UNIVERSIDADE FEDERAL DE SANTA CATARINA
CENTRO DE TECNOLOGIA
PROGRAMA DE PÓS-GRADUAÇÃO EM ENGENHARIA MECÂNICA

Augusto Finger Pacheco

Development of Virtual Kinetics Chemistry for the Prediction of Ignition Delay Time of a Fuel Presenting Negative Temperature Coefficient Behavior

Florianópolis
2022

Augusto Finger Pacheco

Development of Virtual Kinetics Chemistry for the Prediction of Ignition Delay Time of a Fuel Presenting Negative Temperature Coefficient Behavior

Tese submetida ao Programa de Pós-Graduação em Engenharia Mecânica da Universidade Federal de Santa Catarina para a obtenção do título de doutor em Engenharia Mecânica.
Supervisor:: Prof. Amir Antônio Martins de Oliveira Júnior, PhD.

Florianópolis
2022

Ficha de identificação da obra elaborada pelo autor,
através do Programa de Geração Automática da Biblioteca Universitária da UFSC.

Pacheco, Augusto Finger
Development of Virtual Kinetics Chemistry for the Prediction of Ignition Delay Time of a Fuel Presenting Negative Temperature Coefficient Behavior / Augusto Finger Pacheco ; orientador, Amir Antônio Martins de Oliveira Júnior, 2022.
107 p.

Tese (doutorado) - Universidade Federal de Santa Catarina, Centro Tecnológico, Programa de Pós-Graduação em Engenharia Mecânica, Florianópolis, 2022.

Inclui referências.

1. Engenharia Mecânica. 2. Cinética Química Virtual. 3. Tempo de Atraso de Ignição. 4. Mecanismos Cinéticos Reduzidos. 5. Combustão. I. Oliveira Júnior, Amir Antônio Martins de. II. Universidade Federal de Santa Catarina. Programa de Pós-Graduação em Engenharia Mecânica. III. Título.

Augusto Finger Pacheco

Development of Virtual Kinetics Chemistry for the Prediction of Ignition Delay Time of a Fuel Presenting Negative Temperature Coefficient Behavior

O presente trabalho em nível de doutorado foi avaliado e aprovado por banca examinadora composta pelos seguintes membros:

Prof. Leonel Rincón Cancino, Dr. Eng.
UFSC - Campus Joinvile

Prof. Benoît Fiorina, Dr. Eng.
CentraleSupélec, Laboratoire EM2C, CNRS, França

Prof. Luís Fernando Figueira da Silva, Dr. Eng.
Institut Pprime UPR 3346 CNRS, ENSMA and University of Poitiers, France

Certificamos que esta é a **versão original e final** do trabalho de conclusão que foi julgado adequado para obtenção do título de doutor em Engenharia Mecânica.

ICP-Edu
Documento assinado digitalmente
Paulo de Tarso Rocha de Mendonca
Data: 01/09/2022 15:36:15-0300
CPF: 149.822.691-49
Verifique as assinaturas em https://v.ufsc.br

Coordenação do Programa de Pós-Graduação

ICP-Edu
Documento assinado digitalmente
Amir Antonio Martins de Oliveira Junior
Data: 30/08/2022 13:46:50-0300
CPF: 660.526.889-04
Verifique as assinaturas em https://v.ufsc.br

Prof. Amir Antônio Martins de Oliveira Júnior, PhD.
Supervisor:

Florianópolis, 2022.

Este trabalho é dedicado a todas as pessoas que
acreditaram e continuam acreditando em mim.

ACKNOWLEDGEMENTS

Muitas pessoas merecem um espaço nesta seção, e embora não sejam citadas, agradeço muito, sejam pelos conselhos ou discussões. Agradeço ao CNPQ pelos recursos durante essa pesquisa.

De todos os envolvidos, agradeço principalmente aos meus pais, Júlia e Renato, pelo incansável apoio e incentivo durante essa jornada.

RESUMO

A simulação de escoamentos reativos complexos em aplicações com combustão geralmente requer uma grande quantidade de poder computacional, e a parte reativa da solução é geralmente a que consome o maior tempo. Mecanismos detalhados de cinética química podem conter mais de dezenas de milhares de espécies químicas, enquanto que simulações numéricas de escoamentos reativos complexos estão limitadas a mecanismos cinéticos com, no máximo, algumas centenas de espécies. Mecanismos virtuais aparecem como uma estratégia muito eficiente para reduzir drasticamente o tempo computacional na parte reativa das simulações numéricas. Tais mecanismos são formados por espécies e reações químicas artificiais, as quais são otimizadas para reproduzir as características importantes de um problema canônico de interesse. Esta tese apresenta o desenvolvimento de mecanismos virtuais para reproduzir a evolução da temperatura e o tempo de atraso de ignição para a ignição térmica em um reator homogêneo, adiabático, com massa e pressão constantes de uma mistura ar-combustível. O desenvolvimento dos mecanismos virtuais de ignição térmica foi feita em duas etapas: a primeira para a ignição térmica em alta temperatura e a segunda para a ignição térmica em temperaturas baixas e intermediárias de uma mistura com NTC. Para a primeira etapa, modelou-se a ignição térmica de uma mistura de metano e ar, com condições inicias de temperatura de 1000 K à 1500 K e pressões de 1 atm até 3 atm. Para a segunda etapa, modelou-se uma mistura de n-heptano e ar, com temperaturas de 600 K até 1500 K, em pressão atmosférica. A primeira etapa apresenta algumas limitações ligadas, sobretudo, ao limitado número de reações e consequentemente parâmetros do mecanismo virtual. A segunda etapa resolve algumas dessas limitações enquanto que, ao mesmo tempo, aumenta a aplicabilidade da metodologia. Ainda que os erros observados nos atrasos de ignição para os mecanismos virtuais aqui desenvolvidos sejam relativamente elevados, mecanismos reduzidos através de técnicas mais comuns, como DRG, caso produzissem mecanismos com tamanhos similares, apresentariam erros muito superiores. A redução de tempo computacional na simulação com mecanismos reduzidos atinge valores até 1300 vezes.

Palavras-chave: Cinética Química Virtual. Tempo de Atraso de Ignição. Mecanismos Cinéticos Reduzidos. Combustão.

RESUMO EXPANDIDO

Introdução

A predição da evolução da cinética química de espécies químicas é uma das operações que mais demandam tempo computacional em simulações de escoamentos reativos. Grandes mecanismos cinéticos são necessários para descrever com certo grau de precisão reações e caminhos cinéticos para grandes moléculas Lu and Law (2009). Mesmo que mecanismos que compreendem tantos detalhes sejam necessários para a construção de conhecimento acerta da química da combustão, seu uso em aplicações práticas em modelos computacionais complexos é inviável. Para a utilização de alguns mecanismos para grandes moléculas, e.g. o mecanismo de Naik et al. (2011) com 3500 espécies e 17000 reações ou o mecanismo de Pei et al. (2015) com 2885 espécies e 11754 reações, diversas simplificações foram desenvolvidas. Tais métodos podem ser classificados de acordo com o produto final e estratégia utilizada em metodologias que produzem: mecanismos esqueléticos, mecanismos analíticos e metodologias com tabulações. Alumas destas estratégias podem ser utilizadas ainda em estratégias dinâmicas (*on-the-fly*) onde a simplificação ocorre simultaneamente com a solução da parte de transporte do problema.

Ainda que as técnicas de redução tenham atingido altos graus de redução de mecanismos detalhados, um limite é sempre atingido, onde geralmente a precisão se degenera à uma taxa muito superior à taxa de redução. Esta limitação está intimamente ligada à estrutura do mecanismo detalhado e dificilmente pode ser evitada, mesmo ao se empregar uma combinação de estratégias.

A estratégia proposta por Cailler et al. (2017) tem por objetivo superar tal limitação. Ao contrario das metodologias de redução, as quais trabalham de cima pra baixo em um mecanismo detalhado (removendo partes deste), a metodologia de mecanismos virtuais constroem um mecanismo do zero, de modo que este reproduza os mesmos fenômenos observados no mecanismo detalhado. O mecanismo final obtido por tal estratégia pode ser tão preciso quando desejado e pode não apenas representar comportamentos termodinâmicos, mas diferentes aspectos da química (Cailler et al. (2017), Maio et al. (2019) e Cailler et al. (2020)). Além disso, informações adicionais podem ser acopladas ao mecanismo quando desejado. Dessa maneira, o objeto final pode ser composto apenas pelos módulos desejáveis para o problema proposto.

O trabalho de Cailler et al. (2017), Maio et al. (2019) e Cailler et al. (2020) foca na descrição da velocidade de chama laminar e produção de gases poluentes. Nesta tese, mecanismos virtuais para descrever a evolução da temperatura e o atraso de ignição (*Ignition Delay Time* - IDT) para a ignição térmica adiabática, à pressão e massa constantes, de misturas homogêneas de ar-combustível foram propostos e desenvolvidos. Os modelos de cinética virtuais foram implementados e otimizados para predizer o atraso de ignição e a evolução transiente da temperatura durante a ignição em temperaturas médias e altas, baixa pressão para misturas de metano-ar e, misturas de n-heptano em baixas e altas temperaturas em pressões atmosféricas.

Objetivos

Os objetivos gerais deste trabalho podem ser definidos como o desenvolvimento, implementação e avaliação do uso de mecanismos virtuais para predição de tempos de

atraso de ignição e evolução da temperatura em modelos de ignição térmica. Isto vai de encontro ao aprimoramento da metodologia para aumentar a aplicabilidade de tais técnicas como substituto aos mecanismos reduzidos em aplicações práticas.
Para alcançar tais objetivos, as seguintes etapas são propostas: implementação da metodologia de otimização de mecanismos virtuais; desenvolver uma estratégia de avaliação da aptidão através de uma função *fitness* para modelos de auto-ignição; obtenção de mecanismos virtuais para predição de IDT para alta temperatura utilizando metano como referência; obtenção de mecanismos virtuais para predição de IDT para baixas temperaturas utilizando n-heptano como referência; avaliar o uso de mecanismos virtuais para predição de IDT para combustíveis com comportamentos complexos, como NTC.

Metodologia

O desenvolvimento de mecanismos virtuais foi apresentado nos trabalhos de Cailler et al. (2017), Maio et al. (2019) e Cailler et al. (2020), cujo objetivo era representar propriedades termodinâmicas, trasporte velocidade de chama e poluentes em misturas de metano e ar. Os resultados buscados nos estudos eram da ordem de precisão dos mecanismos cinéticos detalhados existentes porém com uma fração mínima do seu número de espécies e reações. Tal metodologia se baseia na otimização de parâmetros termodinâmicos e de cinética química utilizando espécies e reações artificiais para mimetizar o comportamento de mecanismos detalhados.
Para a obtenção de um mecanismo virtual, duas etapas principais são necessárias: Termodinâmica a Cinética Química. Para a primeira etapa, a metodologia empregada segue o apresentado por Cailler et al. (2017), sendo detalhadamente apresentado neste trabalho no capítulo três: *Methodology*. A segunda etapa, responsável pela parte cinética do problema é a grande diferença deste trabalho. A obtenção do atraso de ignição se dá através da solução de modelos zero dimensionais transientes enquanto que modelos para cálculo de velocidade de chama não se importam com a evolução da cinética com o tempo.
Para adaptar a metodologia já desenvolvida para o novo problema, algumas alterações foram necessárias. São dois principais aspectos necessários para reproduzir um mecanismo detalhado durante uma autoignição: a evolução da temperatura e o atraso de ignição propriamente dito.
Um dos grandes problemas em avaliar a diferença dos perfis de temperatura para uma determinada condição e um mecanismo detalhado e um mecanismo virtual durante o processo de otimização é o fato de que o domínio de empo bem como os pontos avaliados não são exatamente os mesmos. Além disso o erro no IDT está diretamente acoplado com um deslocamento do perfil da temperatura em relação ao mecanismo de referência. Tal discrepância nos IDT acaba por introduzir dificuldades em avaliar as diferentes curvas de temperatura. A solução utilizada foi empregar uma metodologia de normalização do tempo, como mostrado na figura a seguir, onde os perfis de temperaturas são normalizados utilizando o atraso de ignição obtido. Deste modo, a ignição passa a ser ancorada no ponto do IDT e duas curvas com IDTs diferentes podem ser comparadas. Além disso, o emprego de tal estratégia faz com que tal metologia esteja muito mais próxima da metologia empregada por Cailler et al. (2017) para avaliação da temperatura.
Para avaliar a parcela referente ao IDT, um cálculo de erro simples da diferença entre o mecanismo virtual e o mecanismo detalhado foi empregado. Além disso, o de-

nominador de tal equação foi modificado para empregar o menor valor entre o IDT do mecanismo virtual e do mecanismo detalhado. Tal estratégia serve como um impedimento à otimização, evitando que casos com valores de IDT abaixo de 1% do observado no mecanismo detalhado sejam agrupados com o mesmo erro.
A aplicação da metodologia utilizou como primeiro objeto de estudo, o mecanismo para o metano, GRI-MECH 3.0. Para tal, condições representando altas temperaturas (de 1000 K até 1500 K) foram selecionadas, em dois níveis de pressão (1 e 3 atm) com uma razão de equivalência estequiométrica. Este primeiro estudo utilizou uma ama de diferentes estruturas de mecanismos para avaliar o efeito da complexidade do mesmo com os resultados.
Um segundo estudo envolvendo o combustível n-heptano foi desenvolvido em seguida. O mecanismo detalhado utilizado foi o mecanismo proposto por Mehl e al. e as condições avaliadas englobaram regiões de NTC e baixa temperatura. Para este caso diversos pontos de alta temperatura (1000 K até 1500 K), NTC (900 K até 650 K) e baixa temperatura (650 K até 600 K) em pressão atmosférica e mistura estequiométrica foram utilizados.

Resultados e Discussões

As discussões dos resultados iniciam-se pelos mecanismos básicos para o metano. Os modelos utilizados mostram que a temperatura adiabática calculada apresentam um desvio de em média, 5% da temperatura de equilíbrio.
Mecanismos simples, contendo apenas uma ou duas reações demonstraram ser capazes de predizer valores de IDT com erros de até 60% para condições extremas, sendo a média, valores abaixo de 40%. Dentre os modelos inicialmente testados, o mecanismo mais simples, One RXN, apresentou os piores resultados na evolução da temperatura. Tal resultado é esperado visto a ausência de qualquer mecanismo que permita emular radicais. Os modelos envolvendo um ou dois intermediários apresentaram curvas de temperatura mais próximas ao mecanismo detalhado, tanto pela presença de intermediários cujos comportamento se assemelham à radicais quanto pela presença de mais reações, o que se traduz em um maio número de graus de liberdade para o modelo. A adição de mai um parâmetro exponencial às reações mostrou uma melhora na evolução da temperatura, com pouco impacto no valor de IDT.
Uma segunda etapa otimizou os mecanismos globais (One RXN) e de um intermediário (One INTER) adicionando reações duplicadas. Isso aumentou os graus de liberdades de tais modelos. Com o aumento do número de reações, houve uma redução nos desvios de atrasos de ignição pra valores menores de 30% nos piores casos.
Como resultado do baixo número de espécies e reações, o tempo computacional obtido para os modelos virtuais ficou abaixo do observado no mecanismo detalhado GRI-MECH3.0. O *speed-up factor* no pior dos casos foi de 1.6 vezes apara altas temperaturas. Em condições de temperaturas mais baixas, i.e. atrasos de ignição mais lentos, os valores de *speed-up factor* chegaram a mais de 100 vezes. A redução na efetividade dos mecanismos virtuais, neste caso, está muito mais ligada ao códio computacional não ser otimizado. Não houve diferenças significativas entre os modelos virtuais.
Para avaliar o desempenho da metologia frente a mecanismos com comportamentos mais complexos, um mecanismo virtual para uma mistura n-heptano-ar foi otimizado. A presença de um NTC seguido de uma mudança de comportamento em baixas temperaturas apresenta grandes dificuldades para a otimização, assim, a mesma estratégia

utilizada para o metano se torna inviável. Um estudo a respeito das estruturas que possibilitariam um NTC foi realizado e como resultado, um mecanismo composto por duas rotas distintas, uma para alta temperatura e outra para baixa, apresentou os melhores resultados.
Ainda, devido ao grande número de parâmetros, uma estratégia baseada em uma otimização em série das reações foi utilizada. Primeiro, um mecanismo piloto para a alta temperatura foi obtido para em seguida ser otimizado apenas na região do NTC. Com as duas regiões otimizadas, uma terceira etapa envolvendo a região de baixa temperatura foi realizada. Por fim, um refino utilizando todas as condições foi feito.
Os resultados obtidos mostram que o mecanismo virtual foi capaz de representar as regiões de alta temperatura, NTC e a mudança de comportamento para baixas temperaturas com erros abaixo dos 20%, exceto na região de transição de alta temperatura para baixa a região de NTC, onde erros de até 40% foram observados. Tais erros poderiam ser diminuídos com a adição de rotas reversas e mais tempo de otimização.
Para a evolução da temperatura, os mecanismos virtuais não conseguiram reproduzir as duas etapas da ignição observadas em baixas temperaturas. No entanto, durante a região de NTC, onde os dois intermediários (de baixa e alta temperatura) eram encontrados em níveis significativos, um comportamento parecido com uma ignição em dois estágios foi observada, indicando que tal comportamento pode ser obtido ao adicionar um novo intermediário no mecanismo.
Para o tempo computacional, devido a grande diferença no tamanho dos mecanismos, os valores de*speed-up factor* observados foram muito superiores, sendo o pior dos casos um fator de 32.5 vezes na região do NTC, muito provavelmente devido a presença dos dois intermediários durante a ignição do mecanismo virtual. Diferentemente dos mecanismos para o metano, os valores para altas temperaturas foram muito superiores, atingindo *speed-up factors* de mais de 1300 vezes, enquanto que em baixas temperaturas, uma média de 80 vezes foi obtida.

Conclusões

Um modelo de mecanismo cinético virtual foi implementado e otimizado para predizer IDT de misturas de metano-ar em médias e altas temperaturas e baixas pressões. O objetivo não se baseia apenas na predição da temperatura adiabática de chama e ao atraso de ignição propriamente dito, mas também a evolução da temperatura da mistura durante uma ignição térmica à pressão e massas constantes.
Os resultados obtidos indicam que a a temperatura adiabática de chama pode ser predita com um erro de até 5% da temperatura de equilíbrio. Os valores de IDT nas condições de 1000 K até 1500 K e pressões de 1 e 3 atm apresentaram bons resultados, com desvios do mecanismo detalhado de no máximo 60 % com a maioria dos casos estando abaixo dos 40 %. Quando estes resultados são observados em gráficos típicos de atraso de ignição, as variações são menores do que as diferenças observadas entre dados experimentais de maquinas de compressão rápida e tubos de choque, e os valores obtidos de mecanismos detalhados. Além disso, os mecanismos virtuais tendem a distribuir o desvio médio através de todo o domínio calculado e mesmo o mecanismo global mais simples (One RXN) apresenta um bom ajuste.
A predição da evolução da temperatura durante a ignição térmica é muito mais complicado do que a predição do IDT. O mecanismo mais simples (One RXN) mesmo apresentando um bom resultado para o atraso de ignição, não apresenta a mesma eficiência na evolução da temperatura. Ele não possui a habilidade de simular a for-

mação e crescimento de radicais, seguido de uma rápida produção das espécies virtuais. Mecanismos virtuais com intermediários (e.g. *Three* "One INTER") apresentam curvas mais próximas do mecanismo detalhado principalmente pela existência de um intermediário, o que facilita a simulação da formação e crescimento dos radicais.
Ao comparar o tempo computacional gasto para resolver o mesmo problema de inição térmica usando o mecanismo detalhado e os mecanismos virtuais, utilizando o mesmo computador, o menor fator de aceleração (*speed-up factor*) obtido foi de 1.6 vezes. Entretanto, para casos com ignição mais lentas, os valores obtidos passam de 100 vezes, ou seja, mecanismos virtuais necessitaram menos de 1% do tempo de um mecanismo detalhado para o mesmo problema.
Uma segunda otimização foi realizado para uma mistura de n-heptano e ar, em baixas e altas temperaturas e pressão atmosférica. O objetivo foi avaliar a capacidade de mecanismos virtuais de predizerem atraso de ignição e distribuição de temperatura para combustíveis que apresentam um comportamento NTC durante a ignição térmica à pressão e massa constantes.
Os valores obtidos de IDT apresentam bons resultados comparados com o mecanismo detalhado para altas temperaturas. Na região do NTC, o mecanismo otimizado foi capaz de reproduzir o comportamento do mecanismo detalhada com erros menores de 20%, exceto para a região de transição entre alta temperatura e NTC. Além disso, o modelo otimizado foi capaz de reproduzir a mudança da região de NTC para a região de baixa temperatura, a qual representava um dos maiores desafios para o mecanismo virtual.
A evolução da temperatura ainda requer melhoras. A estrutura do mecanismo proposto apresenta bons resultados em geral, entretanto a ignição de dois estágios apresentada pelo mecanismo detalhado de Mehl et al. (2011) em baixas temperaturas não foi possível de ser emulada. O mecanismo virtual apresentou um efeito similar durante a transição da alta temperatura para a região de NTC, onde dois intermediários diferentes estavam presentes em quantidades significativas. Isso indica que uma ignição de dois estágios só pode ser obtida com a adição de um intermediário ativo nas condições onde tal comportamento é esperado.
Os efeitos no tempo computacional forma muito superiores ao encontrados para o metano, principalmente pela grande diferença de tamanho entre o mecanismo detalhado e os mecanismos reduzidos. Neste caso, o menor *speed-up factor* observado foi de 32.5 vezes durante a região de NTC. De maneira diferente ao observado nos casos referentes ao metano, temperaturas mais elevadas apresentaram melhores resultados, com casos apresentando *speed-up factor* de mais de 1300 vezes, e para baixas temperaturas, uma média de 80 vezes foi observada. Tais resultados podem ser atribuídos ao aumento da complexidade do mecanismo virtual em baixas temperaturas.

ABSTRACT

The simulation of complex reactive flows in combustion applications generally requires a large amount of computational power, and the reactive part of the solution is usually the most time consuming. Detailed chemical kinetics mechanisms can reach up to tens of thousands species, while numerical simulations of complex reactive flows can handle mechanisms, at most, with a few hundred species. Virtual kinetic mechanisms are a very effective strategy to drastically reduce the computational time spent in the reactive part of numerical simulations. They are formed by artificial species and reaction paths, that are optimized to reproduce the important characteristics of a canonical problem of interest. This thesis presets the development of virtual mechanisms able to reproduce the temperature evolution and ignition delay times of the thermal ignition of a homogeneous, constant mass, constant pressure, adiabatic, fuel-air mixture reactor. The results are divided into two sections: the first one being related to methane-air mixture over a range of temperatures from 1000 K to 1500 K and pressures from 1 atm to 3 atm as a way to test the methodology developed. The second section presents an expansion to the methodology to cover complex fuel behaviors, such as the NTC, using a n-heptane-air mixture tested over a range of temperatures from 600 K to 1500 K and atmospheric pressures. The first section present some limitations of the most due to the small number of reactions and parameters of the kinetic model. The second section address some of those issues while further improving the virtual mechanism methodology applicability. The current IDT errors observed, although having large values, are much smaller than reduced mechanism produced with common strategies such as DRG of the same size.

Keywords: Virtual Chemistry. Ignition Delay Time. Reduced Kinetic Mechanism.

LIST OF FIGURES

LIST OF TABLES

LIST OF ABBREVIATIONS AND ACRONYMS

ANN	Artificial Neural Network
ASER	Automated Simulation Error based Reduction
ATF	Artificially Thickened Flame
CARM	Computer Assisted Reduction Mechanism
CEMA	Chemical Explosive Mode Analysis
CO-DAC	Correlated Dynamic Adaptive Chemistry
CSP	Computational Singular Perturbation
DAC	Dynamic Adaptive Chemistry
DOE	Design of Experiment
DRG	Direct Relation Graph
DRGASA	Direct Relation Graph aided Sensitivity Analysis
DRGEP	Direct Relation Graph with Error Propagation
DRGEPSA	Direct Relation Graph with Error Propagation aided by Sensitivity Analysis
DRGRE	Direct Relation Graph Revised
DSA	Direct Sensitivity Analysis
EDC	Eddy Dissipation Concept
EF	Element Flux
EFA	Element Flux Analysis
EOA	Ellipsoid of Accuracy
FSSA	Full Species Sensitivity Analysis
GA	Genetic Algorithm
GALI	Greedy Algorithm with Local Improvement
HCCI	Homogeneous Charge Compression Ignition
HMTS	Hybrid Multi-Timescale
I-CSP	Automated Computational Singular Perturbation
IDT	Ignition Delay Time
ISAT	*in-situ* Tabulation
JPDF	Joint Probability Density Function
LES	Large Edgy Simulation
NASA	National Aeronautics and Space Administration
NTC	Negative Temperature Coefficient
ODE	Ordinary Differential Equations
PCA	Principal Component Analysis
PDF	Probability Density Function
PE	Partial Equilibrium
PFA	Path Flux Analysis
PFR	Plug Flow Reactor
PMSR*	Pairwise Mixing Stirred Reactor
QSS	Quasi Steady State
RCCE	Rate Controlled Constrained-Equilibrium
RII	Relative Importance Index
ROA	Region of Accuracy
ROP	Rate Of Production
SA	Sensitivity Analysis
SBX	Simulated Binary Crossover
TDAC	Tabulated Dynamic Adaptive Chemistry

TSR	Tangential Stretching Rate

LIST OF SYMBOLS

h	Molar Enthalpy
p	Pressure
k	Rate Constant
A	Arrhenius Pre exponential Coefficient
E_A	Activation Energy
R_u	Universal gas constant
b	Temperature Exponent
$\dot{q}_j$	Rate of Reaction for Reaction j
$\dot{\omega}_i$	Net Production Rates for Species i
$[X]$	Concentration of Species X
c_p	Molar Heat Capacity at Constant Pressure
MW	Molar Weight
P_j	Fitness Penalties
τ	Ignition Delay Time
$d\%$	Relative (%) τ Deviation
γ_{IDT}	Ignition Delay Time Weight Coefficient

CONTENTS

1 INTRODUCTION

The prediction of the time and spacial evolution of the concentration of chemical species is one of the most time consuming operations in reactive flow simulations. Large mechanisms are required to describe the chemical kinetics paths and reactions for large molecules with an adequate degree of accuracy (LU; LAW, 2009). Although comprehensive mechanisms are needed to improve the understanding of the chemistry of combustion, their implementation in complex computational models is largely unfeasible. In order to accommodate the state of the art of kinetic mechanisms for large hydrocarbon molecules, e.g., the mechanisms of Naik et al. (2011) with 3,500 species and 17,000 reactions and Pei et al. (2015) with 2,885 species and 11,754 reactions, several simplification strategies were developed. Such methods can be classified accordingly to the final product and strategy used in schemes that produce skeletal mechanisms, strategies to create analytic mechanisms, and the tabulated strategies. Some of these strategies can also be used in on-the-fly reductions, when the simplification of the mechanism is done simultaneously and in fine tuning with the solution of the transport part of the problem.

Skeletal procedures search and remove unimportant components of the detailed mechanism and therefore reduce its size and complexity. Turányi (1990) published a study in which the importance of species are evaluated by means of removing the reactions where it participates. More recently, graph theory was introduced as a reduction technique by Lu and Law (2005) known as Direct Relation Graph (DRG). Each species is mapped as a node in a directed graph, and the reactions connecting species are mapped as edges. The importance of species in the graph is evaluated and species with negligible effect in the important ones are deemed as redundant and removed. Several studies expanded the basic DRG method, P. Pepiot-Desjardins and Pitsch (2008) introduced Direct Relation Graph with Error Propagation (DRGEP), and importance index variations, such as the Path Flux Analysis (PFA), proposed by Wenting Sun et al. (2010). Presently, a large number of variations exist and several authors studied their applicability and efficiency on reducing very large mechanisms, an activity known as Computer Assisted Reduction Mechanism (CARM). Another application of these methods are the on-the-fly reduction schemes, such as the one proposed by L. Tosatto et al. (2011). Augusto F. Pacheco (2016) presented a comprehensive study on common used reduction techniques, exploring some of the limits of each one.

The main goal of the analytic methods of reduction is to divide the dynamics of the species transformation into fast and slow domains. Analytic reductions aims at reducing the stiffness of the mechanisms by searching for Quasi Steady State (QSS) candidates to be removed from the system, replacing partial differential by algebraic equations. One of the basic methods is the Computational Singular Perturbation (CSP), proposed by S. H. Lam (1985). One of the main advantages of such strategies is the accuracy and robustness of the final mechanism, since the species are not actually removed, but accounted for through QSS relations.

Tabulated chemistry relies on the fact that the chemical trajectory during a combustion process is in a great extent defined by a smaller sub-space, named a manifold. Such space can therefore be solved in advance, the solution is stored as a table and retrieved during the combustion simulation. The density of the table and the number of inputs needed to retrieve a given information is dictated by the complexity of the problem to be solved.

Despite the reduction techniques have achieved several orders of reduction of

complex detailed mechanisms, a limit is always reached, when the accuracy would degenerate at a larger rate than the reduction itself. This limit is intrinsically related to the structure of the detailed mechanism and can hardly be circumvented, even using a combination of strategies.

A strategy proposed by Cailler et al. (2017) aims at surpassing this limitation. Contrary to the reduction methodologies that work down from the detailed mechanism, by removing species and reactions as the method advances, the virtual chemistry method builds a virtual mechanism from the ground up, such that the virtual mechanism reproduces the same effects as the detailed mechanism. The final mechanism provided by such methodology can be as accurate as desired, and can predict not only the thermodynamic behavior, but different aspects of the detailed chemistry. Additional information can be added further and then, the final mechanism can be composed only by the necessary or desired modules for the current problem. (CAILLER et al., 2017; MAIO et al., 2019; CAILLER et al., 2020)

The work by Cailler et al. (2017), Maio et al. (2019) and Cailler et al. (2020) focused on laminar flame speed and production of gas pollutants. In this work, virtual schemes to describe the temperature evolution and the ignition delay time for the thermal ignition of homogeneous, constant mass, constant pressure, adiabatic, fuel-air mixtures are developed. Virtual chemistry models were developed for a methane-air mixture from intermediate to high temperatures and low pressures, and an n-heptane-air mixture from low to high temperatures, at atmospheric pressure. From the results obtained for methane-air, the method was adapted and applied to the n-heptane ignition, to explore the capabilities of the current methodology to predict Negative Temperature Coefficient (NTC) behavior.

In the following sections, the general method is presented and adapted to the prediction of ignition delay time. Several virtual mechanisms are proposed, built from the duplication of basic reaction paths with one or two intermediates. The predicted Ignition Delay Time (IDT) and temperature distributions are compared to the predictions using the GRI-Mech 3.0, for methane-air, and the mechanism by Mehl et al. (2011) for n-heptane-air. The deviations are evaluated, and the computational time relative to the detailed mechanism is assessed.

1.1 OBJECTIVES

1.1.1 General Objective

The main goal of this study is to implement and evaluate the use of virtual mechanisms for predicting ignition delay time and temperature distribution during thermal autoignition, extending the use of virtual schemes as a feasible substitute of detailed and reduced mechanisms in the numerical simulation of practical applications.

1.1.2 Specific Objectives

In order to achieve the general objective, the following specifics goals are proposed:

1. To implement the virtual chemistry optimization scheme;
2. To developed a methodology to evaluate the fitness for autoignition models;
3. To obtain virtual mechanisms for IDT prediction of methane-air mixture;

4. To obtain a virtual mechanism for IDT prediction of n-Heptane-air mixture;
5. To evaluate the use of virtual chemistry for IDT prediction and its limitations when NTC is present;
6. To assess the use of a static virtual mechanism to cover a wide range of conditions.

2 LITERATURE REVIEW

The computational modeling of combustion problems involves the use of thermodynamics, transport and chemical kinetics principles. Thermodynamics provides the basic relations that describe the local state of the combustible media, specially, under local equilibrium, the relation of the species enthalpy h and entropy s to temperature T, pressure p, and species mass concentration c, as well as the pVT relation from the equation of state. The transport of momentum, heat and mass is modeled by macroscopic conservation equations. Meso-scale and micro-scale modeling describe the relation of the transport properties to the local state. Finally, the chemical kinetics describes the interaction between chemical species leading to the transformation from reactants to products. The mass of elements are assumed fixed, although there might be changes in electronic configuration. There are several references that describe the overall challenges of combustion modeling Law (2006), Warnatz et al. (2006), Peters (2000), Oran and Boris (2000), Oppenheim (2008), Echekki and Mastorakos (2010) and Poinsot (2001).

This work focus on the modeling of chemical kinetics, in particular, the reduction of size and complexity of chemical mechanisms aiming at speeding up computation of complex reactive flow, but still retaining the needed accuracy.

This chapter describes the fundamentals of chemical kinetics mechanisms, the mechanism reduction methods mostly used to reduce large detailed mechanisms, emphasizing the principles involved, their advantages, and limitations, and, finally, the development and use of virtual chemistry.

2.1 CHEMICAL KINETIC MECHANISMS

Several works describe the fundamentals of chemical kinetics mechanisms for combustion applications. Here, only the basic concepts needed to the development of the virtual kinetics modeling are described Battin-Leclerc et al. (2014), Turányi and Tomlin (2014), Masel (2001), Pilling (1997) and Peters and Rogg (1993).

2.1.1 Global Reactions

We define a global reaction as an one-step reaction involving one mole of oxidant with a moles of fuel, resulting in n moles of products, generally expressed as

$$F + aOx \rightarrow nPr \tag{1}$$

A global reaction kinetics is a semi-empirical expression that predicts the rate of change of the mass of species k. The Law of Mass Action defines the dependence on the concentration of reactants and the effect of the temperature is accounted for through a rate constant. The global reaction rate generally takes the following form

$$\frac{d[Fuel]}{dt} = -k_G(T)[Fuel]^n[Oxidant]^m \tag{2}$$

Here, the $[Fuel]$ and $[Oxidant]$ represent the molar concentrations of fuel and oxidant, respectively. The property is the apparent rate and is strongly dependent on temperature. The exponents m and n define the fuel and oxidant reaction order and are, generally, empirically fitted to match selected measurements.

The use of global reactions to model chemical kinetics is a simplification of a complex behavior and has found its usefulness in the solution of engineering problems where the rates of transport determine the main outcome of the process. However, the use of global reactions does not provide a solid ground for understanding the details of the reaction process or to determine reaction controlled phenomena, such as ignition, extinction, and some regimes of flame propagation. It is naive to think that exactly n molecules of fuel would collide simultaneously with m molecules of oxidant, producing the final products in a single event of rearrangement of chemical bonds. What is known to occur is a chain of series and parallel elementary reactions, often involving thousands of stable and excited chemical species, known as intermediates. As a consequence, the approach to describe a chemical process involves the determination of the nature of the intermediate species and how they interact with each other in the form of elementary reactions (PACHECO, Augusto F., 2016).

2.1.2 Elementary Reactions

An elementary reaction is an one-step reaction that occurs molecularly in exactly the same way as it is expressed by the chemical equation. In an elementary reaction, the reactants form the products through a single transition state, without the presence of intermediate species. The overall reaction in fact occurs through a sequence of elementary steps.

The reaction molecularity is defined as the number of species that collide to form the activated complex. Only collisions among one, two and three species are statistically probable and they are named unimolecular, bimolecular, and termolecular reactions.

The *Law of Mass Action*, that rigorously applies only to elementary reactions, states that the rate of reaction is proportional to the number of molecules of species appearing as reactants. From the *Law of Mass Action*, the rate of the irreversible bimolecular reaction

$$A + B \rightarrow C + D \tag{3}$$

is expressed as

$$\frac{d[A]}{dt} = -k[A][B] \tag{4}$$

where k is the rate constant and $[I]$ is the molar concentration of species I.

In the same way that a collision between A and B can produce C and D, A and B can also be formed from collisions of C and D. Therefore, in general, a reaction can occur following both directions and two definitions are employed. The first choice uses two different irreversible reactions, while the second choice is to use two kinetic constants, a forward and a reverse kinetic constant. For the bimolecular reaction above, one could write

$$A + B \rightleftharpoons C + D. \tag{5}$$

The rate of production of A by the forward and backward reactions can be expressed, respectively,

$$\left(\frac{d[A]}{dt}\right)_f = -k_f[A][B], \tag{6}$$

$$\left(\frac{d[A]}{dt}\right)_b = k_b[C][D]. \tag{7}$$

where k_f is the rate constant for the forward reaction and k_b is the rate constant for the reverse reaction. Therefore, the total rate of production of A can be expressed as

$$\frac{d[A]}{dt} = \left(\frac{d[A]}{dt}\right)_f + \left(\frac{d[A]}{dt}\right)_b = -k_f[A][B] + k_b[C][D] \tag{8}$$

The relation between the forward and backward constants is the equilibrium constant,

$$\frac{[C]^c[D]^d}{[A]^a[B]^b} = K_{eq} = \frac{k_f}{k_b} \tag{9}$$

where the exponents refer to the stoichiometric coefficients of the reaction.

2.1.3 Reaction Rate for Elementary Reactions

The dependency of the rate constant with temperature may be modeled using an Arrhenius relation in the form

$$k(T) = A\exp\left(\frac{-E_A}{R_u T}\right) \tag{10}$$

where A is the pre-exponential factor, E_A is the activation energy, that can be defined as the energy required to reach the transition state, and R_u is the universal gas constant.

The extended Arrhenius equation includes an additional dependency with temperature in the form

$$k(T) = AT^b\exp\left(\frac{-E_A}{R_u T}\right) \tag{11}$$

where b is the temperature exponent.

2.1.4 Numerical Treatment of Chemical Kinetic Mechanisms

As stated on section 2.1.1, a chemical process takes place through several steps, which can be described by elementary reactions. The set of all the elementary reactions among the chemical species that participate in a chemical reaction is defined as the detailed chemical kinetics mechanism. Consider the following set of reactions in the $H_2 - O_2$ mechanism:

$$\begin{aligned} H_2 + O_2 &\leftrightarrow HO_2 + H && (R.1)\\ H + O_2 &\leftrightarrow OH + O && (R.2)\\ OH + H_2 &\leftrightarrow H_2O + H && (R.3)\\ H + O_2 + M &\leftrightarrow HO_2 + M && (R.4)\\ &\vdots \end{aligned}$$

With the definition of reaction rate for elementary reaction presented in the section 2.1.3, one can define mathematically the production net rates for any chemical species in the mechanism. For example, the net production of O_2 can be calculated as the sum of all the net production rates from all elementary reactions, i.e.,

$$\begin{aligned} \frac{d[O_2]}{dt} &= k_{r1}[HO_2][H] + k_{r2}[OH][O] + k_{r4}[HO_2][M] + \ldots \\ &\quad - k_{f1}[H_2][O_2] - k_{f2}[H][O_2] - k_{f4}[H][O_2][M] - \ldots \end{aligned} \tag{12}$$

The positive terms represent the formation of O_2 and the negative ones, its destruction. This analysis can be extended to all species present on the mechanism.

As the number of elementary reaction in a kinetics mechanism can achieve numbers on the thousands, a compact notation is generally used. An elementary reaction can be represented as

$$\sum_{j=1}^{N} \nu'_{ij}[X_j] \leftrightarrow \sum_{j=1}^{N} \nu''_{ij}[X_j] \qquad \text{for } i = 1, 2, \ldots, L \tag{13}$$

where ν'_{ij} and ν''_{ij} are the stoichiometric coefficients of the reactants and products respectively for species j on reaction i.

This simplified notation allows the use of matrices (in fact, highly sparse matrices) to represent the mechanism, facilitating the numerical treatment.

The rate of reaction of reaction j, $\dot{q}_j$, is calculated from

$$\dot{q}_j = \sum_{i=1}^{L} \nu_{ij} q_i \qquad \text{for } j = 1, 2, \ldots, L \tag{14}$$

where the shorter notation

$$\nu_{ij} = \nu''_{ij} - \nu'_{ij} \tag{15}$$

is used.

Then, the net rate of production of species i, $\dot{\omega}_i$ becomes

$$\dot{\omega}_i = k_{fi} \prod_{j=1}^{N} [X_j]^{\nu'_{ij}} - k_{ri} \prod_{j=1}^{N} [X_j]^{\nu''_{ij}}. \tag{16}$$

2.2 REDUCTION TECHNIQUES

The large size of the detailed chemical kinetics mechanisms, although resulting in a more profound and detailed understanding of the reaction paths, limits their application in the simulation of engineering problems. Therefore, an effort in defining the key pathways in these mechanism is vital to employ all this knowledge in practical applications. Tools that can efficiently analyze and provide information in respect to unimportant aspects and paths have become important modeling tools.

The reduction methods can be separated in two major classes. The first one, the static reduction methods, rely on the use of several solution data to generate a smaller mechanism, able to reproduce the results when used in models within the same conditions. The second, and more recent treatment, consists in using reduction methods dynamically, while the simulation is running.

In the following, the Sensitivity Analysis (SA), Computer Singular Perturbation (CSP), Direct Relation Graph (DRG), and Element Flux Analysis (EFA) are discussed.

2.2.1 Sensitivity Analysis

The sensitivity analysis (SA) identifies the rate-limiting reactions. Following the definition presented by Warnatz et al. (2006), the rate laws for a kinetics mechanism of

R reactions and S species can be written as:

$$\begin{aligned} \frac{d[X_i]}{dt} &= F_i([X_1], \ldots, [X_S]; k_1, \ldots, k_R) \\ i &= 1, 2, \ldots, S. \\ [X_i](t = t_0) &= c_i^0 \end{aligned} \tag{17}$$

The time t is the independent variable, the concentrations$[X]$ of species i are the dependent variables and k_r are the system parameters.

In SA methods, the amount of change of a dependent variable with modifications on system parameters is desired. Frequently, several rate reactions may be modified in detailed chemical reaction mechanisms without causing changes on the concentration of important species. However, there are reactions whose rate constants have a drastic effect on the solution. They may involve both major or minor species. The value of the rate of production may be even relatively small. What matters is its final effect on the solution of the reaction system. These few important reactions are labeled as *rate-determining reactions* or *rate-limiting reactions*.

The dependence of the solution $[X_i]$ on the parameter k_r is called sensitivity and can be defined as absolute and relative following,

$$E_i, r = \frac{\partial [X_i]}{\partial k_r}, \tag{18}$$

$$E_{i,r}^{rel} = \frac{k_r}{[X_i]} \frac{\partial [X_i]}{\partial k_r} = \frac{\partial \ln [X_i]}{\partial \ln k_r}, \tag{19}$$

respectively.

In most of the problems, an analytical solution of the system of differential equations to calculate the sensitivities is not practical. This can be done numerically by differentiating equation 17 as:

$$\frac{\partial}{\partial k_r} \left(\frac{\partial [X_i]}{\partial t} \right) = \frac{\partial}{\partial k_r} F_i([X_1], \ldots, [X_S]; k_1, \ldots, k_R) \tag{20}$$

$$\frac{\partial}{\partial t} \left(\frac{\partial [X_i]}{\partial k_r} \right) = \left(\frac{\partial F_i}{\partial k_r} \right)_{[X_l], k_{l \neq r}} + \sum_{n=1}^{S} \left\{ \left(\frac{\partial F_i}{\partial [X_n]} \right)_{[X_{l \neq n}], k_l} \left(\frac{\partial [X_n]}{\partial k_r} \right)_{k_{l \neq j}} \right\} \tag{21}$$

$$\frac{\partial}{\partial t} E_{i,r} = \left(\frac{\partial F_i}{\partial k_r} \right)_{[X_l], k_{l \neq r}} + \sum_{n=1}^{S} \left\{ \left(\frac{\partial F_i}{\partial [X_n]} \right)_{[X_{l \neq n}], k_l} E_{n,r} \right\}. \tag{22}$$

The Jacobian is defined as

$$J_{ij} = \frac{\partial F_i}{\partial [X_j]}. \tag{23}$$

Finally, we can write,

$$\frac{\partial}{\partial t} E_{i,r} = \left(\frac{\partial F_i}{\partial k_r} \right)_{[X_l], k_{l \neq r}} + \sum_{n=1}^{S} \left\{ J_{i,n} E_{n,r} \right\}. \tag{24}$$

Equation 24 must be solved by numerical integration in order to obtain the deviations of $[X_i]$ due to changes in k_r. When computing $E^{rel}_{i,r}$, the value obtained is a measure of the relative importance of the r^{th} reaction to the concentration of species i at a given time t. If all coefficients for the r^{th} reaction are very small compared to the higher values found, this reaction may be targeted as unimportant. This type of analysis generate graphics such as the one presented in figure 1 (CANCINO, 2009).

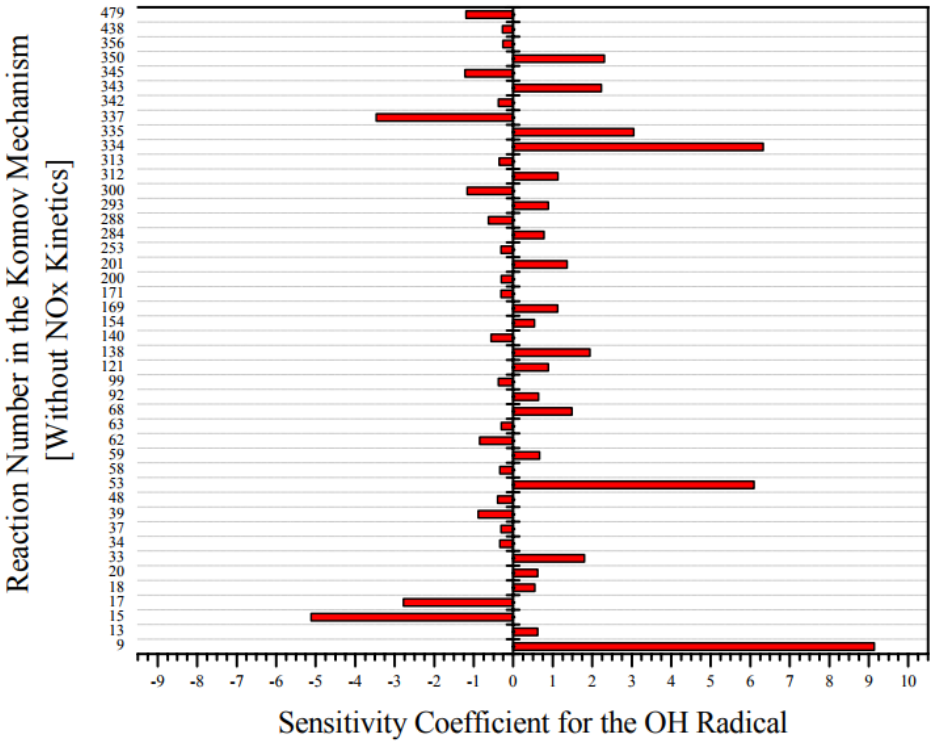

Figure 1 – Typical bar diagram of the sensitivity of the reactions on the concentration of OH radical at a given elapsed time. **Source:** Cancino (2009)

One of the problems faced by SA in thermal ignition problems is that, at each time t, a graphic such as figure 1 is obtained, and when the number of reactions is large, selecting the important reactions for each important species is very time consuming.

Although this method, as several others, was first presented as a way to analyze reaction mechanisms, this can be extended as a reduction technique. After obtaining all the important reactions over all the models and conditions, the reduced mechanism can be constructed with these reactions and the species involved.

This methodology can produce kinetic mechanisms with great accuracy, with a smaller number of reactions. However, its application simultaneously to many different models becomes complex, hindering its use as an exclusive reduction technique.

2.2.2 Direct Relation Graphs

The direct relation graph (DRG) method can be defined as a methodology for searching the important species. For that reason, there are several ways to implement the search, which, mostly, are only marginally different. This section describes several published methodologies based on DRG.

The following presentation is mostly based on Augusto F. Pacheco (2016).

An example of how DRG works can be observed on figure 2. The method operates in a progressive way, from a starting point (an important species list), adding species and reactions until reaching the limit imposed by the threshold. The species in evidence in the diagram are the ones that are progressively added to the final mechanism, i.e., the reduced mechanism. The arrows represent the relation among each species and the thickness of the arrow represents the magnitude of this relation. The process starts in diagram (a), where only species *A* is in the reduced mechanism. In the next step, shown in diagram (b), only species *C*, *D* and *F* have the index greater than the limit and therefore, they are included in the reduced mechanism. At (c), with the presence of species *C*, *D*, and *E* as part of the mechanism, more species become important and are added. The process follows to (d) and finally reaches the reduced mechanism presented in (e). We notice that species *B*, *E*, *G* and *H* never made to the final mechanism because their index never overcame the threshold. In this method, a graph of the mechanism can be build, taking each species as a vertex and the connection between them as the importance index. In the final reduced mechanism there will be a connection between two species *A* and *B* only if the index I_{AB} is greater than the threshold. All the species that do not have a link to the important list are therefore removed from the mechanism as well all the reactions that may involve them.

The first approach to the DRG is presented by Lu and Law (2005). The relation among species was defined as the contribution of a species *B* to the production of the species *A*. The relation r_{AB} can be defined as

$$r_{AB} \equiv \frac{\sum_{i=1,I} |\nu_{A,i}\omega_i\delta_{Bi}|}{\sum_{i=1,I} |\nu_{A,i}\omega_i|} \tag{25}$$

$$\delta_{Bi} = \begin{cases} 1, & \text{if the } i\text{th elementary reaction involves species } B, \\ 0, & \text{otherwise.} \end{cases} \tag{26}$$

If the contribution r_{AB} is sufficiently large, then the removal of species *B* is expected to cause significant error on the prediction of species *A*. In order to control the error, a small threshold value ϵ is used, such that if $r_{AB} < \epsilon$ the dependence between *A* and *B* is negligible. Therefore, two rules are used to construct a DRG:

1. Each node in DRG correspond to a unique species in the detailed mechanism.
2. There exist a direct edge from *A* to *B* if and only if $r_A > \epsilon$

Lu and Law (2005) observed that, while it is straightforward to identify and eliminate unimportant reactions, the identification of the unimportant species is more cumbersome, due mainly to the coupling species. As such, the removal of a species from a mechanism may require the removal of a group of species strong coupled to it.

Therefore, in order to consider a species as important, its relation coefficient to at least one species of interest must be greater than the threshold defined. In this way, the importance coefficient for a species *B* outside of the important species can be written as

$$r_B = \max_{i\in\Omega}(r_{iB}) \tag{27}$$

where Ω represent the list of the important species. Finally, the criteria for elimination of species *B* is

$$r_B = \begin{cases} \geqslant \epsilon, & \text{add } B \text{ to } \Omega, \\ < \epsilon, & B \text{ is not important.} \end{cases} \tag{28}$$

Table 1 – DRG related reduction studies.

Author	**Method**	**Observations (Spc/Rxn)**
Lu and Law (2005)	DRG + CSP	Ethylene: (70/463) to (33/205) and with CSP: (20/16)
Luo et al. (2010)	DRG + isomer lumping + DRGASA	Biodiesel Surrogate: (3329/10806) to (118/837)
Niemeyer and Sung (2011)	DRGEP + different search algorithms	n-Heptane: (561/2539) to (108/406) after sensitivity analysis
Bahlouli, Saray and Atikol (2012)	DRGEP + CSP	n-Heptane: (561/2539) to (118/330)
Tosatto, Bennett and Smooke (2013)	DRG + DRGASA + flux based DRG	JP-8 jet fuel: (234/6997) to 82 92 species
Niemeyer and Sung (2015)	DRGEPSA, isomer lumping, CSP, Greedy SA	Gasoline Surrogate: (1388/5933) to several skeletal mechanisms sizes.
Cheng et al. (2015)	DRG + isomer lumping + SA	Biodiesel Surrogate: (3299/10806) to (92/360)
Pacheco (2016)	DSA, ROP, DRG PFA, DRGEP	Detailed mechanisms for Ethanol
Tang et al. (2017)	DRG, DRGEP, DRGRE, PFA CSP	Diethyl Ether:(174/973) to (80/329)
Qiu et al. (2018)	DRG, DRGEP, SA	Workbench for systematic reduction.
Veerappan, Ramanathan and Kaisare (2019)	DRG + PCA	Automated Simulation Error based Reduction (ASER). Tested against H_2-O_2 and GaAs deposition (gas and surface mechanisms)
Tian, Yan and Li (2019)	DRG related + SA	1-butene: (493/2716) to (52/277)
Minuzzi and de Pinho (2020)	DRG	Ethanol: (57/383) to (37/184)
Rui, Leping and Shiquan (2020)	DRG + SA	Diesel-CH-H tri-fuel: (654/2827) to 262 species
Sui et al. (2020)	DRG	Catalytic and gas-phase mechanisms of H_2/CO/O_2/N_2 over Pt
Liu et al. (2021)	DRG + DRGEP + FSSA	Multi component Diesel Surrogate reduced and merged.

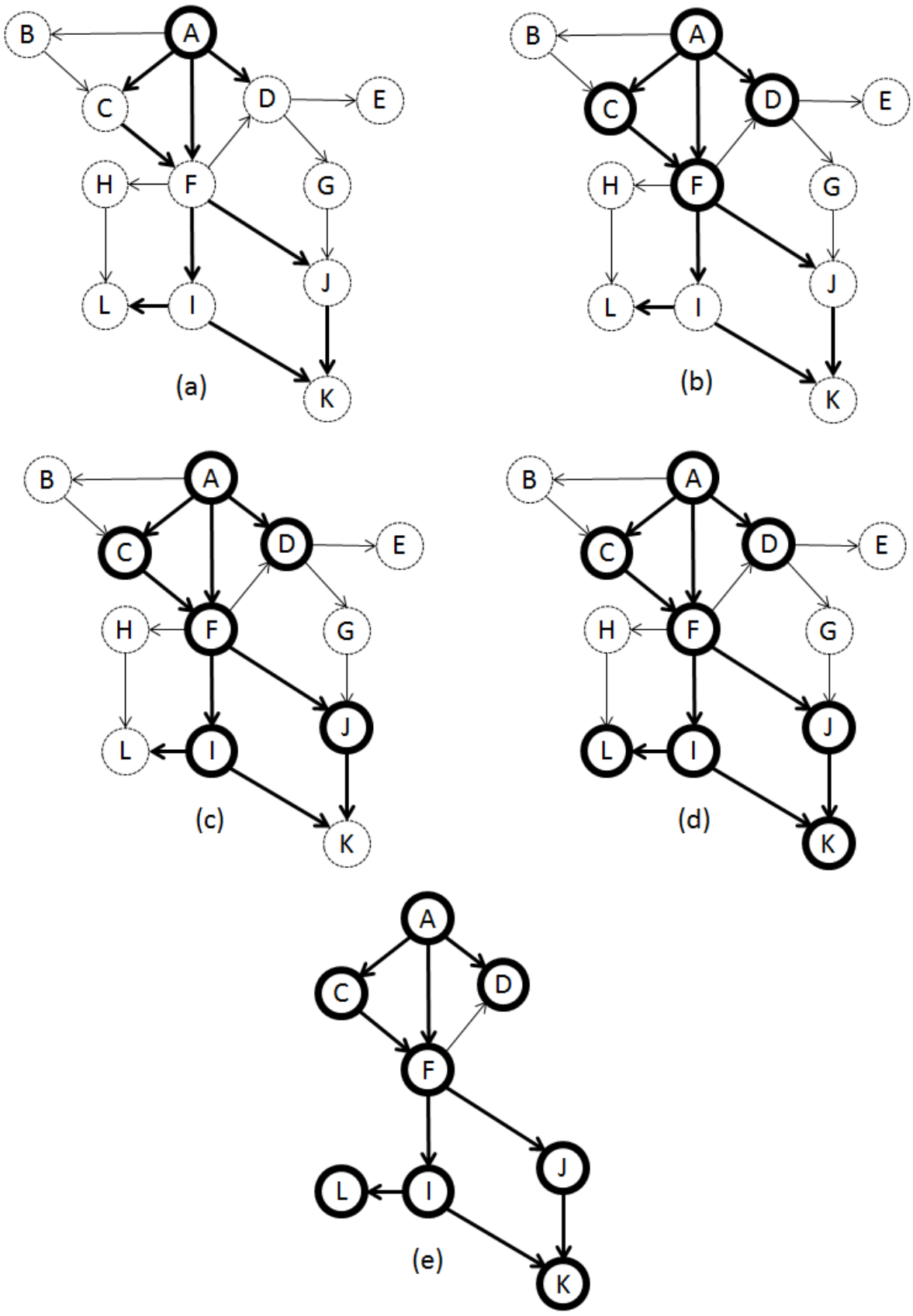

Figure 2 – Example of DRG progression. (a) Initial Mechanism starting with species A as important; (b), (c) and (d) represent the progression of the method; (e) Final reduced mechanism. **Source:** Augusto F. Pacheco (2016)

Based on the DRG method, the Direct Relation Graph with Error Propagation (DRGEP) adds a geometric error to the search, accounting for the distance of a given species from the important species (PEPIOT-DESJARDINS, p.; PITSCH, 2008).

Table 1 presents a summary of works using DRG and some of its variants.

2.2.3 Analytical Methods

As S. H. Lam (1985) stated, the computational singular perturbation (CSP) is an alternative method to formulate the chemical kinetics problem by replacing the detailed mechanism by a reduced mechanism written along the principal directions of the n-coordinates linearized species concentration space. In this method, the behavior of some of the intermediate species is modeled as Quasi-Steady State, while the time variation of the remaining species follows the principal directions of the linearized system.

To develop the main ideas of the CSP method, first the concepts of Quasi-Steady State and Partial Equilibrium are presented.

2.2.3.1 Quasi-Steady State and Partial Equilibrium approximations

The steady state approximation for a chemical species is used when the production rate is approximately equal to the consumption rate, leading to a constant concentration over time. This is the behavior exhibited by species S_2 on figure 3, an example taken from Warnatz et al. (2006).

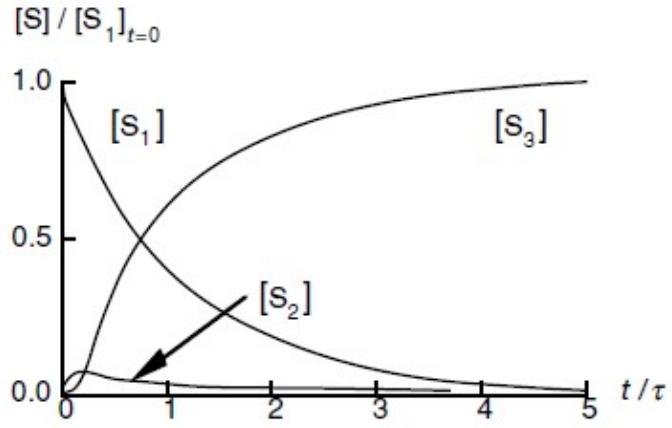

Figure 3 – Variation with time of the non-dimensional concentration of the chemical species S_1, S_2 and S_3 that participate in the simple chain reaction mechanism expressed as $S_1 \rightarrow S_2 \rightarrow S_3$. **Source:** Warnatz et al. (2006)

Very reactive radicals usually follow this behavior. When this is identified, the steady state simplification can be used for the species,

$$\frac{d[X_j]}{dt} = \dot{\omega}_j = \sum_{i=1}^{R} \nu_{ij} q_i = 0 \tag{29}$$

This replaces the differential equation for the species flagged as in QSS from the set of mass conservation equations by an algebraic equation, thus reducing the effort to solve the reactive problem.

The Partial Equilibrium (PE) approximation assumes that the forward and backward reaction rates for a given reaction are equal, resulting in an equilibrium relation among reactants and products. This is illustrated in the following example from Warnatz et al. (2006).

At higher temperatures ($T > 1800K$ and $p = 1$ bar) the following reactions can be assumed to satisfy PE:

$$\begin{aligned} H + O_2 &= OH + O && (R1, R2) \\ O + H_2 &= OH + H && (R3, R4) \\ OH + H_2 &= H_2O + H && (R5, R6) \end{aligned}$$

Assuming that the forward and backward reaction rates are in PE, one obtain the following system

$$\begin{aligned} k_1[H][O_2] &= k_2[OH][O] \\ k_3[O][H_2] &= k_4[OH][H] \\ k_5[OH][H_2] &= k_6[H_2O][H] \end{aligned}$$

This system connects the species concentration in an algebraic way, again reducing the need to solve time evolving differential equations.

2.2.3.2 The CSP method

Methods that simplify kinetic mechanisms by applying QSS and PE approximations may run into problems for very stiff system, when the characteristic time-scales of each species can present differences of several orders of magnitude. The main purpose of CSP is to decoupled fast and slow species, applying QSS for the the group of fast species, reducing the number of ODE to be solved.

S. H. Lam (1985) first presented the CSP methodology for dynamical systems and S. H. Lam and Goussis (1988) presented the use of CSP as a tool for understanding complex chemical kinetics. Following Sau H. Lam (2013), consider the initial value problem:

$$\begin{aligned} \frac{d\mathbf{y}}{dt} &= \mathbf{g}(\mathbf{y}; \epsilon) \\ \mathbf{y}(t = 0) &= \hat{\mathbf{y}} \end{aligned} \tag{30}$$

where $\mathbf{y}$ and $\mathbf{g}$ are N-dimensional column vectors, all components of $\mathbf{g}(\mathbf{y}; \epsilon)$ are algebraic functions of $\mathbf{y}$ and ϵ is a small dimensionless parameter which equation 30 is known to be stiff in this small limit.

When there are M linearly independent fast reactions in the reaction system, a fast subspace projection of $N \times N$ can be defined as

$$Q^{fast}(M) \equiv \sum_{m=1}^{M} \mathbf{a}_m \mathbf{b}^m \tag{31}$$

where $\mathbf{a}_m$ and $\mathbf{b}^m$ are linearly independent basis vector, which are, by definition, orthonormal,

$$\begin{aligned} \mathbf{b}^m \cdot \mathbf{a}_{m'} &= \delta_{m,m'} \\ m, m' &= 1, \ldots, M. \end{aligned} \tag{32}$$

CSP uses these definitions to write **g** as

$$\mathbf{g}(\mathbf{y};\epsilon) = \mathbf{g}^{fast}(\mathbf{y};\epsilon) + \mathbf{g}^{slow}(\mathbf{y};\epsilon), \tag{33a}$$

$$\mathbf{g}^{fast}(\mathbf{y};\epsilon) \equiv Q^{fast}(M)\cdot\mathbf{g}(\mathbf{y};\epsilon), \tag{33b}$$

$$\mathbf{g}^{slow}(\mathbf{y};\epsilon) = \mathbf{g}(\mathbf{y};\epsilon) - \mathbf{g}^{fast}(\mathbf{y};\epsilon). \tag{33c}$$

After the fast reactions are identified, the term $\mathbf{g}^{fast}(\mathbf{y};\epsilon)$ is expected to rapidly decay to $O(\epsilon)$, so it can be neglected. Therefore, the problem can be rewritten as

$$\frac{d\mathbf{y}}{dt} = \mathbf{g}^{slow}(\mathbf{y};\epsilon) + O(\epsilon) \tag{34}$$

For reduction purposes, CSP finds all fast modes that better describe the fast domain. After this, some fast species can be selected and described as QSS, reducing the stiffness of the system and thus, simplifying the model.

Table 2 presents some of the recent studies using CSP.

Table 2 – Some recent CSP studies.

Author	Method	Observations
Wu, Qiao and Huang (2013)	CSP	Automated CSP (I-CSP) Dimethyl ether: (55/290) to (26/20)
Wu, Qiao and Huang (2014)	CSP	AutomatedCSP (I-CSP) reduction algorithm.
Ciottoli et al. (2017)	CSP	Applied on a polybutadiene mechanism (561 species, 2538 reactions) generating reduced mechanism with less than 20 species.
Koniavitis, Rigopoulos and Jones (2017)	CSP	Reduced mechanism with (RCCE) using CSP.
Galassi et al. (2018)	CSP + TSR	Automated CSP framework. Does not requires target species.
Zhao and Lam (2019)	CSP	Review of Linear CSP and Non-linearCSP methods.
Si et al. (2021)	DRG + CSP + ANN	Reduction of GRI-MECH3.0 using DRG+CSP and optimization using ANN.

2.2.4 Element Flux Analysis - (EFA)

When analyzing kinetics mechanisms, the evaluation of how species are transformed is generally necessary. Another possibility is to evaluate the element flux between species, which is the maim purpose of the Element Flux Analysis (EFA).

Androulakis et al. (2004) presented the method of EFA as a mean to develop time-dependent flux diagrams to identify key reaction pathways with minimum effort.

The idea is to calculate the atomic fluxes for each atom (C, H, O, N, ...) at each time using reaction rates, obtaining the major source and sink for each element. The instantaneous chemical flux of atom *A* from species *j* to species *k* through reaction *i* is defined as

$$\dot{A}_{ijk} = q_i \frac{n_{A,j} n_{A,k}}{N_{A,i}} \tag{35}$$

where $n_{A,j}$ is the number of atoms A in species j and $N_{A,i}$ is the total number of element A in reaction i. Using this reaction, one can obtain the flux of any given atom A that flows from species to species. The total transfer of element for a pair of species as a function of time can be expressed as

$$\bar{A}_{FROM,TO}(t) = \sum_{i=1}^{N_R} A_{i,FROM,TO}(t) \tag{36}$$

As stated in equation 36, the atom flux is fixed for a given time t. For reduction purposes, one reduced mechanism can be obtained at each time and the global mechanism is the sum of all of them. For a more complete analysis, a time-integration can be performed, building a flux over all reaction trajectory. Androulakis et al. (2004) proposed a way of accounting for it,

$$\hat{A}_{FROM,TO} = \frac{\int_{t=0}^{\tau} \bar{A}_{FROM,TO}(t)dt}{\sum_{FROM'} \sum_{TO'} \int_{t=0}^{\tau} \bar{A}_{FROM',TO'}(t)dt} \tag{37}$$

And another normalization can be defined as

$$\hat{A}_{FROM,TO} = \frac{\int_{t=0}^{\tau} \bar{A}_{FROM,TO}(t)dt}{\max \int_{t=0}^{\tau} \bar{A}_{FROM',TO'}(t)dt} \tag{38}$$

This analysis can be used to identify key pathways in terms of source-sink relationships.

When using this method as a reduction mechanism tool, a table for each element is obtained which contains all source-sink pairs. An example by Androulakis et al. (2004) is presented in table 3. After sorting the element flux, the normalized value of equation 38, presented in the last column of the table, can be used as a measure of importance of the species. If a reduction is to be made, a threshold is set to include all pairs with at least 10% of the contribution. In this example, a reduced mechanism containing seven species is obtained.

For a complete reduced mechanism, the same approach must be made for every element in the detailed mechanism, and the reduced mechanism obtained encompasses all the species selected as important and all the reactions that include them.

Some studies using EFA as a reduction technique are summarized in table 4. Here, only studies using EFA as the main method are presented. Several other studies associate EFA with *on-the-fly* methods, or use EFA as a form of reaction pathway analysis.

As presented in the last section, there are several methods and strategies to simplify detailed kinetics mechanisms. These methods, however, only represent accurately the chemical kinetics under a certain range of experiments and conditions previously used to generated them. For a more general use, strategies based on the on-the-fly reduction were proposed. These approaches use the previous methods to generated a single reduced mechanism which is valid only at the current time or space coordinates. In this way, they provide a more accurate mechanism at each condition with the expense of solving the reduction problem at run-time clock.

Table 3 – Sample Interpretation of the Time-Integrated Element Flux Pointers. Adapted from Androulakis et al. (2004)

FROM	**TO**	$\hat{A}_{FROM,TO}$	**SUM**	**% of maximum** $\hat{A}_{FROM,TO}$
CH4	CH3	16.8	16.8	100.0
CO	CO2	16.8	33.6	100.0
HCO	CO	14.8	48.4	88.1
CH2O	HCO	14.2	62.6	84.5
CH3O	CH2O	12.2	74.8	72.6
CH3	CH3O	12.1	86.9	72.0
CH3	CH2O	1.9	88.8	11.4
C2H5	C2H4	1.1	90.0	6.8
CH3	C2H6	1.1	91.1	6.7
C2H6	C2H5	1.1	92.2	6.6
CH3	CH2(S)	1.0	93.2	6.0
CH2(S)	CO	0.9	94.1	5.5
C2H4	C2H3	0.6	94.7	3.4
CH3	CO	0.5	95.2	3.0
CH2CHO	CH2CO	0.5	95.7	2.8
HCCO	CO	0.4	96.1	2.5
CH2CO	HCCO	0.4	96.5	2.4
C2H3	CH2CHO	0.4	96.8	2.1
CH3	HCO	0.2	97.1	1.4
CH2O	CH4	0.2	97.3	1.4
C2H4	CH2CHO	0.2	97.5	1.2
CH3OH	CH2OH	0.1	97.6	0.8
CH3	CH3OH	0.1	97.7	0.6
C2H4	HCO	0.1	97.8	0.6
C2H4	CH3	0.1	97.9	0.6
CH2OH	CH2O	0.1	98.0	0.6
C2H3	HCO	0.1	98.1	0.5
C2H3	CH2O	0.1	98.2	0.5
CH3OH	CH3O	0.1	98.3	0.5
CH2	CO2	0.1	98.4	0.4
CH3	CH2	0.1	98.4	0.4
CH2	CO	0.1	98.5	0.4
CH2(S)	CH2	0.1	98.6	0.4

2.2.5 Dynamic Reduction

As presented before, the Dynamic Reduction or *on-the-fly* reduction scheme works by simplifying the chemical kinetics locally based on the local state of the mixture and an acceptable error metric.

The fuel oxidation in a zero-dimensional problem, such as a constant pressure reactor, results in a time evolution of the temperature and concentration of chemical species. At the start, few species, such as the fuel and the oxidizer, exist, the temperature is not too high, and the kinetics present low rates. As the elapsed time increases,

Table 4 – EFA reduction method studies.

Author	Method	Observations
Androulakis, Grenda and Bozzelli (2004)	EFA	Coupled EFA and automated mechanism generation to evaluate the method.
Perini et al. (2012)	EFA + GA	Reduction method coupling EFA with GA, comparing the results with and without GA.
Wang et al. (2013)	EFA + SA + CEMA + CSP	Tri-component surrogate mixture: (209/1673) to 34-species global reduced mechanism
Pachler et al. (2016)	EFA + SA	Reduced over 70% of a mechanism without significant errors
Gao, Yang and Sun (2016)	EFA	Uses EF to build a Element Graph and identifies Global pathways

other intermediary species appear, requiring a more complete chemical kinetics mechanism.

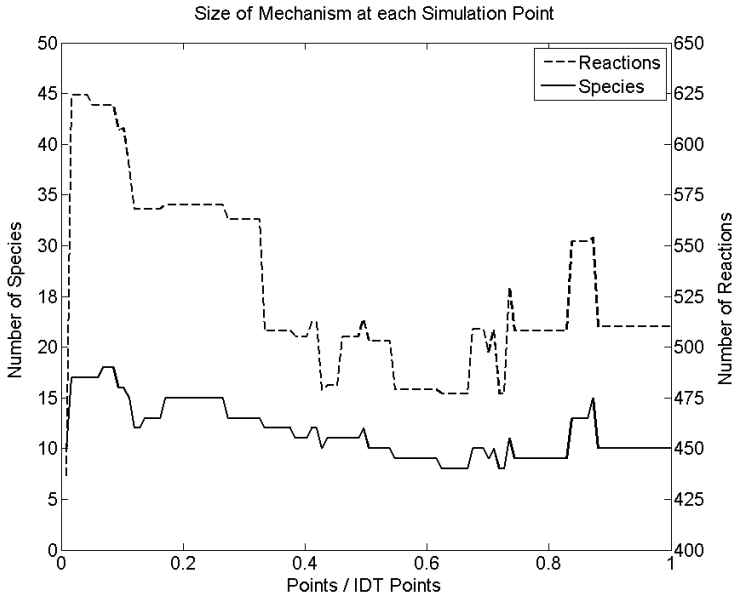

Figure 4 – Size of the minimum reduced mechanism at each timestep, calculated by DRG, for a constant pressure reactor ethanol-air oxidation, at 10 bar, 900 K, using Mittal's, 111 species, 710 reactions, detailed mechanism. **Source:** Augusto F. Pacheco (2016)

Therefore, in the start, a small mechanism would be enough to describe the fuel decomposition, but, as time passes, increasingly more complex mechanisms are needed. The application of the DRG reduction scheme at each time step in this problem allows to observe the minimum number of species and reactions to model the mass and energy rates within a prescribed threshold error. Figure 4 presents these results

for ethanol oxidation at 10 bar and 900 K, using Mittal's detailed chemical kinetics mechanism (PACHECO, Augusto F., 2016).

Augusto F. Pacheco (2016), using the same threshold that generated figure 4, obtained a reduced mechanism with 41 species and 240 reactions able to model the entire thermal ignition. From figure 4, we notice that the largest size needed to model the ignition locally is 18 species. However, the identity of the important species change along the ignition and that is why one needs more species to model the entire ignition problem. Therefore, the dynamic reduction aims at capturing this evolution and represent it optimally as time evolves.

The on-the-fly reduction are applies to local spacial conditions. L. Tosatto et al. (2011) used a *on-the-fly* reduction to solve a 2D axisymetric flame with different kinetic mechanisms. Figure 5 presents results of a steady-state combustion for three different fuels. The number of active species needed to locally model the chemical kinetics is also shown to vary from a maximum of 16 species for methane to a maximum of 222 species for JP-8.

From figure 5, the size of the mechanism required in pre and post-flame regions is much smaller than the full detailed mechanism. For instance, in figure (c), the majority of the cells require kinetic mechanisms with less than 50 % of the number of species of the detailed mechanism.

From these two examples, the more inhomogeneous the problem is, in terms of species concentrations or temperature, the greater is the potential for improving the time spent to simulate these problems. Since in almost all combustion flows there are large variations of local state properties, the dynamic reduction is very attractive in these applications. However, the method still needs the solution of a local reduction problem, the tabulation of the reduced kinetics mechanism, and the treatment of mass continuity, which will them present a computational time trade-off, depending on the size of the detailed chemical mechanism.

2.2.5.1 *in situ* Tabulation – (ISAT)

The *in situ* Tabulation (ISAT) is an algorithm intended to reuse solutions on computationally demanding problems, achieving this by storing results and using specif data pointers to retrieve them (CONTINO et al., 2011). When the local conditions during the simulation are within a given range, the ISAT just interpolates from the results already stored. As the simulation proceeds, more solutions are added to the table, improving the accuracy of further estimates.

S. B. Pope (1997) presented a very thorough description of the mathematical foundations of the ISAT method. The presentation in this section follows the works of Ren et al. (2014) and Contino et al. (2011).

As stated before, the purpose of ISAT is to tabulate a function $\mathbf{f}(\mathbf{x})$, where $\mathbf{f}$ and $\mathbf{x}$ are vectors with dimensions n_f and n_x respectively. Given a new vector $\mathbf{x}^q$, ISAT returns $\mathbf{f}^q(\mathbf{x}^q)$ as an approximation to $\mathbf{f}(\mathbf{x}^q)$ if possible. As the simulation advances, the table is built up accordingly to the received queries. These results are stored in a binary tree, where the entries, named leaf, are composed of the n^{th} leaf of its location, $\mathbf{x}^{(n)}$, the function value, $\mathbf{f}^n = \mathbf{f}(\mathbf{x}^{(n)})$ and the Jacobian matrix, $\mathbf{A}^{(n)}$, defined as

$$A_{ij} = \frac{\partial f_i}{\partial x_j}. \tag{39}$$

During the computation, given a new point $\mathbf{x}^q$, ISAT computes a linear approxi-

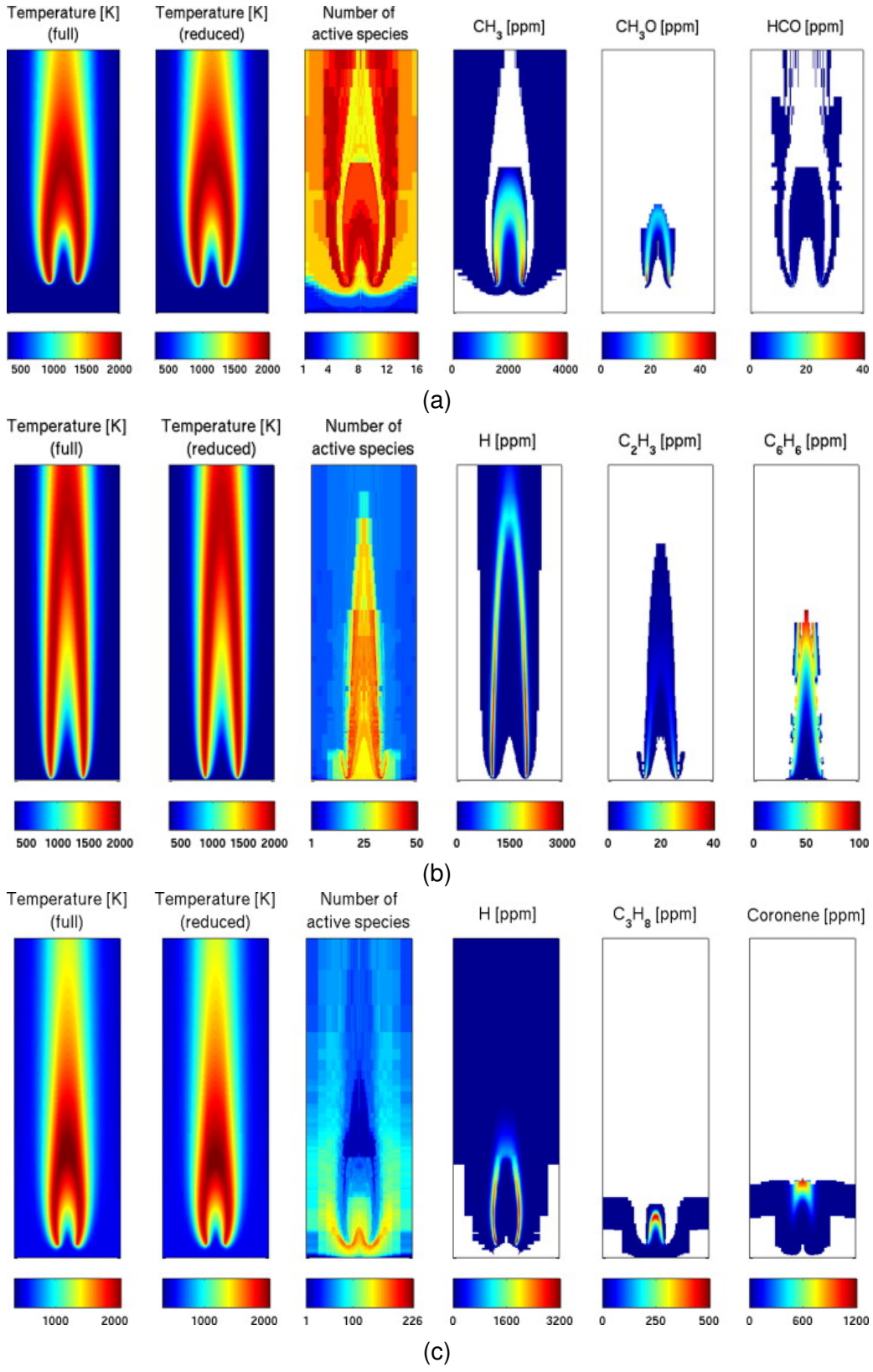

Figure 5 – Steady Flame for different fuels and kinetic mechanisms. (a) methane, 16 species; (b) ethylene, 50 species; and (c) JP-8, 222 species. **Source:** L. Tosatto et al. (2011)

mations of $\mathbf{f}(\mathbf{x}^q)$ on the n^{th} leaf as

$$\mathbf{f}(\mathbf{x}^q) \approx \mathbf{f}^l(\mathbf{x}^q) = \mathbf{f}^{l,n} = \mathbf{f}^n + \mathbf{A}^{(n)}(\mathbf{x}^q - \mathbf{x}^n) \tag{40}$$

The linear approximation defined by equation 40 is valid only in the Region of Accuracy (ROA) which is the connected region containing $\mathbf{x}^n$ and $\mathbf{x}^q$, according to the local error,

$$\epsilon^{(n)}(\mathbf{x}^q) = ||\mathbf{f}^{l,n}(\mathbf{x}^q) - \mathbf{f}(\mathbf{x}^q)|| \leqslant \epsilon_{ISAT} \tag{41}$$

where ϵ_{ISAT} is a user defined limit.

The ISAT, therefore, returns a linear approximation with a local error smaller than an user defined threshold. As stated above, the ROA is the region of solution where the method can ensure equation 41. But, in general, the ROA is computed using a conservative hyper-ellipsoid called Ellipsoid of Accuracy (EOA),

$$EOA \equiv (\mathbf{x}^q - \mathbf{x}^n)^T \widetilde{\mathbf{A}}^T \mathbf{B}^T \mathbf{B} \widetilde{\mathbf{A}} (\mathbf{x}^q - \mathbf{x}^n) \leqslant \epsilon_{ISAT}^2 \tag{42}$$

where $\widetilde{\mathbf{A}}$ is the modified matrix $\mathbf{A}$ and $\mathbf{B}$ is an optional scaling matrix.

Contino et al. (2011) implemented a modified equation to evaluate the EOA,

$$EOA \equiv (\mathbf{x}^q - \mathbf{x}^n)^T \mathbf{L}\mathbf{L}^T (\mathbf{x}^q - \mathbf{x}^n) \leqslant 1 \tag{43}$$

where $\mathbf{L}$ is the Cholesky factorization of $\widetilde{\mathbf{A}}\mathbf{B}^T\mathbf{B}\widetilde{\mathbf{A}}/\epsilon_{ISAT}^2$. This formulation is more efficient to check if a point lies in the EOA by evaluating $||\mathbf{L}^T(\mathbf{x}^q - \mathbf{x}^n)|| \leqslant 1$.

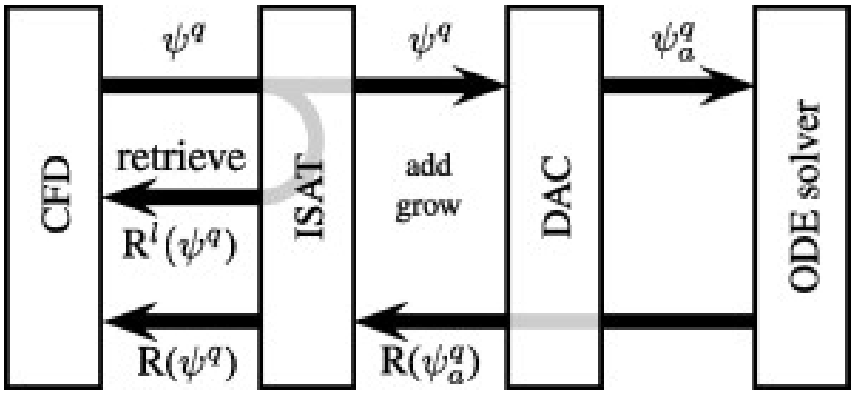

Figure 6 – TDAC method - Combination of ISAT with DAC techniques. **Source:** Contino et al. (2011)

During a simulation using ISAT, for each query $\mathbf{x}^q$, one of the following operations is performed:

1. Retrieval: If the query point is within the EOA of $\mathbf{x}$, the linear approximation to $\mathbf{f}(\mathbf{x}^q)$ based on that leaf is returned.

2. Growth: If a retrieval attempts failed, $\mathbf{f}(\mathbf{x}^q)$ is directly evaluated and returned. Some leaves close to $\mathbf{f}(\mathbf{x}^q)$ are selected and the error (equation 41) is evaluated and if it is less than ϵ_{ISAT}, the leaf's EOA is grown to cover $\mathbf{x}^q$).

3. Addition: If no grown can be performed to achieve an error smaller than ϵ_{ISAT}, a new leaf associated with x^q is add to the ISAT table.

As only one of the operation calls the ODE solver, the speed up of ISAT is directly related to the number of growth operations to the retrieve ones.

One of the limitations of the algorithm is the fact that the table can grown to huge sizes if left without control, methods to maintain it at a practical size are required.

Although ISAT, as its core, is an *on-the-fly* method, it its already used in combination to others reduction techniques to further improve its applicability. The main idea in this hybrid strategies is to first try to retrieve a solution for the problem. If it is possible, the ISAT runs as intended. If it is not possible and a solution is required, a reduction algorithm is called and used to reduce the number of active species for the ODE solver, reducing the computational time spent on the growth operation. Figure 6 represents the workflow for these approaches. Variable ψ represents the $\mathbf{x}$ and R the $\mathbf{f}$.

Table 5 presents a list of studies based on the application of ISAT with others reduction techniques and/or at different problems and models. The list is not exhaustive, but includes representative studies for each approach.

2.2.5.2 DRG related methods

As stated on previous chapters, the use of reduction techniques in *on-the-fly* schemes is a promising way to reduce the computational time of reactive flow simulations, mainly on multidimensional problems.

For that, a compromise between the time spent in the reducing technique and the time saved while using the reduced mechanism is a must. Therefore, reducing methodologies that are proven to be computationally inexpensive are fitted to this task. In this scheme, the DRG related methods are great candidates.

Despite the peculiarities associated to *on-the-fly* methodologies, the implementation of DRG related methods are much the same as for static methods. The difference is that the reduced mechanism obtained at each time step or spacial location are promptly used to solve the local problem.

In zero-dimensional problems, with only time variation, the implementation resumes generally in applying the selected DRG method at the current elapsed time. The species targeted as unimportant are, in the simplest way, treated as inert while the solver integrates the remaining, advancing the timestep. In the new time, the reaction rates are re-evaluated for all the species, and a new set of inert species are chosen.

Another approach to treat the unimportant species is used by L. Tosatto et al. (2011), in which the species set as unimportant have their mass fraction set to zero and all their reactions are deactivated. To deal with the removal of mass from the system, some adaptations are used for the mass fraction. As the models used are multidimensional, L. Tosatto et al. (2011) also included a transport term to the evaluation of the DRG importance index. In this approach, species that are heavily transported from neighboring regions also become important species.

As the number of dimensions grows, the number of cells to solve reactive flows increase. With this in mind, strategies called Correlated Dynamic Adaptive Chemistry (CO-DAC) were created. Weiqi Sun et al. (2015) and Weiqi Sun and Ju (2017) present studies on the implementation of this method. The basis is that several times, the conditions in neighbors are too similar to those at a point where a reduced mechanism already represents the local state. In this way, during the simulation, sub zones with similar conditions share the same reduced mechanism, decreasing the number of *on-the-fly* reductions needed. This is also applied to temporal domains.

Table 5 – ISAT studies

Author	**Observations**
Pope, S. (1997)	ISAT
Saxena and Pope (1999)	ISAT in JPDF
Mazumder (2005)	ISAT with Surface Reactions
Gordon et al. (2007)	ISAT in PDF
Contino et al. (2011)	ISAT+DRG
Hiremath, Ren and Pope (2011)	ISAT+RCCE+GALI
Pang, Ng and Gan (2012)	ISAT+Parallel Processing
Hiremath et al. (2012)	ISAT+Parallel Processing in LES/PDF
Ren et al. (2013)	ISAT in EDC and PDF
Cui et al. (2013)	ISAT in EDC models
Hiremath et al. (2013)	ISAT+RCCE+Parallel Processing in LES/PDF
Ren et al. (2014)	ISAT+DRG
Emami et al. (2015)	ISAT inLES/ATF
Zhou and Wei (2016)	ISAT+DRG
Adhikari, Sayre and Chandy (2017)	ISAT
Li et al. (2018)	TDAC (ISAT + DAC – DRG, DRGEP, PFA, EFA)
An et al. (2019)	ISAT (DAC with tabulated reduced mechanisms)
Kamma and Suvanjumrat (2021)	TDAC (ISAT + DAC – DRG, DRGEP, PFA, EFA)

Two other points on the applicability of the DRG related methods are: (1) how to select the initial important species and, (2) How to select the threshold used.

For the first point, due to the generally inhomogeneous nature of the combustion problems, one can find that a given target can be very effective in a fuel rich zone, while being much less important on far away zones. Curtis et al. (2015) presented an alternative to this, called Relative Importance Index (RII) to automatically select the target species at each point. The methodology takes into account the fact that some intermediate species present a larger number of other interacting species, which

tends to make its importance index to be too low to be included in the mechanism. By asserting this, a RII rank can be constructed and the target species picked from it. The main contribution of this approach is to obtain local reduced mechanisms with higher quality and therefore a more accurate *on-the-fly* solution. A more in-depth definition is provided by the authors, as well as an example of the method.

For the second point, there are still not many studies on automating the selection of the user threshold. Generally, more knowledge about both the system and the detailed mechanism used is necessary. Most studies compare the use of different values of threshold, and their magnitude is highly dependent on the size of the detailed mechanism used and the desired accuracy.

Table 6 presents a list of studies of *on-the-fly* reduction techniques using DRG related methods.

Table 6 – DAC with DRG related methods.

Author	**Method**	**Observations**
Liang, Stevens and Farrell (2009)	DRGEP	HCCI with a speed-up factor of more than 30.
Tosatto, Bennett and Smooke (2011)	flux-based DRG	2D Flames, with a speed-up factor of almost 20.
Gou et al. (2013)	Error Controled + PFA	0D Auto Ignition and Unsteady Flame Propagation
Viggiano and Magi (2014)	DRGEP	Single zone HCCI and multidimensional HCCI.
Sun et al. (2015)	Correlated + PFA + HMTS	0D Auto Ignition and 1D Flame Propagation, comparing the time spent calculating each term.
Curtis, Niemeyer and Sung (2015)	RII + DRGEP	Automated Selection of Target Species.
Sun and Ju (2017)	Correlate + PFA + HMTS	Spherical Premixed Flames and 1D diffusion Flames, improvements of two orders of magnitude for computational efficiency.

2.2.5.3 EFA based methods

EFA was modified to be applied in dynamic reduction in the same way that the DRG method was. EFA is used to calculate a local element flux, at a given time and spatial position, and this analysis is used to support a local reduction. The overall *on-the-fly* algorithm is similar as that used for DRG. Table 7 presents a list of studies using EFA in *on-the-fly* schemes.

Table 7 – EFA based studies

Author	Method	Observations
He et al. (2010a)	EFA	PFR and PMSR*
He, Ierapetritou and Androulakis (2010)	EFA	HCCI multidimensional model with a speed up of almost 20.
He, Ierapetritou and Androulakis (2011)	EFA	HCCI multidimensional model with a new method of computing the source term.
Zhang et al. (2012)	EFA	PFR and HCCI implementations
Zhang, Androulakis and Ierapetritou (2013)	EFA + QSS	PFR and 2D HCCI model with QSS and EFA being used.
Zhang et al (2014)	EFA + Automated Mechanism Generation	PFR Generates at each time step a new detailed mechanism and than uses EFA for reduction and simulation.

2.3 VIRTUAL CHEMISTRY

Virtual chemistry takes on a different path when compared to all the previous methods. All the previous methods, except ISAT, simplify the detailed mechanism by removing unnecessary reactions and species. They all suffer from a fundamental limitation which is the minimum structure needed to model the production rates of the important chemical species. Laminar flames far from extinction are strongly controlled by thermodynamics and transport. Thermal ignition, however, is strongly determined by chemical kinetics, mainly the reaction paths for propagation and ramification. This produces a limitation to the minimal size needed for a reduced mechanism and therefore, limits the applicability of a given reduced mechanism. Figure 7 presents how the virtual and reduced mechanisms are related to the detailed mechanism regarding their development. Contrary to the reduced mechanisms, virtual mechanisms are built bottom-up.

The virtual chemistry aims to avoid the limitations of the reduced models. They are built from scratch to reproduce the main outcome of a detailed chemistry in a given combustion problem. Therefore they are not bound by the intrinsic requirements of reproducing specific reaction paths as are the reduced models, and as a consequence, they can be much smaller than reduced mechanisms. To accomplish this, virtual mechanisms requires two major steps: the first is dedicated to optimize the properties of virtual species to match the mixture thermodynamic properties. The second optimizes the kinetic parameters aiming at reproducing a desired combustion characteristic, such as flame speed, ignition delay time, and pollutant formation. The combination of targets is, in principle, limitless and, although the behavior calculated with the detailed mechanism is usually the model to emulate, measurements could be used to further improve the quality of the virtual model. In this section, only general aspects of virtual mechanisms will be presented. The details will be left to the chapter on methodology.

Cailler et al. (2017) presents one of the first uses of virtual chemistry in the

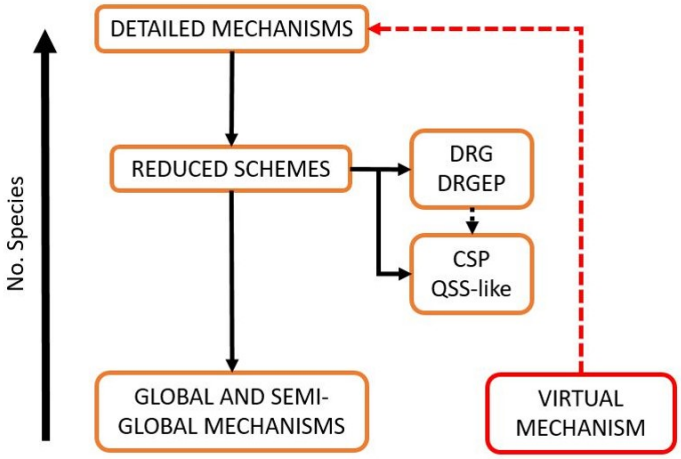

Figure 7 – Relation among virtual, reduced, and detailed mechanisms.

place of commonly reduced methodologies. The authors introduce the virtual species, optimize the thermodynamic properties using NASA polynomials, and the mixture transport properties. Their method calculates a virtual mechanism at each desired condition. Then, a correction function *f* is developed to interpolate among the tabulated solutions for that condition of interest during the simulation.

Their method was used to simulate a methane-air laminar premixed flame using the GRI-MECH3.0 as detailed chemistry. The authors produced figure 8 which compares the laminar flame speed obtained with the detailed chemistry (black lines), a semi global mechanism (green squares), and two virtual structures, one reaction as blue dots and two reactions as red triangles. The virtual mechanisms presented results with no distinction from the detailed mechanism.

The virtual mechanisms were further tested for diffusion flames. The results obtained by the authors present a better accuracy than the semi-global results, but not as close as the predictions of laminar flame speeds. The absence of diffusion flames in the optimization phase of the virtual chemistry was the most probable cause of the discrepancy.

Maio et al. (2019) introduced the concept of satellite mechanisms, where additional targets and functionalities are built and optimized using a virtual scheme. Thermodynamic properties were optimized using equilibrium temperatures under adiabatic and non-adiabatic conditions. The virtual mechanisms obtained under those hypothesis present correction factors to allow simulations of a wide range of problems. The CO prediction was obtained using a satellite mechanism.

The virtual schemes were tested against 1D laminar premixed flames submitted to radiative heat losses. Figure 9 presents the prediction of laminar flame speed with the proposed models. The non-adiabatic procedure was able to represent the detailed chemistry with a great accuracy.

The virtual models were then used in a Large Edgy Simulation (LES) of a non-adiabatic turbulent premixed flame. The non-adiabatic mechanisms produced better results for CO prediction than the adiabatic mechanism, although the prediction overestimates the peak CO. A solution to mitigate this effect was to include strain effects as strained flamelets to the optimization.

A more comprehensive study is presented by Cailler et al. (2020). In this study,

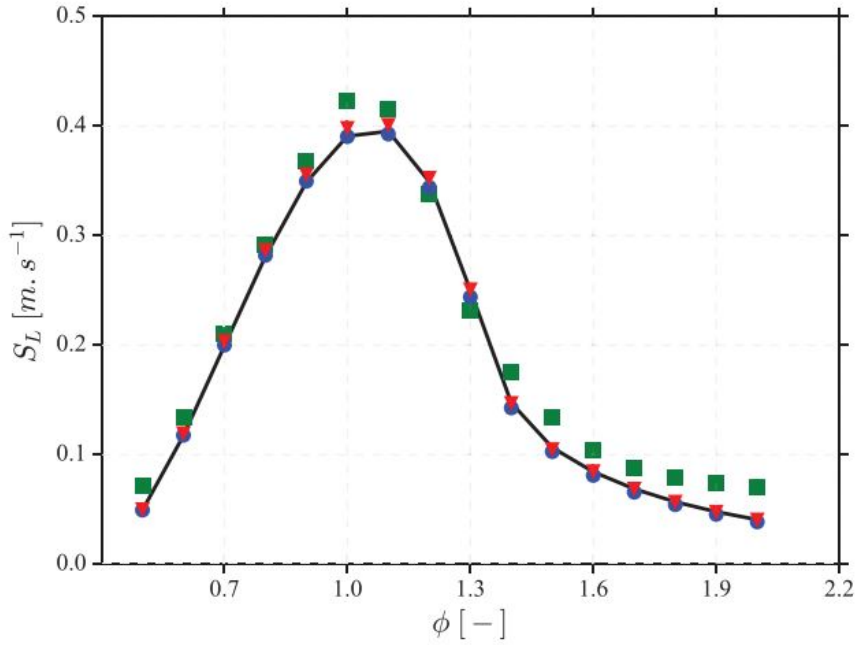

Figure 8 – Laminar Flame Speed versus equivalence ratio for a premixed methane/air flame at 300K and pressure of 1 atm. **Source:** Cailler et al. (2017)

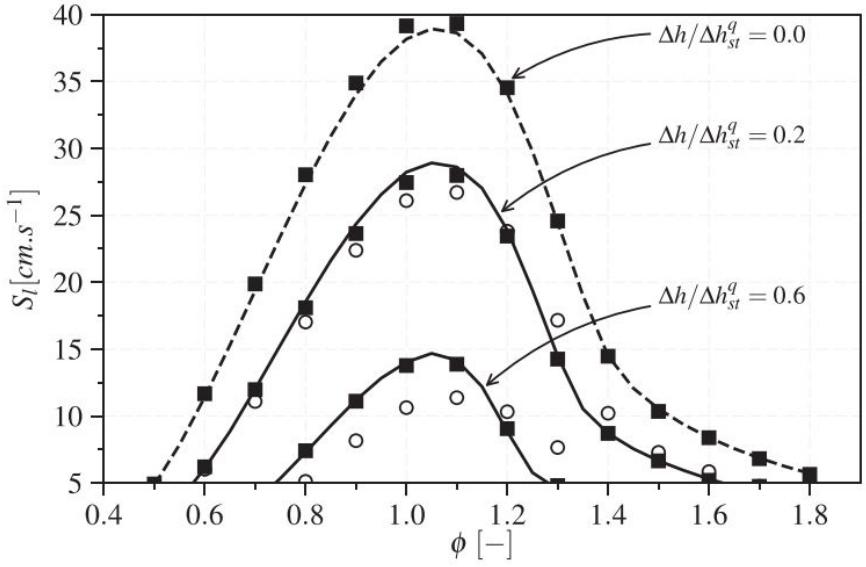

Figure 9 – Laminar Flame Speed for different configurations using: detailed chemistry (Lines); non-adiabatic virtual mechanism (squares) and adiabatic virtual mechanism (circles). **Source:** Maio et al. (2019)

the authors further provided details on the implementation of the optimization of thermodynamic and transport properties. Figure 10 presents the authors's diagram of the optimization procedure. The implemented work flow starts with the optimization of thermodynamic properties followed by the kinetic parameters. This part of the problem targets the temperature and transport properties of the virtual scheme. The satellite

mechanism is built after the solution of the flame problem, starting in the third and fourth step. The sub-mechanisms used for prediction of the concentration of small species are energetically neutral and the transport aspects are copied from the main virtual mechanism to reduce computational cost.

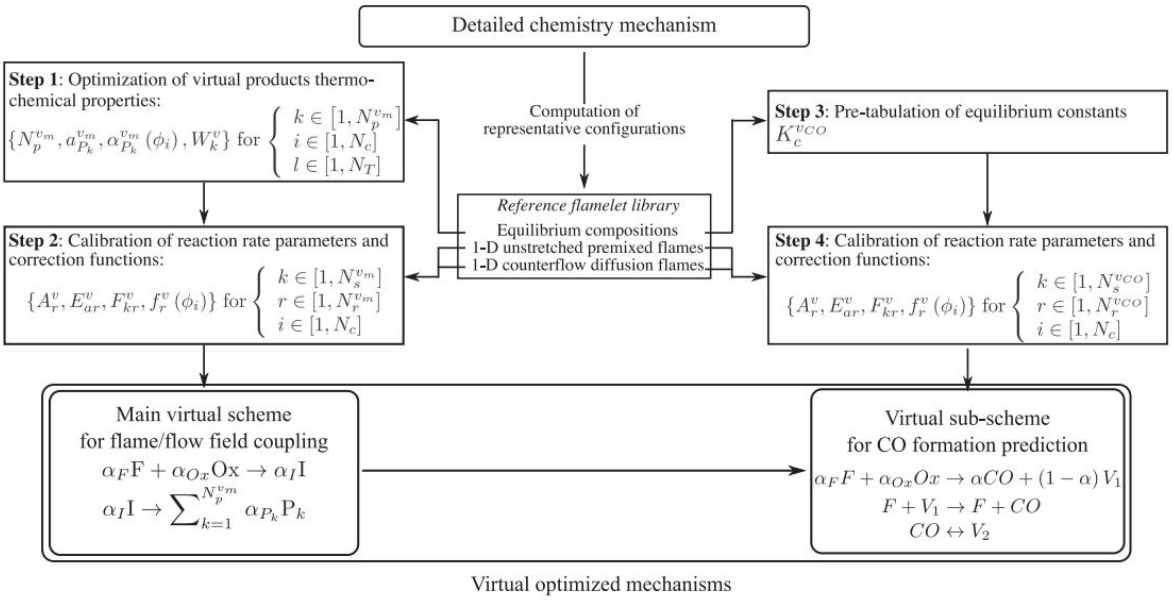

Figure 10 – Virtual optimization procedure. **Source:** Cailler et al. (2020)

The methodology was further validated against methane-ar non-premixed counterflow laminar flames, unstretched laminar premixed flames, and counter-flow diffusion flames. A comparison among virtual mechanism, analytic schemes, tabulated chemistry, and detailed mechanism was performed. The virtual mechanisms were able to reproduce the results within a computational time comparable to the time spent using semi-global schemes. A second validation used a 2D laminar partially-premixed burner. In this example, the analytically-reduced chemistry and the virtual chemistry approach recovered well the detailed solution.

Additional studies on virtual chemistry for heavy fuels were performed to assess the capabilities of the virtual methodologies. Figure 11 shows that the virtual chemistry methodology is not exclusive for lighter fuels such as methane, which was used in previous works.

As it stands, virtual chemistry is a promising methodology for reproducing detailed chemistry in CPU constraining problems, such as LES simulation of combustion problems. Additionally, the flexibility provided by the methodology ensures that critical targets can be modeled without modifying or requiring a re optimization of a virtual mechanism, but instead they can be added and removed from a base mechanism as the current problem requires. Additionally, as the scope of this method is not constrained by the target, there are many opportunities for addressing different objectives, such as the simulation of phenomena not included in the optimization step, or creating mechanisms for other combustion characteristics, such as ignition delay time.

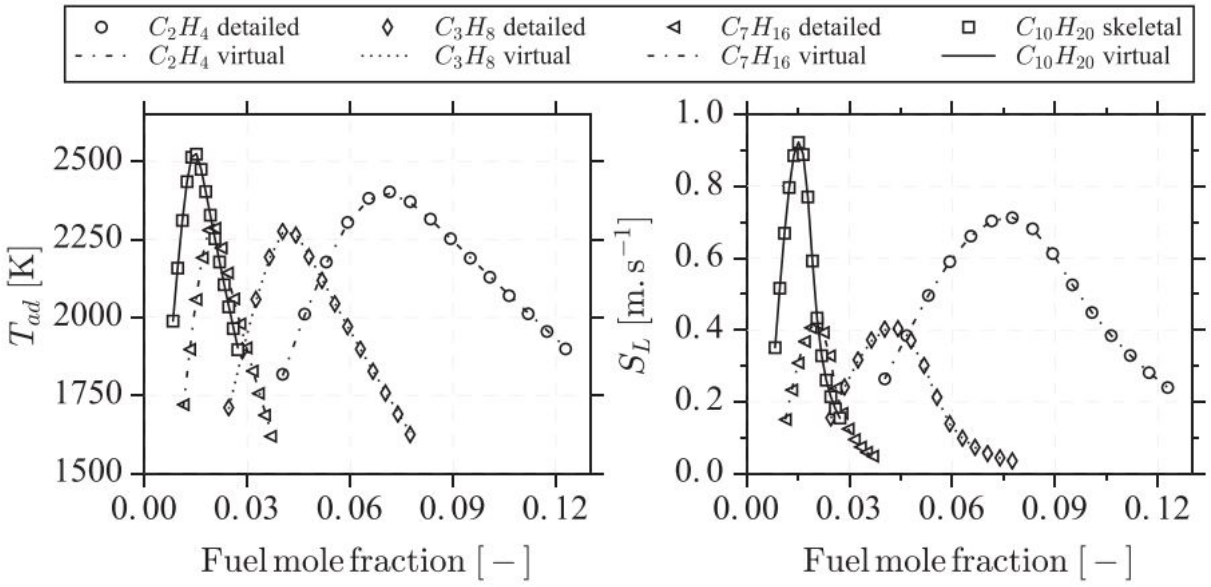

Figure 11 – Adiabatic Temperature and Laminar Flame Speed for hydrocarbon+air mixtures. **Source:** Cailler et al. (2020)

3 METHODOLOGY

3.1 VIRTUAL CHEMISTRY OPTIMIZATION

This thesis is an extension of the works of (CAILLER et al., 2017), (MAIO et al., 2019), and (CAILLER et al., 2020). Those works targeted laminar flame speed as the base problem, while the main target for the current work is to represent the transient thermal ignition. The Virtual Chemistry requires the optimization of two major parts of the kinetic mechanism. The first is related to the virtual species and mixture thermodynamics properties, while the second is related to the target objectives of the virtual mechanism. In this work, the thermodynamic optimization follows almost the same methods of the previous works, with only some minor adjustments. The kinetics part of the optimization is, however, modified to account for specific requirements and these differences are explained in the corresponding section.

The next sections cover the basic steps for obtaining a virtual chemistry, summarized as follows:

1. Mechanism Structures: Describes how the virtual mechanisms were built, going from the simple one global reaction to more complex structures;
2. Thermodynamic Properties Optimization: Presents the math used to obtain the thermodynamics properties, as well some specific issues related to the optimization;
3. Reaction Parameter Optimization: Describes how the optimization was set-up to obtain the reaction parameters as well as how the fitness function modeling.

3.1.1 Mechanism Structures

In this work, the base mechanisms were defined in an *ad-hoc* manner. The basic guidance is to start from the simplest possible structures and increase their complexity as needed.

The first is a global reaction, labeled as "One RXN", presented in eq. 44,

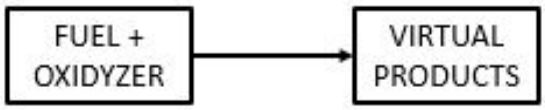

Figure 12 – One RXN model.

$$c_f[fuel] + c_o[oxidant] \rightarrow \sum_{v=1}^{n_{virtual}} c_v[virtual]_v \tag{44}$$

where c_i represents the stoichiometric coefficient of species i, with the underscripts f, o, and v representing the fuel, oxidant and the virtual species, respectively, and graphically represented in figure 12.

A second and slightly more complex model is a mechanism composed by two reactions and one additional intermediary virtual species, as presented in eq. 45 and

figure 45. These models are labeled "One INTER" models. The first reaction comprehends the consumption of fuel and oxidizer to produce an additional virtual species, named Intermediary Species and represented by the letter *I*. This species is used as an additional control parameter to better model the radical pool effect existing in the thermal autoignition. The second reaction is therefore the consumption path for the Intermediary, leading to the production of the $n_{virtual}$ species.

Figure 13 – One INTER model.

$$c_f[fuel] + c_o[oxidant] \rightarrow c_I[I] \tag{45a}$$

$$c_I[I] \rightarrow \sum_{v=1}^{n_{virtual}} c_v[virtual]_v \tag{45b}$$

A still more complex mechanism is built by duplicating the former model using two distinct intermediaries. Such mechanism is used to better model the radical pool effect. This model is labeled "Two INTER". Its graphical representation is in figure 14 and a more formal description is presented in equation 46.

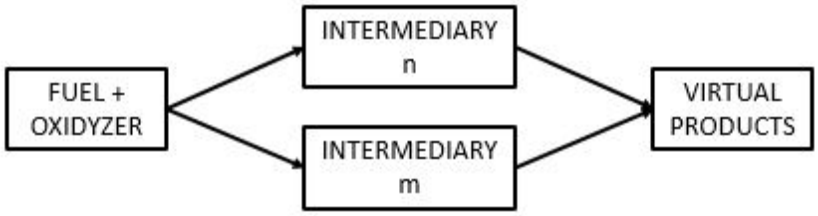

Figure 14 – Two INTER model.

$$c_f[fuel] + c_o[oxidant] \rightarrow c_{I_1}[I_1] \tag{46a}$$

$$c_{I_1}[I_1] \rightarrow \sum_{v=1}^{n_{virtual}} c_v[virtual]_v \tag{46b}$$

$$c_f[fuel] + c_o[oxidant] \rightarrow c_{I_2}[I_2] \tag{46c}$$

$$c_{I_2}[I_2] \rightarrow \sum_{v=1}^{n_{virtual}} c_v[virtual]_v \tag{46d}$$

Additionally, as stated by several authors, some reactions rates are too complex to be model only with on Arrhenius equation and therefore may encompass duplicate reactions to better approximate their temperature dependency. The same is valid for virtual schemes and the act of duplicating reactions extended to the whole model and it is labeled here as combined models.

3.1.2 Thermodynamic Properties Optimization

The methodology used to obtain the proper thermodynamics parameters was based on the works of (CAILLER et al., 2017), (MAIO et al., 2019) and (CAILLER et al., 2020). In the following deductions, the authors will not be constantly cited in order to improve the reading flow of the equations.

As stated, the virtual chemistry at first must be able to reproduce the thermodynamics properties of the mixture, i.e constant pressure specific heat function, c_p, and the mixture molar weight. The first is usually implemented in the form of NASA7 polynomials (Eq. 47 and 48). Therefore, each virtual species in the mechanism requires six coefficients for the NASA7 polynomial with the addition of one stoichiometric coefficient for every equilibrium condition used.

$$\frac{c_p}{R} = a_1 + a_2 T + a_3 T^2 + a_4 T^3 + a_5 T^4 \tag{47}$$

$$\frac{h}{RT} = a_1 + \frac{a_2}{2} T + \frac{a_3}{3} T^2 + \frac{a_4}{4} T^3 + \frac{a_5}{5} T^4 + \frac{a_6}{T}. \tag{48}$$

Moreover, each species requires the definition of a molar weight (*MW*), demanding 7 parameters for each virtual species to be defined. For the thermodynamic part, the fitness function must therefore be able to represent those parameters and was defined as:

$$\epsilon_{thermo} = \sum_{i=1}^{N_c} \left(\Psi^{eq}_{det}(T, P, \phi)_i - \Psi^{eq}_{vir}(T, P, \phi)_i \right) \tag{49}$$

where N_c is the number of conditions used, $\Psi^{eq}_{det}(T, P, \phi)_i$ represents the current detailed parameter being optimized, being the equilibrium temperature or the molar weight for the condition i, and $\Psi^{eq}_{vir}(T, P, \phi)_i$ is the virtual counterpart. From here, the under script i will represent the $(T, P, \phi)_i$ in order to help the visualization. The Ψ function for the enthalpy is represented as

$$\Psi^{eq}_i = \sum_{s=1}^{N_s} Y_{i,s} h_{i,s} \tag{50}$$

If all the thermodynamics of the detailed mechanism used the NASA7 coefficients formula, we can rewrite the above equation as

$$\Psi^{eq}_i = \sum_{s=1}^{N_s} Y_{i,s} a^{det}_{1,s} + \frac{T_i}{2} \sum_{s=1}^{N_s} Y_{i,s} a^{det}_{2,s} + \cdots + \frac{T_i^4}{5} \sum_{s=1}^{N_s} Y_{i,s} a^{det}_{5,s} + \frac{1}{T_i} \sum_{s=1}^{N_s} Y_{i,s} a^{det}_{6,s} \tag{51}$$

where $a^{det}_{n,s}$ is the n^{th} NASA coefficient for the detailed species s.

For the detailed part, all the values are known and thus, this equation become the target for the optimization and takes the form of

$$\epsilon_{thermo} = \sum_{i=1}^{N_c} \left(\Psi^{eq}_i|_{det} - \Psi^{eq}_i|_{vir} \right) \tag{52}$$

We can expand the $\Psi^{eq}_{vir,i}$ as equation 53 (the *i* is suppressed to help the viewer). As the final target is to present the same behavior of the detailed mechanism, therefore some virtual species are modeled based on real ones (such as the fuel, oxidizer and diluent).

$$\Psi^{eq}_{vir} = \underbrace{Y^{det}_F \Psi_F + Y^{det}_O \Psi_O + Y^{det}_D \Psi_D}_{A} + Y^{det}_P \underbrace{\left(c_1 \Psi_{V_1} + \cdots + c_{N_s} \Psi_{V_{Ns}} \right)}_{Virtual} \tag{53}$$

$$Y^{det}_F + Y^{det}_O + Y^{det}_D + Y^{det}_P = 1 \tag{54}$$

Where *P* represent all the detailed species except the species on the group *A* (fuel *F*, oxidizer *O* and diluent *D*). The V_k is used to represent the virtual species *k*. The c_k is the virtual stoichiometric coefficients and by definition is written as

$$\sum_{k=1}^{N_{vir}} c_k = 1. \tag{55}$$

The species modeled based on real ones present the same set of NASA coefficients, and at initial and equilibrium conditions are expected to present the same molar fraction as the real ones. With that in mind, we can simplify the optimization by removing such contribution from the equation as

$$\epsilon_{thermo} = \sum_{i=1}^{N_c} \left(\Psi^{eq}_i|^*_{det} - \Psi^{eq}_i|^*_{vir} \right) \tag{56}$$

$$\Psi^{eq}_i|^*_{det} = \Psi^{eq}_i|_{det} - \Psi^{eq}_i|_{det,A} \tag{57}$$

where *A* represent the group of common species between the mechanisms. The virtual part can be formulated by assuming that the virtual species must match the properties of the detailed species not contained in *A*, obtaining the following equation.

$$\Psi^{eq}_i|^*_{vir} = Y^{det}_{i,P} \sum_{k=1}^{N_{vir}} c_{i,k} \Psi_{i,k} \tag{58}$$

where $Y^{det}_{i,P}$ is the sum of all the *P* detailed species molar fractions, $c_{i,k}$ is a stoichiometric coefficient for species *k* at condition *i* and $\Psi_{i,k}$ is the calculated properties for virtual species *k* at condition *i*.

Equation 56 when fully developed requires the optimization of all the virtual NASA coefficients with the stoichiometric values for each one at every condition *i* used, which can lead to very unfeasible problems. In the best case, the fitness value should be zero, indicating that the virtual scheme has exactly the same properties as the detailed one. Using this consideration, we can rewrite eq. 56 as

$$\Psi^{eq}_i|^*_{det} = Y^{det}_{i,P} \sum_{k=1}^{N_{vir}} c_{i,k} \Psi_{i,k}. \tag{59}$$

By expanding the Ψ functions in the form of eq. 51, we obtain

$$B_{1,P}^{det} + \frac{T}{2}B_{2,P}^{det} + \cdots + \frac{T^4}{5}B_{5,P}^{det} + \frac{1}{T}B_{6,P}^{det} = B_1^{vir} + \frac{T}{2}B_2^{vir} + \cdots + \frac{T^4}{5}B_5^{vir} + \frac{1}{T}B_6^{vir} \tag{60}$$

$$B_{n,P}^{det} = \sum_{s}^{N_P} Y_s^{det} a_{n,s}^{det} \tag{61}$$

$$B_n^{vir} = Y_P^{det} \sum_{k}^{N_{vir}} c_k a_{n,k}^{vir} \tag{62}$$

which is valid over all conditions i. By comparing and matching the coefficients with the same Temperature order for a given condition we can further work in eq. 60:

$$\begin{cases} Y_P^{det} \sum_{k}^{N_{vir}} c_k a_{1,k}^{vir} = B_{1,P}^{det} & \text{(63a)} \\ \cdots & \\ Y_P^{det} \sum_{k}^{N_{vir}} c_k a_{m,k}^{vir} = B_{m,P}^{det} & \text{(63b)} \end{cases}$$

where m represent the number of NASA parameters in the optimization. If we add the additional consideration of equation 55 of the virtual stoichiometric c_k sum, we can rewrite the above system of equations as

$$\begin{cases} \sum_{k=1}^{N_{vir}-1} a_{1,k}^{vir} c_k + a_{1,N_{vir}}^{vir} \left(1 - \sum_{k=1}^{N_{vir}-1} c_k\right) = \frac{B_{1,P}^{det}}{Y_P^{det}} & \text{(64a)} \\ \cdots & \\ \sum_{k=1}^{N_{vir}-1} a_{m,k}^{vir} c_k + a_{m,N_{vir}}^{vir} \left(1 - \sum_{k=1}^{N_{vir}-1} c_k\right) = \frac{B_{m,P}^{det}}{Y_P^{det}} & \text{(64b)} \end{cases}$$

In the system of equations above, all the right side variables are known as they are obtained from the detailed mechanism. In the left hand side, two sets of unknowns are present, the thermodynamic coefficients $a_{m,k}^{vir}$ of the virtual species and the virtual stoichiometric coefficients c_k, which the last one may be distinct for each initial condition.

If $m = N_{vir} - 1$, the current system present $N_{vir} - 1$ equations and by setting c_k as unknown variables and with a given set of $m \times N_{vir}$ thermodynamics parameter $a_{m,k}^{vir}$, this system can be solved and the c_k coefficients can be calculated for each condition i. Therefore, with a $m \times N_{vir}$ guess of $a_{m,k}^{vir}$, we can obtain the correspondent c_k.

With this im mind, the thermodynamic optimization is divided into two parts. The first one requires the solution of the system of equations represented in Eqs. 64, by optimizing the $m \times N_{vir}$ initial thermodynamics coefficients. By entering a candidate of

coefficients in the equations 64, one can obtain all the corresponding c_k. To validate the set of thermodynamics used, the fitness evaluation change the focus to analyze if the c_k obtained are valid, for that, the following equations are therefore used.

$$\epsilon_{thermo,1} = \sum_{i=1}^{N_c} \sum_{k=1}^{N_{vir}} v_{i,k} \tag{65}$$

$$v_{i,k} = \begin{cases} 0 & \text{if } 0 < c_{i,k} < 1 \\ 1 & \text{otherwise} \end{cases} \tag{66}$$

for every c_k obtained, is checked if it falls inside the interval proposed by equation 66, if it is a valid value, nothing is added to the fitness function, otherwise, one is added. The optimization stops as soon as $\epsilon_{thermo,1}$ reaches zero, meaning that all the calculated c_k are valid.

The second part targets the $N_{vir} - m$ parameters left, using the previous calculated stoichiometric values c_k for every condition following equation

$$\epsilon_{thermo,2} = \sum_{i=1}^{N_c} \sum_{l=m}^{N_{thermo}} \left(B_{i,l}^{vir} - B_{i,l,P}^{det} \right) \tag{67}$$

The target of the second part focus on better predicting the adiabatic temperature, by calculating the corresponding one for the full set of thermodynamics.

Finally the molar weight optimization takes place, equation 49 is used, with the Ψ function being the mixture molar weight and the previous c_k as the stoichiometric coefficients.

3.1.3 Kinetic Optimization

As for the kinetic optimization, the methodology is divided into Intermediary modeling, Reactions parameter selection, Penalties and finally the fitness evaluation per se.

3.1.3.1 Intermediary and Thermodynamics Optimization

Additional intermediate species may also be used, which requires another set of NASA-7 parameters to be optimized. These new species are not considered in the thermodynamics optimization step as they are not desired to exists at the equilibrium state, therefore its NASA-7 coefficients are optimized with the kinetic parameters.

As the virtual structure becomes complex and more intermediaries are required, its optimization becomes more expensive computationally, mostly due to the sheer amount of parameters every species adds to the procedure. As for the thermodynamics properties, three methodologies were considered and can be summarized in the order of the number of parameters as:

1. Method all NASA: The more basic method where all the six NASA coefficients are optimized independently. This results is a great increase of the number of optimization parameters and several solver problems arise, since the range of each parameter can be very wide. Despite these drawbacks, the method may provide the best match to the detailed mechanism, but such benefit is hard to quantify. Probably, it is more suitable as a refining step of the final solution.

2. Method of the enthalpy of formation: To overcome the problems of the All NASA procedure, the methodology presented by (CAILLER et al., 2017), (MAIO et al., 2019), (CAILLER et al., 2020), and also described by (PACHECO, A. F. et al., 2020) can be used. It is very similar to the All NASA methodology, but it optimizes five instead of six parameters. The last parameter is calculated using the enthalpy of formation of the virtual products as follows:

$$a_6 = \frac{\Delta H_V}{R} - \left(a_1 T_0 + \frac{a_2}{2} T_0^2 + \frac{a_3}{3} T_0^3 + \frac{a_4}{4} T_0^4 + \frac{a_5}{5} T_0^5\right) \tag{68}$$

$$\Delta H_V = \sum_{k=1}^{N_v} c_k h_{V_k} - \left(h_F + \frac{c_O}{c_F} h_O\right) \tag{69}$$

Here, ΔH_V is evaluated at 298 K. This ensures that the Intermediary properties would always produce a valid set of coefficients, bound to produce a intermediary result between the reactants and the virtual products.

3. Method of the linear combination: This method represents a simpler approach, where only one parameter is optimized. The method assigns a weighted average between the reactants and the virtual products, as shown in equations 70,

$$\sum_{i}^{N_{reac}} c_i[i] \rightarrow c_I[I] \rightarrow \sum_{j}^{N_{prod}} c_j[j] \tag{70a}$$

$$c_I a_I^{vir} = \alpha \sum_{i}^{N_{reac}} c_i a_i + (1-\alpha) \sum_{j}^{N_{prod}} c_j a_j^{vir} \tag{70b}$$

where α is a general weighting factor.

With this method, the number of parameters and solver issues are reduced to the minimum. However, this results in a very small degree of freedom to improve the temperature profile. Therefore, it is a very efficient starting strategy, but not the most accurate one.

The approach used here when applying the linear combination method uses the NASA coefficients at 1000 K only. This is one additional drawback of the implementation, since detailed thermodynamics data sets generally present more than one set of NASA coefficients with different reference temperatures.

A second discussion is regarding the number of the intermediaries to be optimized. A priori, each intermediary requires its own set of coefficients. In order to ease the optimization, different approaches can be done. If all the intermediaries are optimized at the same time, their properties could be mirrored, halving the number of parameters required. An individual optimization of the properties can be performed at later stages.

3.1.3.2 Reactions Parameters

Virtual reactions are modeled following the elementary reaction structure. The rate constant of each reaction is modeled by an Arrhenius equation (Eq. 71), therefore each reaction requires at least two parameters, the pre-exponential factor *A* and the

activation energy E_a. For more control over the solution, the temperature exponent b is also used.

$$k_r = AT^b exp(-E_a/RT) \tag{71}$$

$$q_r = k_r \prod_{r=0}^{n_{reactants}} [r]^{\alpha_r} \tag{72}$$

Equations such as Eq. 71 requires at least one parameter to be optimized. Generally two or three parameters are used (A, b and E_a). The combination of the A and E_a produces a rate with and exponential dependency over the Temperature, the temperature exponential b parameter has a similar effect and therefore both can present a type of competition on the optimization. Several chemical mechanisms do not require the temperature exponent, and for some optimization cases, such parameter can be ignored, being added as a refinement at the end of the process. This is more common on high temperature ignitions, while the NTC requires a different type of temperature dependency. For those cases, the easiest way to achieve an inverse relation with the temperature is by utilizing a negative b coefficient. A negative E_a could also be used to achieve that type of dependency, but care should be taken to avoid overlapping with the effect of a negative b. Therefore, not using the b parameter can be an advantage to the optimization, since this removes one parameter and avoids the aforementioned competition.

As for the reaction orders α_r in Eq. 72, their main effects in virtual schemes are the adjustment of the chemistry over different pressure levels and the accommodation of different stoichiometric conditions. For small fuel molecules, i.e., methane (CH_4), with a stoichiometry ratio of 2 oxygen molecules for each fuel molecule, the exponent $\alpha_r = 2$ does not compromise the convergence of the method. However, for large fuel molecules, such as heptane (C_7H_{16}), the stoichiometric coefficient for the oxygen is 11, which leads to a concentration raised to the eleventh power. The instability created by such large powers hinders even more the optimization and in most cases, nullify the reaction rate. Therefore an effort to limit such values is a reasonable choice.

3.1.3.3 Penalties

As the solution surface presents several local minima, some penalties are required to help the optimization to progress. Aside from penalties to address solver and convergence problems, additional penalties are used. A penalty is used to ensure the complete consumption of all intermediaries at the end of the ignition. Another penalty ensures that all fuel is also consumed at the end of the ignition. Finally, another penalty defines the time required to fully consume a portion of the fuel, to avoid instantaneous consumption of the reactants.

All penalties are modeled by the penalty function P_j (to be used in equation 79) defined as

$$P_j = \begin{cases} 0 & \text{if condition is within the parameters} \\ C & \text{otherwise.} \end{cases} \tag{73}$$

where C is fixed, either as a large number, or as a linearly increasing number, depending on the target.

3.1.3.4 Fitness Evaluation

Ignition delay time and the temperature transient profile are the main targets of this study. The model used is a homogeneous, constant mass, constant pressure, adiabatic reactor (Eq. 74 and 75) and IDT was defined as the point where the temperature increases by a certain amount.

$$\frac{dT}{dt} = -\frac{1}{\rho c_p} \sum_k h_k \dot{\omega}_k \tag{74}$$

$$\frac{dY_k}{dt} = \frac{MW_k}{\rho} \dot{\omega}_k \tag{75}$$

Here, $\dot{\omega}_k$ is the net production rates for species k.

The objective function has two components. The first is directly defined as the relative error between the IDT predictions with the virtual scheme and with the detailed mechanism as

$$u^j_{idt} = \frac{|\tau^j_d - \tau^j_v|}{min(\tau^j_d, \tau^j_v)} \tag{76}$$

where τ refers to the IDT and the subscripts d and v are used for detailed and virtual mechanisms respectively while j represent the condition. The minimum in the denominator is used to discourage the genetic optimization to be trapped in very fast ignition cases.

The second component is calculated from the error between the temperature profiles over a time domain normalized by the IDT (Eq. 77), to ensure that the shape of the temperature curve is taken into account separated from the effect of the IDT.

$$t^j_{n,i} = \frac{t_i}{\tau_j} \tag{77}$$

$$u^j_T = \sqrt{\int_{t_n=0}^{t_{n,max}} \left(\frac{T^v(t_n) - T^d(t_n)}{T^d(t_n)} \right)^2 dt} \tag{78}$$

This methodology helps to adjust of the time domain used for the optimization by using a normalization space and all the error integrals presented in Eq. 78 are performed between 0 <= $t^j_{n,i}$ <= 1.5 for the methane cases and 0 <= $t^j_{n,i}$ <= 2.0 for the n-heptane ones except for the 1500 K conditions where a $t_{n,max}$ = 3.5 was used instead. This selection encompass all the ignition up to a burnt state, as we can observe at figure 15 for the methane.

By limiting the temperature profile to be evaluated, we ensure that all the oxidation occurs without introducing more errors in the form of the difference in the equilibrium temperatures, as at this step there is little to no control over it. Additionally, it helps to better describe the final end of ignition which can be difficult for some global schemes, as smaller values for the final t_n could not capture some of this behavior.

The fitness calculation for each condition is calculated by Eq. 79, which couple both errors (IDT and Temperature). The objective function is them defined as Eq. 80 using a mean square average and the optimization targets become the minimization of this function.

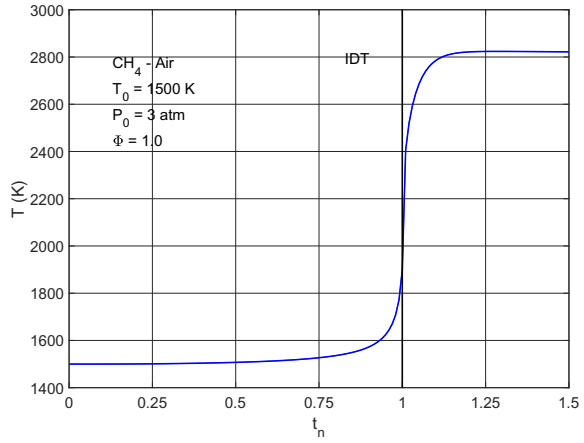

Figure 15 – Temperature Profile with normalized time

$$\epsilon_k^j = [(1 + u_{idt}^j)(1 + u_T^j) - 1] + P_j \tag{79}$$

$$\epsilon_k = \frac{1}{n_{cond} + 1} \sqrt{\sum_{j=1}^{n_{cond}} (\epsilon_k^j)^2 + max(\epsilon_k^j)^2} \tag{80}$$

Additionally, the $max(\epsilon_k)^2$ on equation 80 is used as an weight for the max error case. Additional weight parameters can still be used, mainly to help improve the IDT predictions.

3.2 ALGORITHMS

All codes used in this work were developed in Python language. The cantera library (GOODWIN et al., 2017) was used for handling thermodynamic properties for the detailed mechanisms, while an in-house thermodynamic library was developed to deal with the virtual mechanisms. The SCIPY package (VIRTANEN et al., 2020) was used for solving the set of differential equations, while an in-house code handles the chemistry part. The optimization problem was solved using an in-house genetic algorithm, summarized in the next section.

3.2.1 Genetic Optimization Algorithms

The surface solution for a chemical kinetics problem is generally very complex, and solver errors may lead to local optima. Optimization algorithms that use a rule to search the solution space, such as gradient search, can be very problematic to use in the current conditions, possibly trapping the algorithm in a local minima. In addition, the calculation of gradients are not straight forward in reactive problems and can present a computational time challenge when the number of parameters being optimized grows.

Genetic optimization is a powerful optimization technique to handle local minima and large number of parameters. It uses random individuals to explore the whole optimization domain, removing the necessity of gradient calculations and allowing for an effective search of complex surface solutions. Such methods rely on the evolution of a population following the evolutionary theory proposed by Darwin in 1859.

The optimization was implemented in a in-house algorithm which reproduces the evolutionary theory using the following steps:

1. Initialization - The initial population is initialized with random genes;
2. Evaluation - The performance of all individuals are evaluated using a fitness equation;
3. Evolution - The evolution of the population occurs as follow:
   (i) Selection - First, the parents are selected. Here, a *k*-tournament was used;
   (ii) Cross Over - A new set of children are produced from the parents via cross-over models. Here, the SBX model was used;
   (iii) Mutation - Some individuals, chosen at random, have some of their genes mutated to introduce additional variance to the population;
4. Evaluation and Reduction - The performance of the children population is evaluated and a new generation is selected. Here, the best *n* individuals are added to the next generation and the evolution step starts again.

There are some points to consider for the current problem. First, the range of values of the parameters vary over a few orders of magnitude and the selection of a reasonable domain in this range is not trivial. Second, it is more probable that a solution crashes or does not result in ignition, than a valid ignition. Third, the population may converge around a single individual, which is called the early convergence problem. To avoid these conditions, after a small number of generations without improvement, the optimization algorithm randomizes a large part of the population and enforces an evolution.

3.3 CASE STUDIES

Two basic cases were studied. The first addresses the more general behavior of high-temperature IDT curves, i.e., a monotonic relation with the temperature. The methane autoignition is one example of such behavior and was used to provide a better understanding of the feasibility of the methods devised.

The second addresses those fuels presenting negative temperature coefficient (NTC) behavior. These fuels present a region in the IDT curve where there is a negative relation of IDT with temperature, i.e. increasing the temperature causes also an increase in the IDT. The n-Heptane (nC_7H_{16}) has a very pronounced NTC. A complex and extensive chemical kinetics mechanism is needed to correctly predict the behavior in the NTC region. The complex chemistry together with the aggressive NTC makes this fuel an interesting test for the capabilities of the virtual schemes.

Since a genetic optimization method is used, there is no guarantee that a global minimum is found. Therefore, there is a need to define when the optimization should stop:

1. Adiabatic Temperature: since the optimization is computationally fast when compared to the kinetic phase, the stop criteria is defined as, either (a) a zero value for the fitness function or, (b) a given number of generations without any improvement. In this case, a 10^4 number of generations is used.

2. Molar Weights: following the previous case, two stop criteria are used: (a) a fitness function smaller than 10^{-3} or; (b) 10^3 generations without improvement.

3. Kinetic Parameters: (a) the zero conditions still applies, and (b) the maximum number of generations without significant improvements (over 0.1%) is set to 10^3.

3.3.1 Methane

As discussed and presented in the Thermodynamics Optimization section, a set of stoichiometric coefficients are calculated for each unburned condition. Due to the large temperature window, spanning values above and below 1000 K, two sets of NASA-7 coefficients are needed to calculate the properties of the unburned mixture, one for the lower (< 1000 K) and the other for the higher temperatures (> 1000 K). As a result, a significant variation of the stoichiometric coefficients was noticed, imposing difficulties in reaching the required adiabatic flame temperature.

To minimize this effect, the temperature range was kept between 1000 K and 1500 K, and, for this range, a single set of NASA-7 coefficients are needed. A fraction of these coefficients were used to obtain the best set of stoichiometric coefficients that could represent all the unburned mixtures of interest, while the remaining fraction was optimized to predict the adiabatic flame temperature. In this way, no correction function for the product coefficients in the virtual reactions was needed. Although this procedure brought benefits for the optimization of kinetics parameters, it also resulted in deviations in the predicted adiabatic flame temperatures. Therefore, it was necessary to reach a compromise between the capacity to predict the adiabatic flame temperature, versus the capacity to predict the time evolution of the temperature during the ignition delay.

The method was applied to a methane-air mixture, using the GRI-Mech 3.0 (SMITH et al., 2018) as the detailed mechanism. The thermodynamic optimization was performed at three temperatures ($1000K$, $1300K$ and $1500K$), two pressures (1 atm and 3 atm) and several equivalence ratios (from 0.8 to 1.2). For the kinetic optimization, the same conditions were used except the equivalence ratio, which was kept at stoichiometry.

As for the mechanism structure, the three reaction paths presented in Table 8 were used.

Table 8 – Summary of the base kinetic structures.

Name	Mechanism	No. of rxn	No. of int	No. of param
One RXN	$\nu_F F + \nu_{Ox} O \rightarrow \sum_{i=0}^{n_v} \nu_i V_i$	1	-	4
One INTER	$\nu_F F + \nu_{Ox} O \rightarrow I$ $I \rightarrow \sum_{i=0}^{n_v} \nu_i V_i$	2	1	13
Two INTER	$\nu_F F + \nu_{Ox} O \rightarrow I_1$ $I_1 \rightarrow \sum_{i=0}^{n_v} \nu_i V_i$ $\nu_F F + \nu_{Ox} O \rightarrow I_2$ $I_2 \rightarrow \sum_{i=0}^{n_v} \nu_i V_i$	4	2	24

Model One RXN is an one-step global reaction producing n_V products. Model One INTER is formed by two series reactions with one intermediary species (I). Model

Two INTER has two parallel paths, each of them formed by two series reactions with one intermediary species (I_1 and I_2). The number of kinetics parameters to be optimized increases with the number of reactions and intermediaries, from 4 to 24.

For each set of initial conditions, the virtual chemistry was optimized until there is no improvement in the objective function after a given number of subsequent generations.

A first optimization was performed without using the *b* exponent in the power-law temperature dependence of the Arrhenius model. Then, a second optimization was performed adding the *b* exponents as part of the kinetics parameters. Finally, a third optimization was performed duplicating and triplicating each mechanism. For example, the first and second optimizations use the single global reaction "One RXN" as shown in Table 8. Then, the third optimization uses the Two "One RXN" and the Three "One RXN" as mechanisms, resulting in the following sets:

$$\begin{array}{lll} \text{''One RXN''} & : & \nu_F F + \nu_{Ox} O \rightarrow \sum_{i=0}^{n_v} \nu_i V_i, \\ \text{Two ''One RXN''} & : & \nu_F F + \nu_{Ox} O \rightarrow \sum_{i=0}^{n_v} \nu_i V_i, \\ & : & \nu_F F + \nu_{Ox} O \rightarrow \sum_{i=0}^{n_v} \nu_i V_i, \\ \text{Three ''One RXN''} & : & \nu_F F + \nu_{Ox} O \rightarrow \sum_{i=0}^{n_v} \nu_i V_i, \\ & : & \nu_F F + \nu_{Ox} O \rightarrow \sum_{i=0}^{n_v} \nu_i V_i, \\ & : & \nu_F F + \nu_{Ox} O \rightarrow \sum_{i=0}^{n_v} \nu_i V_i, \end{array} \tag{81}$$

The same logic was applied to the other two mechanisms. This provided additional degrees of freedom that result in improvement of the prediction of the temperature evolution during ignition delay, as it is presented below. Table 9 presents a summary of the number of species and reactions of the virtual mechanisms developed here.

Table 9 – Summary of the number of species and reactions

Mechanism	**num. of Species**	**num. of Reactions**
One RXN	8	1
Two "One RXN"	8	2
Three "One RXN"	8	3
One INTER	9	2
Two "One INTER"	9	4
Three "One INTER"	9	6
Two INTER	10	4

3.3.2 n-Heptane

The methane optimization explores the use of virtual chemistry for describing fuels with simple IDT behavior. n-Heptane presents a strong NTC region and thus it is selected as a model fuel to address the issue of modeling NTC using virtual mechanisms.

Figure 16 presents the ignition delay times for the n-Heptane/Air mixture (defined as the time needed to reach a 600 K temperature increase over T_o), at stoichiometric condition and atmospheric pressure, calculated with Mehl et al. (2011) mechanism. The detailed mechanism presents 1389 species and 9603 reactions.

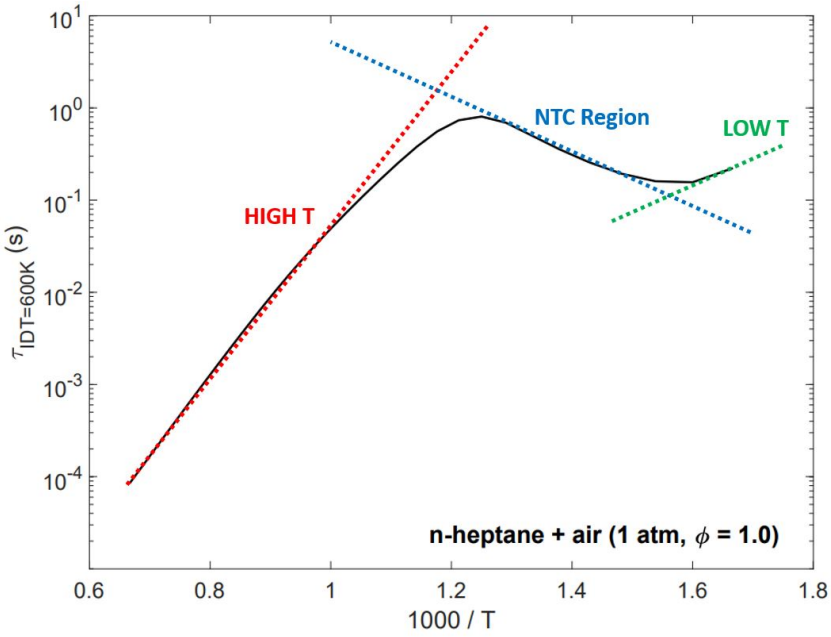

Figure 16 – IDT prediction for n-Heptane/Air mixture using Mehl et al. (2011) detailed mechanism

The IDT behavior can be divided into three different regime. The first is the high temperature ignition (represented by the red line). It follows the general monotonic behavior of decreasing IDT when the temperature increases. At about 800 K ($1000/T$ = 1.2), the effect of a slower ignition due to low temperature starts to fade off, changing the behavior to the NTC region between 800 K and 650 K (blue line). At lower initial temperatures ($1000/T > 1.5$, green line), the behavior changes again to a simple monotonic temperature dependency. This is the low temperature regime.

In this work, the initial temperature ranged from 600 K to 1500 K. This ranges crosses over the reference temperature of 1000 K, where the low temperature set of NASA coefficients changes to the high temperature set. Since the virtual mechanism uses a single set of thermodynamic parameters for the entire temperature range, the detailed adiabatic temperature is not predicted perfectly in the entire temperature range. Additional computational details will be discussed with the results.

The virtual mechanism was developed at one pressure (1 atm) and stoichiometric condition.

As for the mechanisms structures, the higher temperature reaction path, mostly active for conditions of $T > 1000K$, is composed by two "One INTER" Structures as presented by equations below. The underscript 1 is used to represent the high temperature reaction paths.

$$\nu_F F + \nu_{Ox} O \rightarrow I_1 \tag{82a}$$

$$I_1 \rightarrow \sum_{i=0}^{n_v} \nu_i V_i \tag{82b}$$

$$\nu_F F + \nu_{Ox} O \rightarrow I_1 \tag{82c}$$

$$I_1 \rightarrow \sum_{i=0}^{n_v} \nu_i V_i \tag{82d}$$

The low temperature path is modeled using a single One INTER structure, with a distinct intermediary species from the high temperature path. The underscript 2 is used to differentiate the low temperature structure from the high temperature reaction path.

$$\nu_F F + \nu_{Ox} O \rightarrow I_2 \tag{83a}$$

$$I_2 \rightarrow \sum_{i=0}^{n_v} \nu_i V_i \tag{83b}$$

4 RESULTS

First, the results for methane are presented, mainly discussing the use of progressively complex virtual models. Then, the results for n-heptane are presented, with focus on the modeling of NTC region.

4.1 METHANE

The results for methane virtual mechanisms are presented in three separate sections. The first presents the predictions obtained with the base global (One RXN), series (One INTER), and parallel (Two INTER) virtual mechanisms. The second presents the predictions obtained from duplicating and triplicating each base mechanism. Finally, the last section presents the improvements observed in computational time.

4.1.1 Base Model Results

Figure 17 presents the predictions of IDT using the three base virtual mechanisms presented in Table 8, for equivalence ratio of 1, pressures of 1 bar and 3 bar and temperatures from 1000 K to 1500 K. All virtual mechanisms present a good agreement with the detailed mechanism when the predicted IDT is observed in the typical Arrhenius graph.

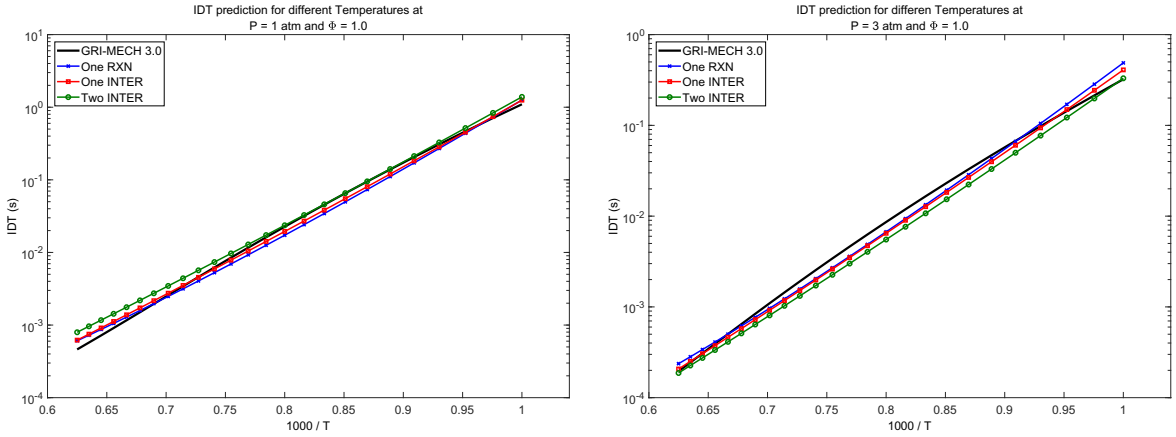

(a) (b)

Figure 17 – Comparison of IDT calculated with the virtual and detailed mechanisms for (a) 1 atm and; (b) 3 atm.

In order to evidence the deviations from each model, Figures 18a and 18b present the relative deviation of the predictions for each virtual mechanism in respect to the predictions of the detailed mechanism. The $d\%$ is defined as

$$d\% = \left(1 - \frac{\tau_v}{\tau_d}\right) \tag{84}$$

where τ_v and τ_d are the ignition delay times predicted with the virtual and the detailed mechanisms, respectively.

Deviations larger than 50 % are observed at the lower temperatures. The model with one intermediate presents the best compromise overall. All the virtual mechanisms

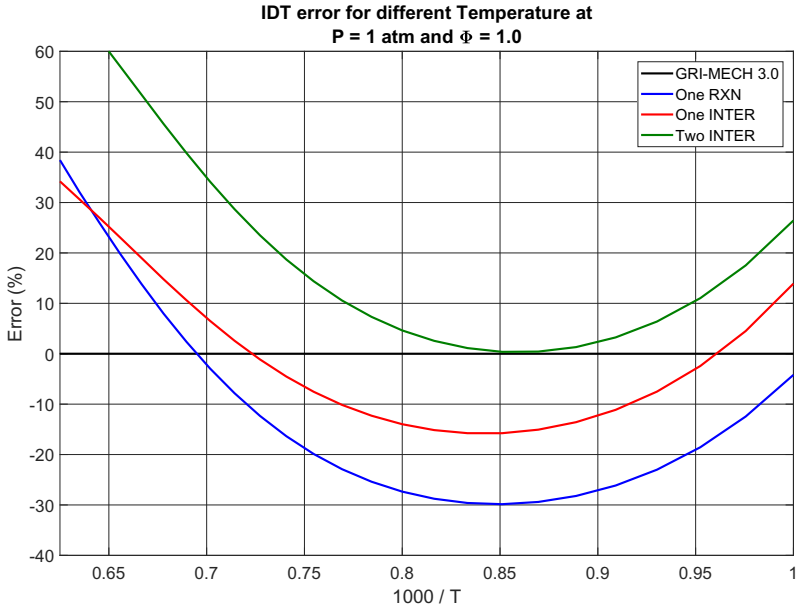

(a)

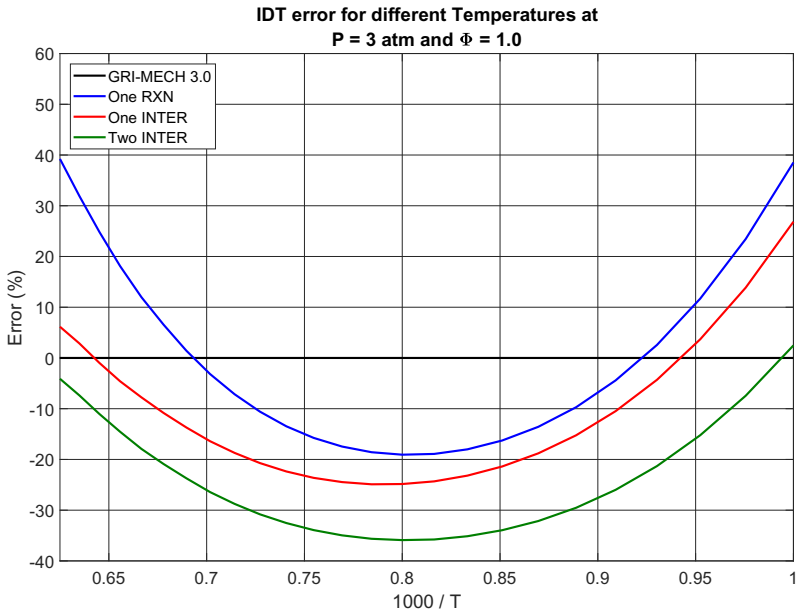

(b)

Figure 18 – Relative error of IDT at (a) 1 atm and; (b) 3 atm.

predicted the IDT with a very similar behavior indicating that the small number of reactions and parameters used is not enough to properly model autoignition problems.

Figures 19a and 19b present the predictions of the temperature evolution prior do IDT at initial conditions of 1000 K and 1 atm and 1500 K and 3 atm, respectively, which correspond to the slowest and fastest ignition delay times in this study. A difference on burned temperature calculated from the virtual and detailed mechanisms of approximately 50 K is observed and is described in the beginning of the last section.

The predictions for other conditions follow the same trends and are not shown here. The closest prediction of the overall temperature profile is provided by the two

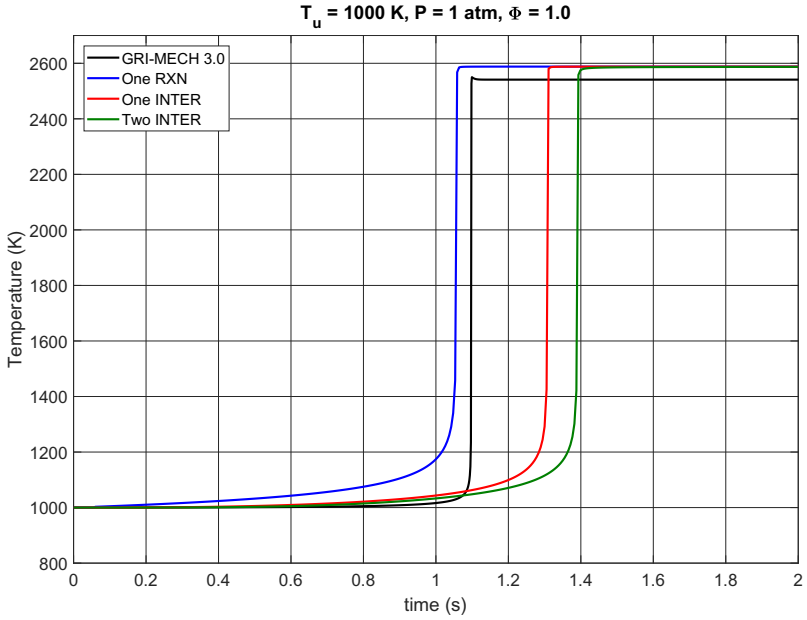

(a)

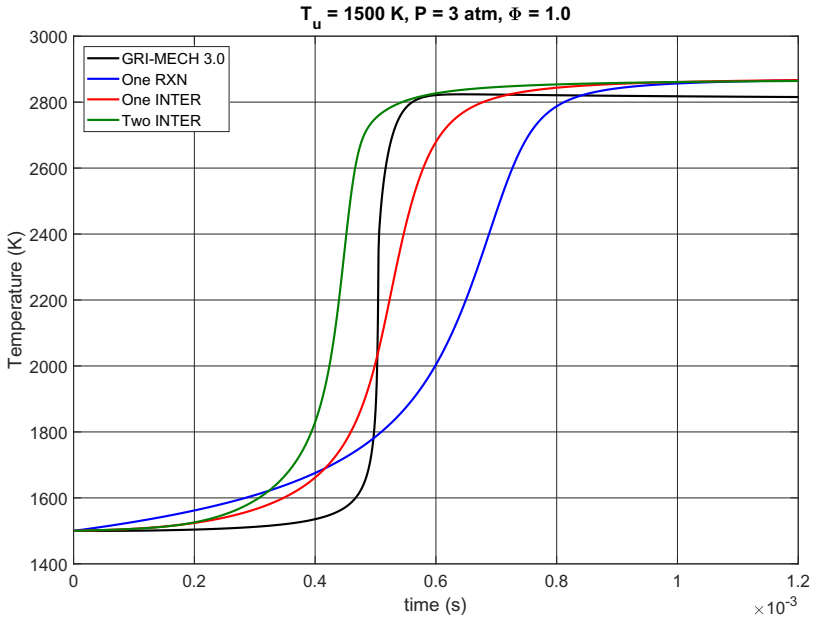

(b)

Figure 19 – Temperature evolution comparison at (a) T_u = 1000 K and P = 1 atm; (b) T_u = 1500 K and P = 3 atm.

intermediates model, followed by the one intermediary although the One RXN has a better prediction on the lower Temperature case.

The temperature exponent (parameter *b*) in the Arrhenius expression was included in the One, One INTER, and Two INTER mechanisms as a way of improving the prediction of IDT. The concurrent optimization of the temperature exponent *b*, the pre-exponential factor *A*, and the activation energy E_a may lead to values of *b* unreasonably high because both, the temperature exponent and the Arrhenius exponential, lead to an exponential effect of the temperature in the reaction rate, which may result

in a compensating effect. Therefore, to avoid reaching upper bounds for b, first the pre-exponential factor A and the activation energy E_a were optimized, assuming $b = 0$, and then, for the optimum A and E_a, parameter b was optimized.

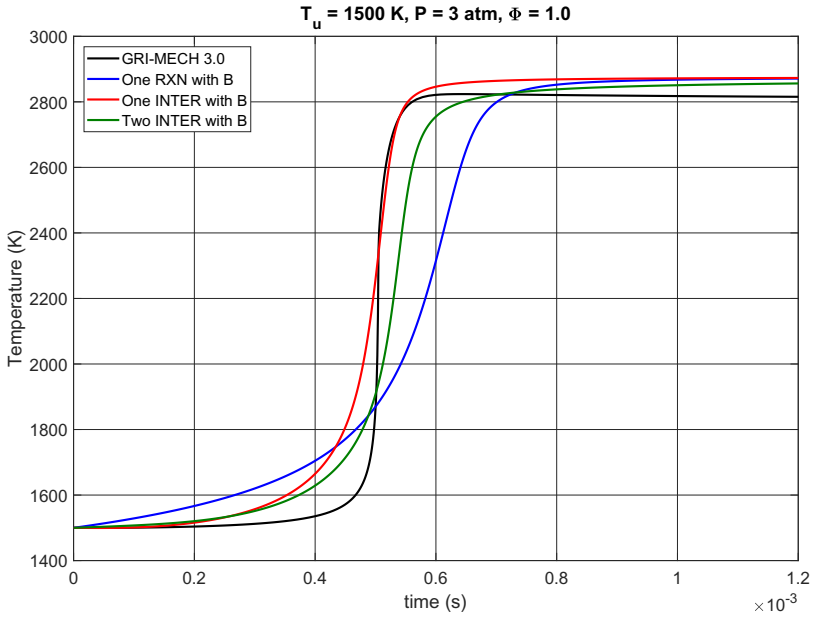

(a)

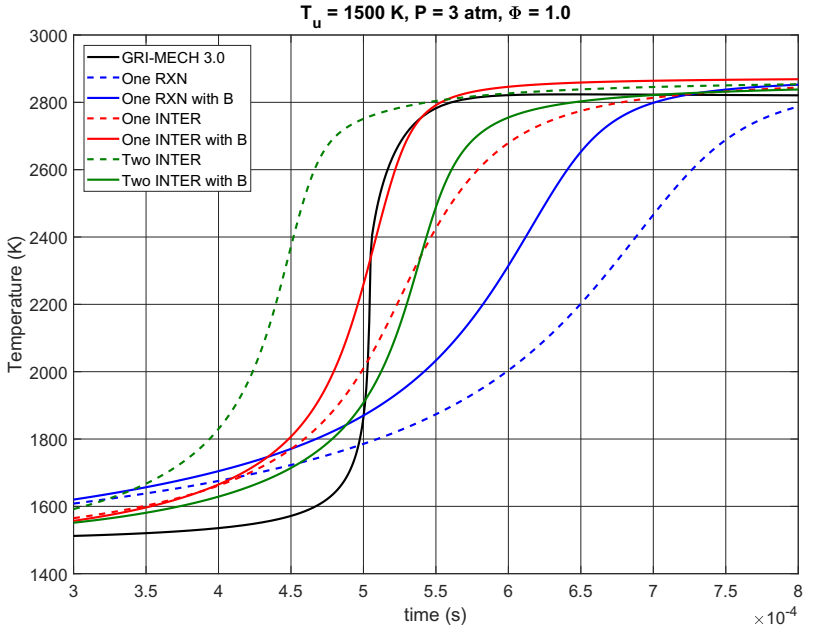

(b)

Figure 20 – Temperature profiles at T_U = 1500 K and P = 3 atm (a) predicted using mechanisms One, One INTER, and Two INTER with the inclusion of parameter “b”, and (b) compared to the base models with a zoom in the time range around the ignition time.

Although very little improvement occurred in the prediction of IDT, some improvement was observed in the prediction of the temperature profile, as presented in Figures 20a and 20b. Figure 20a presents the entire temperature profile predicted using param-

eter b for T_U = 1500 K and p = 3 atm. These conditions lead to smaller IDT where a stronger effect of the parameter b is observed. Figure 20b presents a comparison of the predictions of temperature with and without using parameter b for the time range near the ignition. The optimization of parameter b leads to a steeper temperature increase near the ignition, as observed specially in the One RXN and One INTER mechanisms. The same marginal improvement was observed for the reactants at lower temperature and pressure (not shown in the figures).

4.1.2 Combined Model Results

The predictions of IDT of the detailed mechanism does not follow a simple exponential curve in the IDT versus $1/T$ graph. This suggests that the addition of more parallel paths may lead to a better prediction. Here we test the effects of the duplication of the base reaction mechanisms in the prediction of IDT and temperature profile. This strategy was applied in the One RXN and One INTER models, originating the Two "One RXN", Three "One RXN", Two "One INTER", and Three "One INTER" models.

The mechanism named "One RXN" presents two and three global reactions, with the prefixes differentiating one from the other. The "One INTER" cases follows the same rule however, both the reactions are duplicated i.e. the reaction that consumes fuel and produces intermediary and the reaction that consumes the intermediary to produce the virtual species.

All the cases using sets of "One INTER" uses a common intermediary, therefore only one set of Thermodynamic coefficients are optimized in the kinetics phase. The “Two INTER” mechanism was not duplicated because the large number of parameters to optimize lead to a slow convergence, when compared to mechanisms generated by the duplication of the “One INTER” base mechanism. Since the differences observed in the IDT curves becomes imperceptible in the IDT versus $1/T$ graph, the following figures present the percent difference between the predictions with the virtual and detailed mechanisms.

Figures 21a and 21b shows the deviation of the virtual schemes to the detailed mechanism for the two pressure levels.

The additional reaction paths, including Temperature exponents, add additional degrees of freedom to the models, resulting in a smaller overall percent deviation in respect to the detailed mechanism. The maximum error was also smaller than the ones encountered in the base structures. For the IDT prediction, the structures with "One RXN" yield better results even with values of the fitness functions higher than those for the "One INTER" model. Additional improvements of the prediction of IDT could still be obtained by increasing the IDT weighting factor of the fitness calculations.

Figure 22 shows the temperature evolution along the thermal ignition for methane-air mixtures, at equivalence ratio 1, temperatures 1000 K, 1300 K, and 1500 K, and pressures of 1 atm and 3 atm. The first observation is the difference in equilibrium temperature among the mechanisms. This is due to difficulties on optimizing the thermodynamic parameters, as already discussed above. However, in the worst scenarios, the deviations reach, at most, 5 % in the final equilibrium temperature (at 1500 K, 1 atm).

More interesting, are the differences observed in the temperature evolution. The analysis of the temperature evolution reveals the differences in the use of the "One RXN" and the "One INTER" mechanisms.

First, although the "One RXN" mechanisms result in a good prediction of IDT,

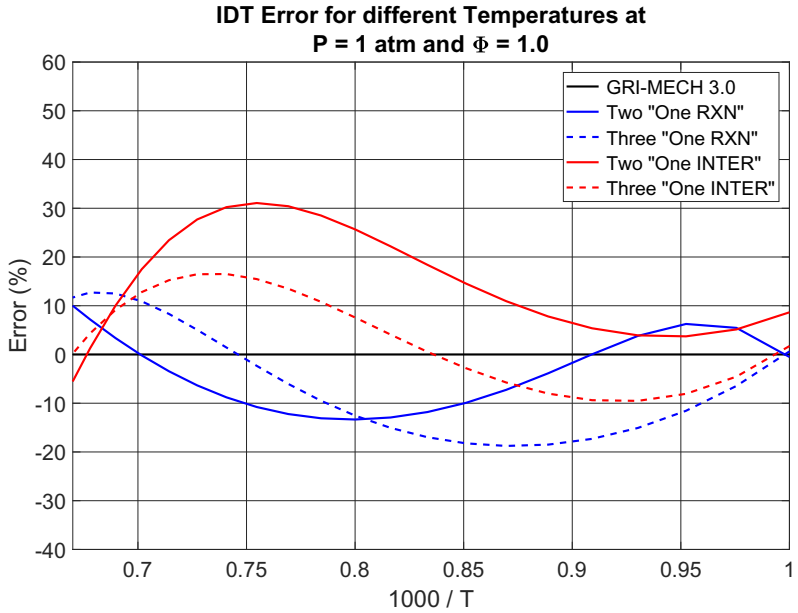

(a)

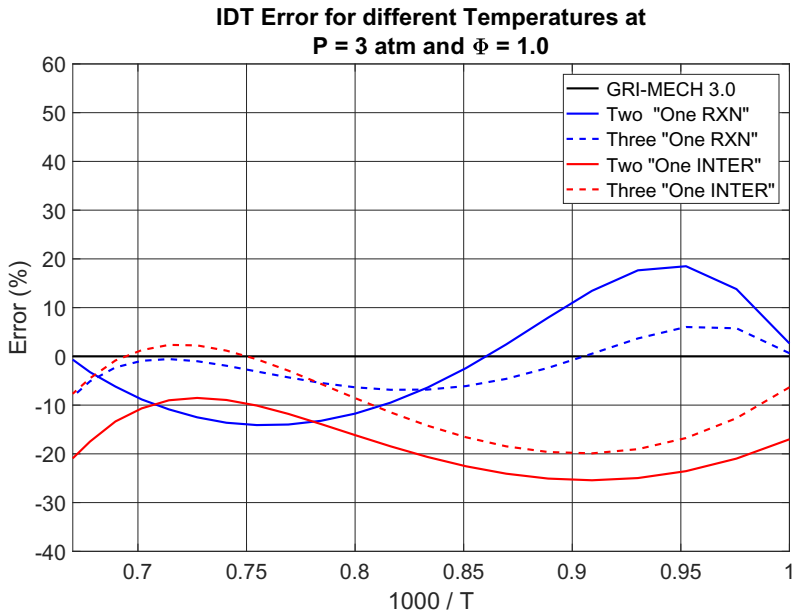

(b)

Figure 21 – Relative error of IDT base structure combination at (a) 1 atm and; (b) 3 atm.

they are not as well effective in predicting the temperature evolution. They lack the ability to emulate the formation and growth of a radical pool followed by a fast production of virtual species. Therefore, Figure 22e and 22f show that while the Two “One RXN” presents a thermal ignition much slower than the detailed mechanism, the Three “One RXN” presents a very abrupt temperature distribution after ignition. The behavior of both "One RXN" cases indicate, practically, the limits of global mechanisms, producing either an explosive temperature curve or a "slow burn" curve.

Secondly, the "One INTER" mechanisms present a worse IDT prediction, how-

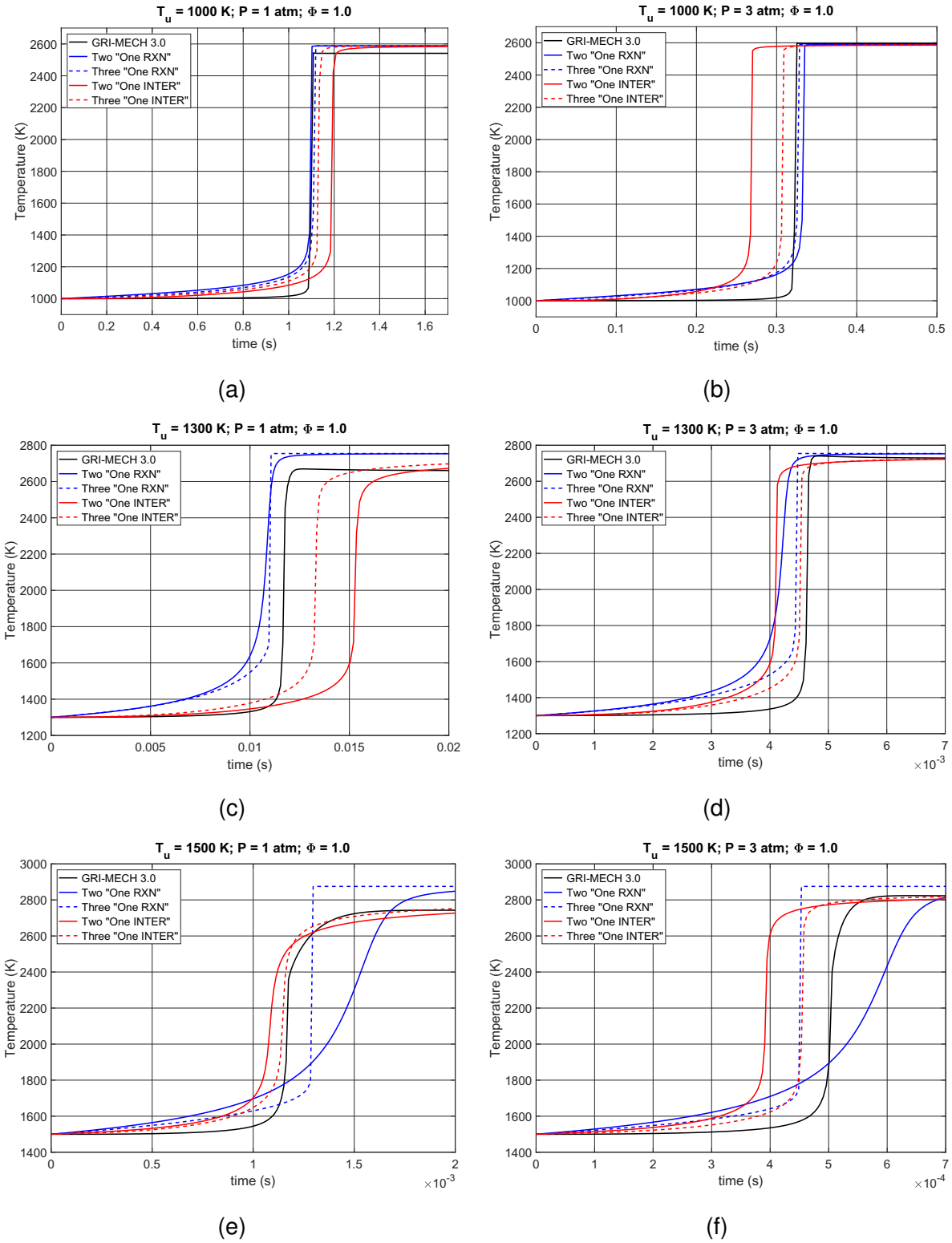

Figure 22 – Temperature evolution along the thermal ignition for methane-air mixtures, at equivalence ratio 1, at temperatures and pressures: (a) 1000 K, 1 atm, (b) 1000 K, 3 atm; (c) 1300 K, 1 atm; (d) 1300 K, 3 atm; (e) 1500 K, 1 atm; and (f) 1500 K, 3 atm.

ever the temperature distributions approach more closely the results of the detailed mechanism. The Three "One INTER" model presents the closest agreement with the

detailed temperature distribution. This agreement is mostly due to the presence of an intermediary species, which allows for the emulation of the formation and growth of a radical pool. Also, the presence of small fractions of the intermediary in the burned mixture helps the optimization of the final burned temperature, as it can be observed in Figures 22c, 22e and 22f.

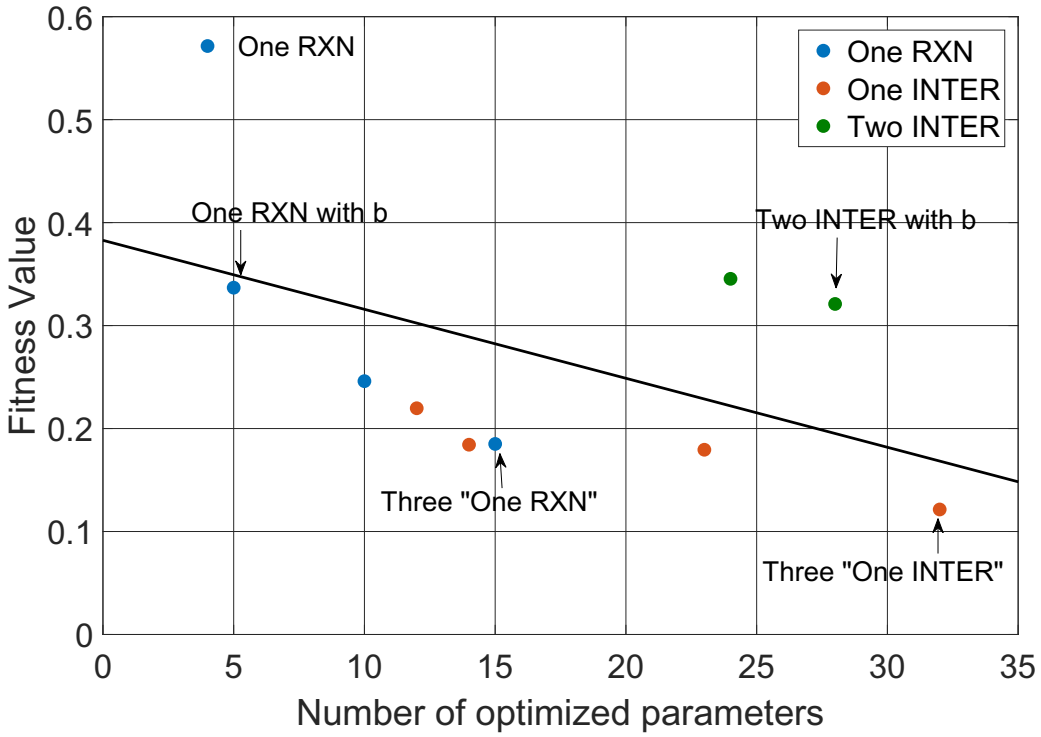

Figure 23 – Fitness value versus number of parameters

It is difficult to assess which virtual mechanism provides the best results, since there are two components in the optimization, the IDT and the temperature distribution. If only the IDT prediction is required to be accurate, then figures such as 18 and 21 can be used. In the figures presented here, however, both, the IDT and temperature profiles were used in the penalty function. In figure 23, all the virtual mechanism are presented according to their final fitness values. Each color corresponds to a given base model. In this figure, the Three "One INTER" presents the best solution, as well as, the largest number of parameters to be optimized. Within the same base model, increasing the number of parameters improves the solution, as it can be observed in the One RXN cases (blue dots). Although, generally, a larger number of parameters results in a better solution (as in the blue and orange dots), we observe that the Two INTER models (green dots) presents the same quality as the One RXN with b model, while requiring seven times more parameters.

4.1.3 Computational Time

The computational time when using the reduced mechanisms is always much faster than when using the detailed mechanism, as expected. Also, the difference in

computational time increases as the IDT increases. However, the relative computational time among the different mechanisms is not as well as clear.

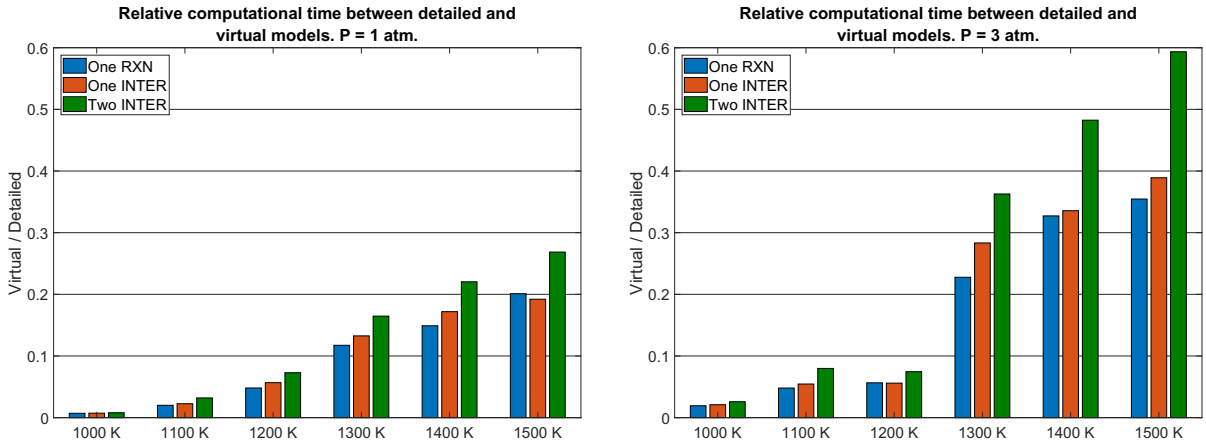

(a) (b)

Figure 24 – Relative computational time between detailed and virtual models for (a) 1 atm and, (b) 3 atm.

Figure 24 presents the relative computational time between the detailed and the virtual mechanisms for (a) 1 atm and (b) 3 atm. All similar mechanisms were combined into the same category (One RXN, One INTER and Two INTER) due to very small differences observed on the computational time within the same category. Even considering that the present computational code is not optimized for fast computation, in the worst case scenario, the time spent when using the virtual mechanisms was smaller than 60 % of the detailed mechanism for the slower mechanisms (Two INTER). Overall, the Two INTER mechanisms are the slowest mostly due to the presence of the second intermediary. The One RXN and One INTER mechanisms presented a similar CPU time, being the former slightly faster most due to its simpler structure and absence of intermediaries.

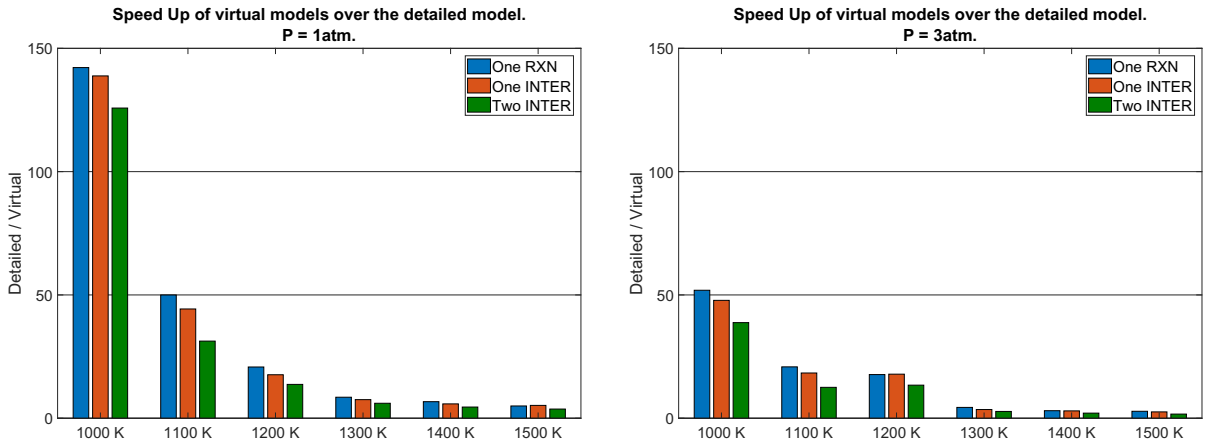

(a) (b)

Figure 25 – Speed up of the virtual mechanism over the detailed one for (a) 1 atm and, (b) 3 atm.

Figure 25 is another way of presenting the relative CPU time, in terms of the speed up of the virtual mechanisms when compared to the predictions of the detailed mechanism. The smallest speed-up factor found was 1:6 for the Two INTER cases, which is already a very good result. For the slower ignition cases (1000 K), the speed-up was over 100 times the CPU time needed to compute the solution with the detailed mechanism. We also observe that the speed up grows exponentially as the IDT increases, becoming even more significant as the temperature decreases. Finally, it is expected that a more optimized algorithm would increase the advantage even further.

4.2 N-HEPTANE

The results for n-Heptane are presented in three sections. The first presents discussions regarding the differences between the methane optimization and the n-heptane. The second presents the results for the predictions and virtual optimization of the virtual mechanism. Finally, the last section presents the improvements observed in computational time.

4.2.1 Mechanism Structure and Optimization

The NTC behavior requires more complex chemistry to be described, which can be translated to a more challenging virtual mechanism optimization. Differently from methane, when the IDT curve follows an Arrhenius relation, the n-heptane presents three distinct regimes, as shown in figure 16. The presence of a high temperature regime, followed by an NTC behavior, and finally by an Arrhenius low temperature regime, requires a more detailed approach.

During the methane optimization, adding more reactions to an already optimized virtual mechanism was required to ease the optimization. However, that strategy alone is not enough to produce a viable virtual chemistry for n-heptane. As an example of the limitations of the previous approach, a virtual mechanism composed by a Two INTER base model optimized using the same procedure used for methane is presented in figure 26.

Even the optimization achieving the stop criteria of more than 1000 generations without improvements, the results are far from representing the NTC and the low temperature regime. Although the high temperature regime ($0.6 \leqslant 1000/T \leqslant 1.1$) is well represented and there is a very weak NTC, there is no transition from the negative relation to a direct relation in the low temperature domain ($1000/T \geqslant 1.6$).

The example in figure 26 is only one of the many attempts of optimizing the NTC behavior using the same methodology used for methane. To properly address the modeling chalenges of the NTC and low temperature regimes, first a general discussion about the required structure of the mechanism is presented, followed by the optimization strategies and results for partial and final mechanism.

4.2.1.1 A parametric study

In any complex chemistry, the structure of the mechanism has a major role on the chemistry process. Simpler solutions, such as global reactions, lack the capacity to solve all regimes with a single set of parameters. Generally, detailed mechanisms for fuels with NTC present a large number of species and reactions and their reduced forms are likely to fail on the NTC region. This occurs as a consequence that reduction strate-

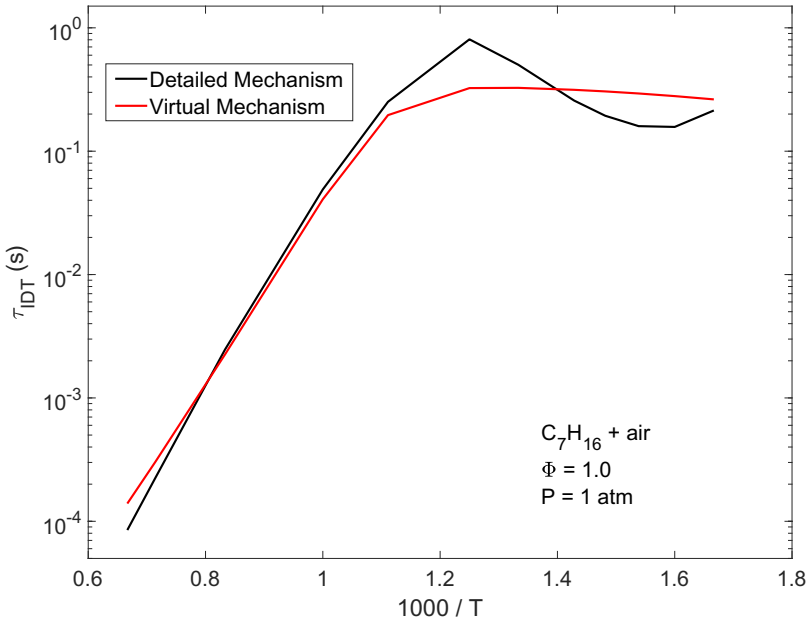

Figure 26 – Virtual optimization attempt for n-heptane detailed mechanism

gies usually eliminate reaction paths that have very small contribution to production rates, even though their combined effect is important to produce the NTC behavior.

Proposing a more complex virtual chemistry has a great impact on the complexity of the optimization, since the number of parameters increase, but, with no assurance of a better overall result. For the complex behavior of the n-heptane, the selection of the virtual chemistry structure has a major impact on whether a consistent and accurate solution can be achievable.

As a tool to address the virtual structures to model NTC behavior, a small Design of Experiment (DOE) was performed on a very simple kinetics model that emulates an auto ignition process. Such study used the following simplifications:

1. It was based on the 0D, constant mass, constant pressure, adiabatic reactor equations described in equation 75 without the energy equation;

2. The reaction rates are constant through each case and are defined based on the initial temperature;

3. The IDT was defined as the time required to produce a certain amount of virtual products.

The above simplifications allow for an easy test of any given virtual structure. The DOE was performed by modifying the dependence of the reaction rates in respect to the initial temperature for every reaction in the structure. The objective was to found possible candidates that are capable of capturing the NTC behavior, and for that reason, only the cases with such capability were selected.

To automate the selection of possible candidates, each one was categorized based on the IDT prediction. A solution has a valid NTC if only one local maximum and one local minimum are present within the temperature range, not in the boundaries. If that condition is met, a normalization of the logarithm of IDT was performed and the difference between those normalized values was calculated. If this value is greater

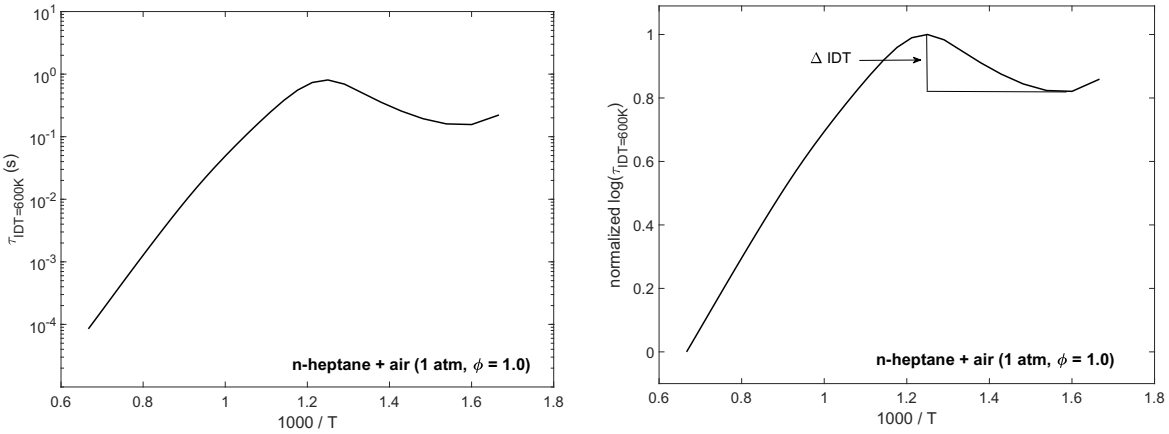

(a) (b)

Figure 27 – n-Heptane IDT. (a) Normal case and; (b) Normalized times.

than 0.05 the current solution is selected. Figure 27 presents an illustration of such procedure for the n-heptane detailed mechanism, where (a) is the original IDT curve and (b) is the normalized IDT curve. The ΔIDT indicated in figure (b) is calculated for each candidate. To collapse the results into an easily readable figure, each case was represented as a point in a 2D diagram, where the x-axis is the temperature difference between the maximum and minimum normalized IDTs around the NTC region and the y-axis is the the calculated normalized Δ_{IDT}.

Two basic structures tested are shown in Figure 28. Figure 28(a) represents one of the basic models, the Two "One INTER" case. Figure 28(b) represents an extension of the first mechanism by adding a second intermediate product and a third path to consume reactants.

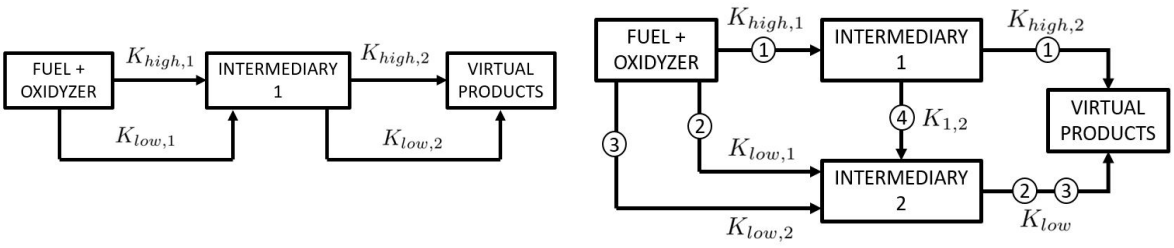

(a) (b)

Figure 28 – Virtual mechanism structures. (a) Two "One INTER" and; (b) Two INTER, with all the reactions paths.

Figure 28(b) presents three reactions paths, one for the High Temperature chemistry (reaction path 1) and two for the Low Temperature (reaction paths 2 and 3). Reaction 4 was used to connect the two paths. By combining those paths, three partial and one final structures were obtained: Two INTER (paths 1 and 2), Two INTER High to Low (paths 1,2 and 4), Two INTER Low to High (paths 1, 2 and a reversed 4), and the final complete structure (paths 1, 2, 3 and 4).

The DOE results of the five structures are presented in figure 29. Figure (a) shows all the NTC points for each case while figure (b) presents the region of the

diagram covered by each structure. The number of points is directly related to the number of parameter used on the DOE, and we can assume that any point inside the delimited region can be achieved by a given structure.

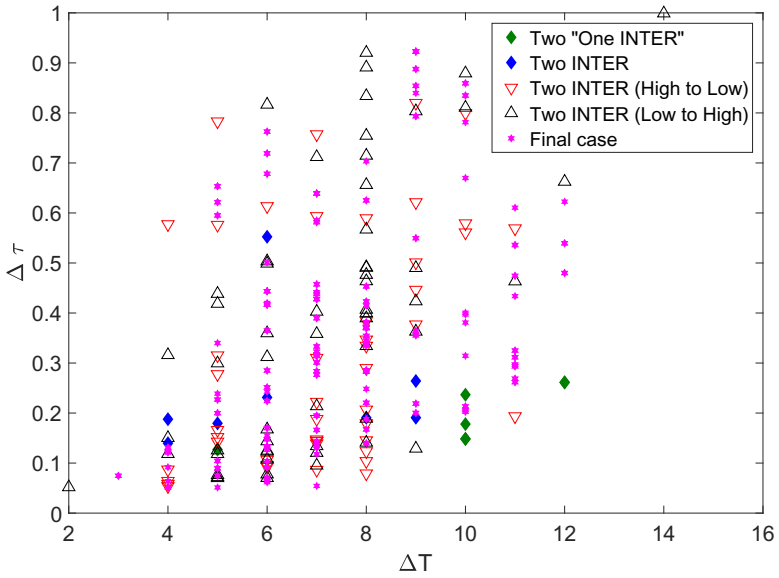

(a)

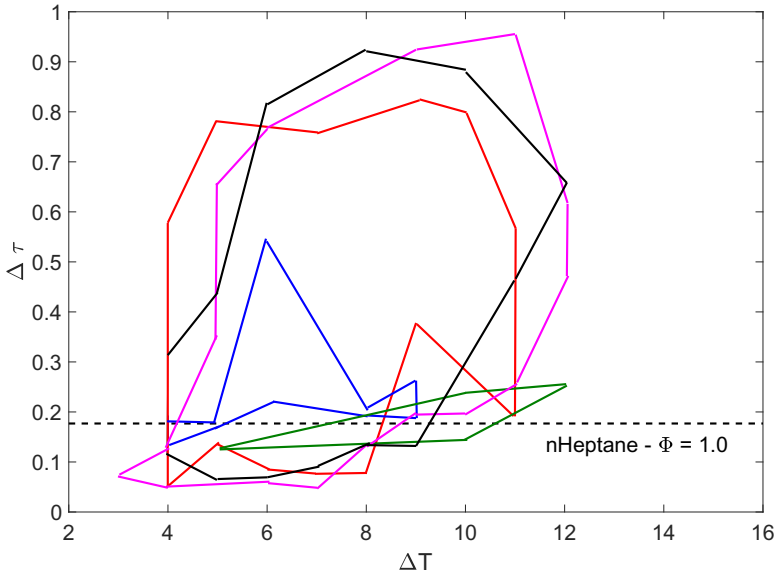

(b)

Figure 29 – DOE results. (a) All points and; (b) Enclosed regions.

Small enclosed regions, such as the one presented by the green (Two "One INTER") and blue (Two INTER) lines can be translated as too narrow to obtain an NTC, whereas large regions such as the red and black (Two INTER) and pink (Final) are sufficiently large to contain more NTC behaviors. The caveat here is the fact that a large set of parameters increases the optimization complexity, therefore there is a

trade-off between the cost of optimizing a virtual structure versus the possible benefits of using it.

As a final note regarding the virtual structure, structures with a single intermediary may not be suitable for mechanism with multiple exponential IDT regions. The structure used here lies between the Two INTER and the Final structures. This will be better discussed in the following sections.

4.2.1.2 Optimization Specifics

The methane optimization modeled the thermodynamics of the intermediary using the enthalpy of formation. For the n-heptane, the following simplifications were used:

1. Intermediary thermodynamics: linear interpolation;
2. Fixed reactants order: the reactant order was not optimized; and
3. Partial conditions optimization: the optimization was performed adding different conditions progressively at each time step and adding reaction paths as needed.

The major difference between the methane and n-heptane implementations can be related to the the third point, the use of a sub-set of the optimization conditions at each optimization step. As presented in figure 16, the n-heptane IDT curve can be divided into the High temperature, the NTC and the low temperature regimes. The High temperature and the NTC regions can be optimized independently of each other, since for parallel reactions paths, the faster one will always be the one that controls the chemistry. In this particular case, at high temperature conditions, the high temperature reaction path will be much faster than the NTC one and therefore will dictate the IDT behavior. Similarly, in the NTC conditions, the NTC specific reaction path will be faster than the high temperature one and therefore will control the chemistry.

The last discussed property of high temperature and NTC reaction paths made possible to first optimize only the high temperature reaction paths, considering only the appropriated conditions. With the former solution already optimized, the NTC region can be obtained only considering the temperatures where it appears and with exclusive negative *b* coefficients. That methodology of optimizing each region independently was one of the major improvements over the methane optimization. By using such strategy, an NTC can be achieved in a fraction of the time spent to obtain the failed virtual mechanism in figure 26. Additionally, this way an NTC mechanism could be obtained consistently from scratch using different penalties and parameters with a very small time cost.

The main problem appears on the transition between NTC and the low temperature, as this part presents the behavior of series reaction paths: The slow reaction path in this case must be the one controlling the chemistry. Again, the same procedure can be used, where the previous optimized mechanism, now already covering the high temperature and NTC regions, is augmented with the proper reaction paths for the current regime and only those new reactions are optimized.

Following these discussions, the next section presents the results of one particular structure that better represents the n-heptane IDT behavior.

4.2.2 Model Results

Differently from the methane thermal ignition, the modeling of the n-heptane thermal ignition was performed at only one pressure (one atmosphere). The optimization for different pressures would follow the same steps, generating a different set of thermodynamic and kinetics parameters. The remaining conditions were presented in the chapter on Methodology. In the following, the results are organized in terms of prediction of ignition delay, prediction of temperature time distribution, and behavior of the chemical species during thermal ignition.

4.2.2.1 Ignition delay time

As stated, the optimization proceeds as a set of sequential mostly independent steps. The first one is the optimization of the high temperature regime. This part of the problem can be treated in the same way used for the methane. It started with a basic initial One INTER model, using a linear interpolation for the high temperature intermediary. As soon as the basic solution was obtained, the One INTER model was duplicated and optimized. Three temperatures were used: 1500, 1200, and 900 K.

Figure 30 presents the IDT predicted using the partially optimized high temperature virtual mechanism. The current solution presents a high deviation from the detailed solution. The relative deviations are presented in Figure 31.

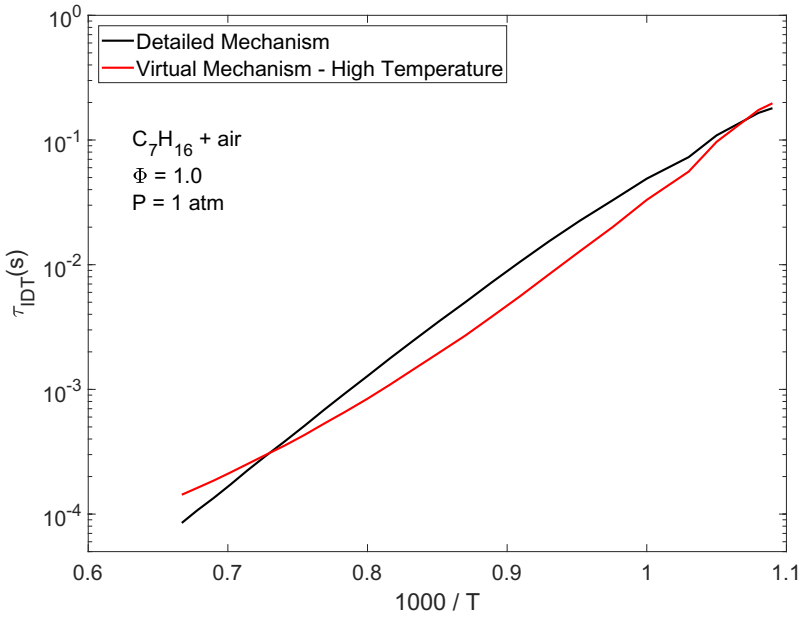

Figure 30 – Virtual optimization attempt for n-heptane detailed mechanism at high temperature conditions

The current virtual mechanism presents a much higher deviation (up to 60% at 1500 K) than the methane model with the same structure (30% at 1300 K and 1 atm). The main reason for this is the amount of computational time dedicated to the optimization. For the methane, the virtual mechanism obtained could be considered as a final product from the methodology while for the n-heptane virtual mechanism, it is a partial solution, from which the final virtual mechanism will be built upon. The optimization in this phase was halted earlier as the addition of the NTC reactions could

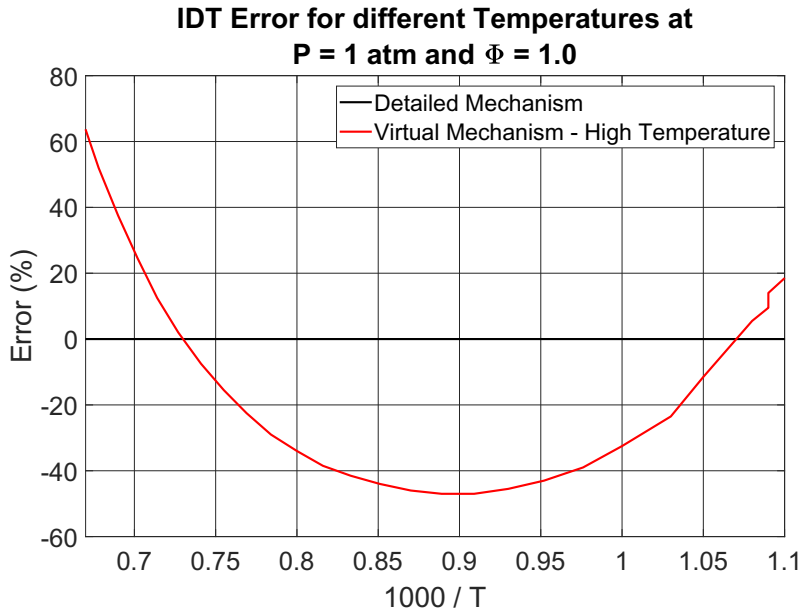

Figure 31 – Relative error of IDT for high temperature cases for n-heptane.

negatively impact the current solution. Therefore, the current deviation was purposely left on the mechanism to provide more leeway to the optimization of the next steps being refined in the final solution. Additionally, the use of linear interpolation greatly reduces the amount of freedom the model has in exchange for a fast convergence. As for the number of parameters, 13 were optimized in this phase, being one for the linear thermodynamic interpolation and three for each of the four reactions.

Using the previous mechanism as a base, a second One INTER model was added to represent the NTC and low temperature reaction paths using a distinct intermediary (Figure 28(b)). This NTC model used an exclusively negative *b* coefficient. Additionally, the previous high temperature models were not optimized, maintaining its coefficients during this step.

The NTC regime could be pinpointed to occur between 800 K ($1000/T = 1.25$) and 625 K ($1000/T = 1.25$) and the initial temperatures used for the optimization were 900, 850, 775, 675, and 625 K. The inclusion of 900 K as an optimization condition acted as an anchor, restraining the current mechanism to move too far from the high temperature solutions. The use of 850 K instead of 800 K reduced the error in the transition between regimes.

During this phase, only 7 parameters were optimized: 1 for the thermodynamic linear interpolation of the intermediary species I_2 and 3 for each of the two reactions. Additionally, the IDT part of the fitness evaluation was used with a weight $\gamma_{IDT} > 1$, as

$$u^j_{idt} = \gamma_{IDT} \frac{|\tau^j_d - \tau^j_v|}{min(\tau^j_d, \tau^j_v)} \tag{85}$$

where γ_{IDT} is the weighting factor. The optimization of the NTC region relies heavily on this coefficient to further force the virtual mechanism to represent the IDT behavior, despite the temperature.

Figure 32 presents the IDT predictions of the partial NTC virtual mechanism for the temperature range of 900 K to 625 K and Figure 33 presents the relative deviation

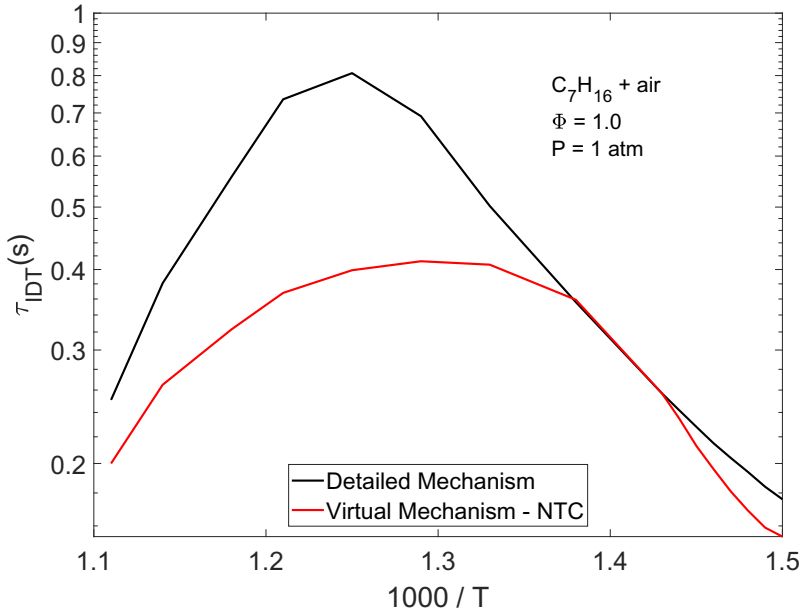

Figure 32 – Virtual optimization attempt for n-heptane detailed mechanism at NTC region conditions

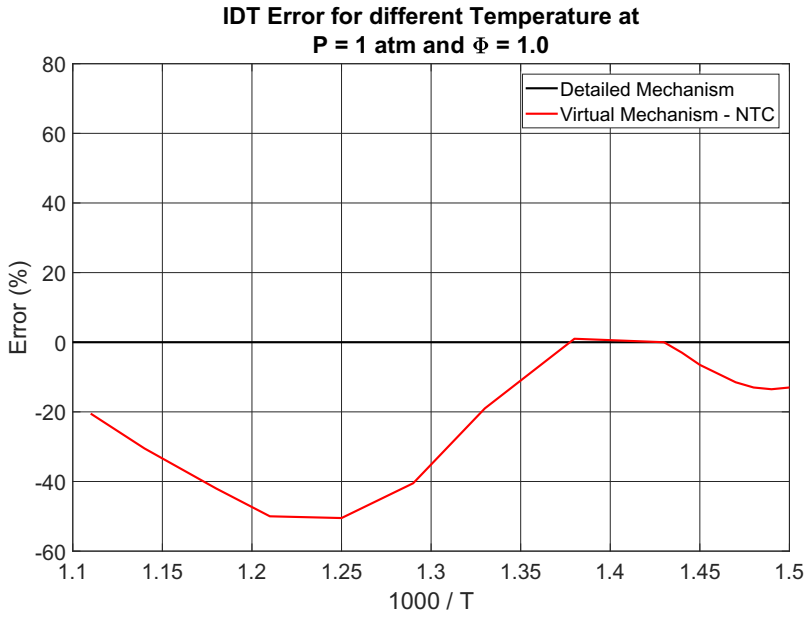

Figure 33 – Relative error of IDT for NTC cases for n-heptane.

of the current solution. The virtual mechanism presents a faster ignition in almost all the conditions, with higher errors (up to -50 %) during the transition from the high temperature to the NTC regimes. That deviation is mostly related to the combined effects of the corresponding reaction paths. As the temperature enters the NTC (below the 800 K or $1000/T = 1.25$), the solution approaches the detailed one. At the edge of the low temperature range (near 625 K), the effects of the negative coefficients fall-off and the virtual mechanism starts to increase the predicted IDT.

The penalties used for reactant consumption were one of the bottlenecks dur-

ing this phase. A more relaxed penalty ended up producing mechanisms with almost instantaneous consumption of fuel. Therefore, aside from the IDT weighting factor, the penalties for early species consumption became more important.

The low temperature regime presents the higher challenge for the optimization phase. As mentioned in previous sections, the basics of parallel reaction paths cannot be used to easily obtain a new IDT mode as the NTC and high temperature cases. Several possible solutions could be used, such as adding reverse reactions to slow down the production of intermediaries and or the virtual products. The solution used here was far simpler, it consisted in further refining the NTC reaction path with a increasing γ_{IDT}.

The effect of a negative *b* coefficient can be better understood as a parameter that reduces the magnitude of the pre-exponential factor *A* (in equation 86) as the temperature increases.

$$k_r = \frac{A}{T^{|b_{neg}|}} exp(-E_a/RT) \tag{86}$$

By calibrating the b_{neg}, one can effectively change the temperature anchor point were this change of behavior occurs. That was the strategy employed in the low temperature regime. To achieve that, a higher value of $|\ b_{neg}\ |$ was allowed with an increase on the IDT weighting factor. Therefore, the number of parameters was the same as the last optimization.

The temperatures used for this optimization were 700, 675, 650, 625, 615, 610, 605, and 600 K. As the previous cases, temperatures outside the region (700, 675, and 650 K) were used to act as anchors to prevent from damaging previous solutions. Figure 34 presents the IDT prediction and figure 35 the relative deviation.

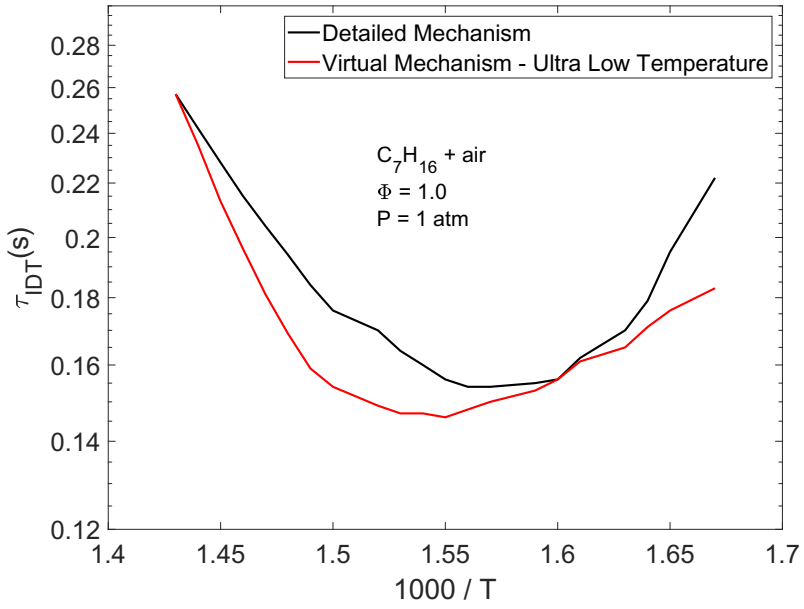

Figure 34 – Virtual optimization attempt for n-heptane detailed mechanism at low temperature conditions

The predictions for the low temperature region are much more accurate than the NTC region. In figure 35 the maximum error in this temperature range is smaller than 20% at the temperature limit of 600 K. It is interesting to note that to proper represent

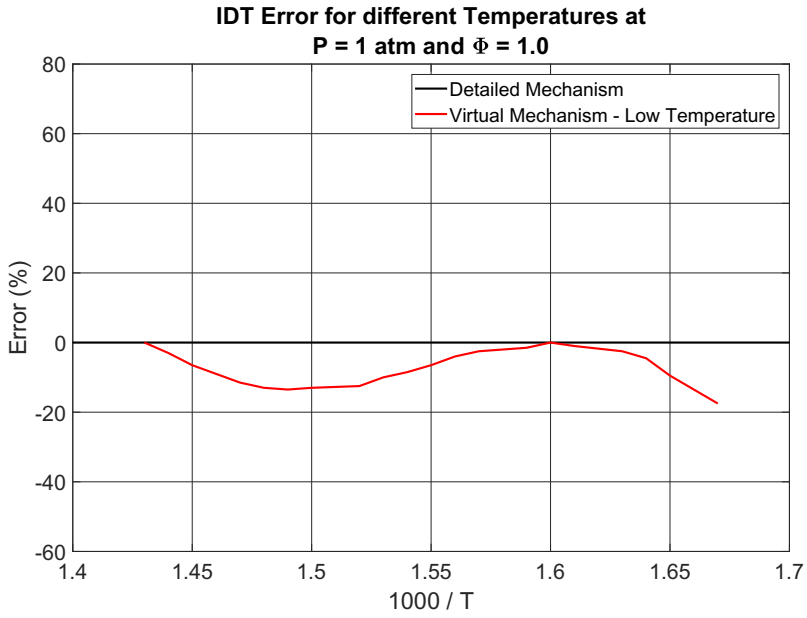

Figure 35 – Relative error of IDT for low temperature cases for n-heptane.

this part of the IDT curve, very small errors are required, since the maximum difference between the detailed prediction (comparing the 700 K and the 625 K) is of the order of 0.08 seconds or 60% of the IDT at 625 K. That small window of values restrict even more the optimization of the IDT part of the problem.

The final mechanism can be used to predict all the temperature range, from 600 to 1500 K. Figures 36 and 37 present the IDT curve for the virtual mechanism and the relative deviation across all the conditions.

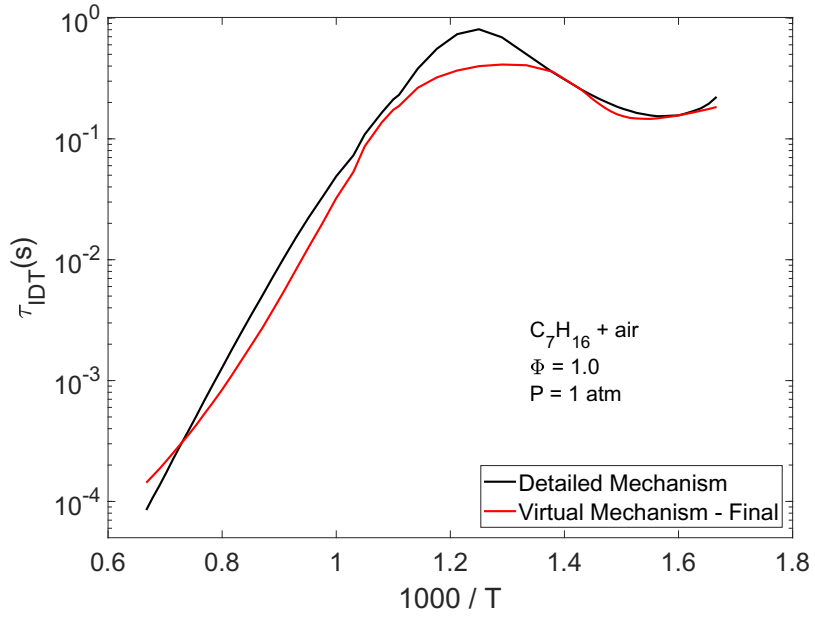

Figure 36 – Virtual optimization attempt for n-heptane detailed mechanism at all the conditions

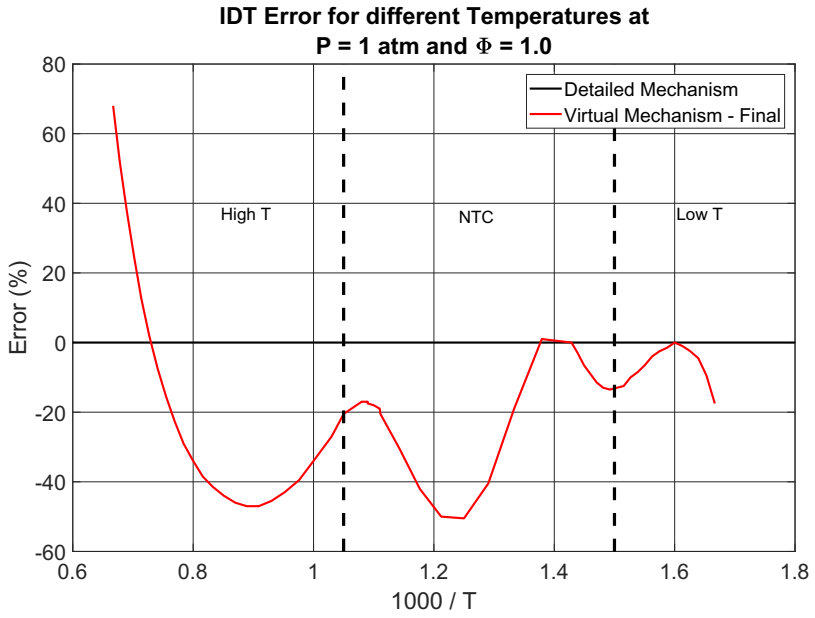

Figure 37 – IDT predictions comparison between the detailed mechanism and the refined virtual mechanism

The overall prediction presented in Figure 36 has a good agreement over the entire range albeit with significant deviations on the high temperature and in the transition phase. The relative deviation obtained are decreased as the temperature decreases and could be associated to the increase on the IDT weighting factor.

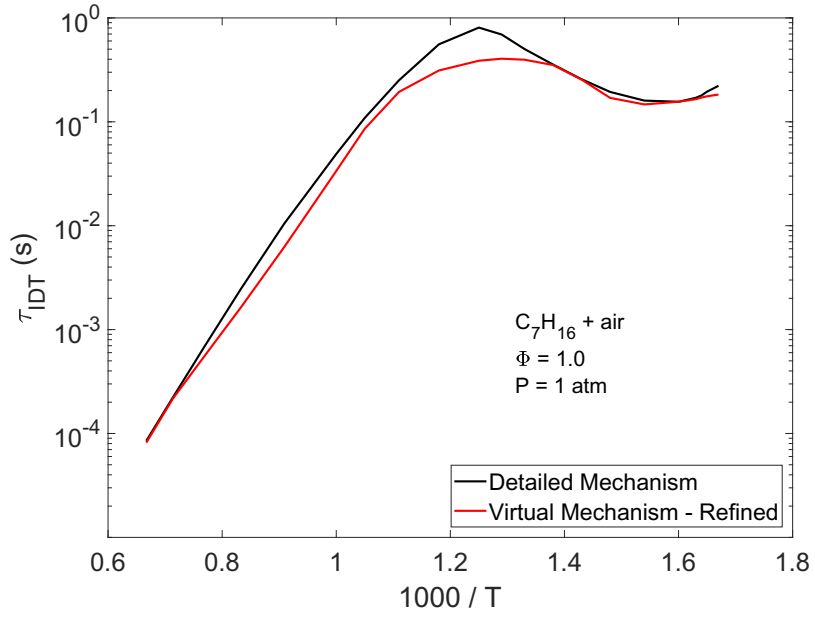

Figure 38 – IDT predictions comparison between the detailed mechanism and the refined virtual mechanism

A final effort of refining the high temperature reactions was performed. Only the high temperature parameters were used and all the temperature range was evaluated.

The final virtual mechanism, named as Refined, is presented in figures 38 and 39. The refined version presents a better prediction over the high temperature conditions, with a maximum absolute error of 40 % against a previous 70 % in the same high temperature region. The NTC region was practically not affected by the refinement. Additional refinements or the addition of reverse reactions could still be considered to reduce the errors further.

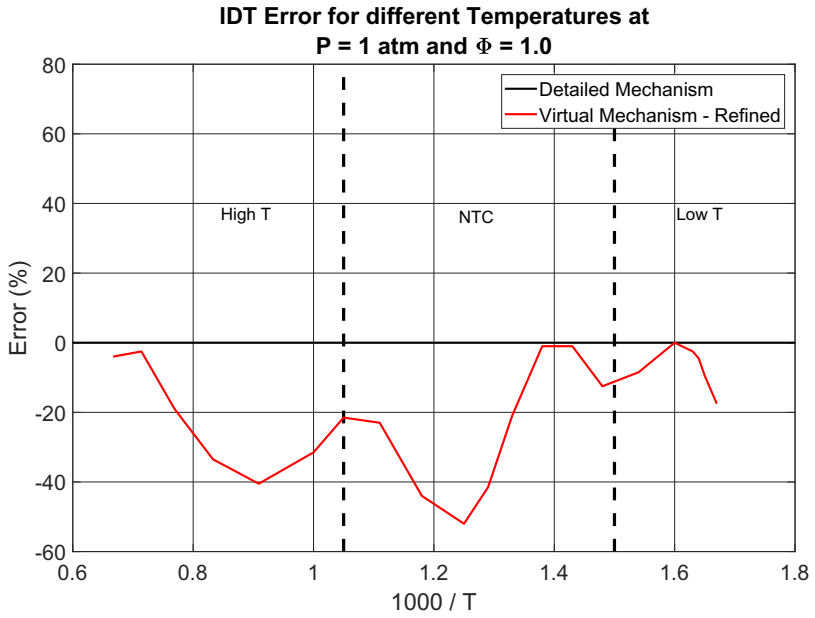

Figure 39 – IDT predictions comparison between the detailed mechanism and the refined virtual mechanism

4.2.2.2 Temperature

The second part of the optimization targets the temperature distribution. In the following discussions, the results for the refined mechanism for high temperature (from 1500K to 900K), NTC (900K to 625K) and the Low Temperature cases (625K to 600K) are presented.

Figure 40 presents the high temperature distribution for temperatures above 900K. The general shape of the virtual distributions are similar to the predictions of the detailed mechanism. The current virtual mechanism can predict the temperature distribution changing from the lower temperature shapes where there is enough time to a radical pool to be formed (900 K) to a more explosive and fast ignition (1500 K).

The thermodynamic difference between the virtual species and the detailed mechanism can be observed in the equilibrium temperature. At 900 K, the virtual mechanism presents the equilibrium temperature 100 K higher than the detailed mechanism, meaning a 3.9 % deviation. At the higher temperature, 1500 K, the deviation is still 100 K, with a relative deviation of 3.5%. The linear interpolation procedure used to model the intermediaries may be the main responsible for the initial part of the differences in the temperature distribution, as it allows for very few improvements.

The NTC region is presented in figure 41. Figure 41(d) shows one of the worst IDT prediction cases, being the point of the maximum relative deviation (-50 %), at the

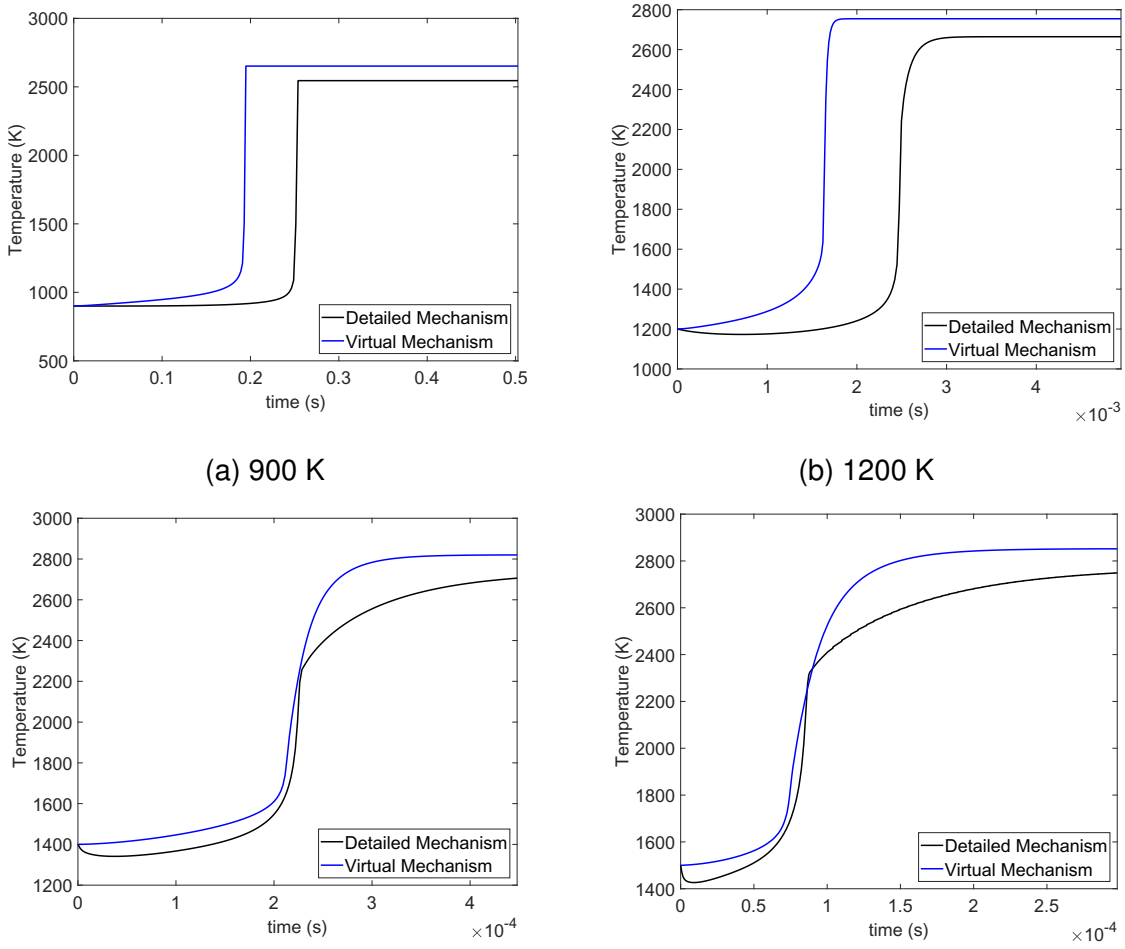

(a) 900 K

(b) 1200 K

(c) 1400 K

(d) 1500 K

Figure 40 – Temperature distribution comparison between the detailed mechanism and the refined virtual mechanism at High Temperature cases (n-heptane + air, at stoichiometric ratio and 1 atm).

transition from high temperature to the NTC. The equilibrium temperature still presents a deviation, decreasing its magnitude as the initial temperature decreases.

In the temperature range presented in figure 41, the detailed mechanism started to present a two stage ignition, which can be clearly observed in figure 41(a), where the detailed temperature rises almost 200 K before ignition. The virtual chemistry presents a similar effect, at 700 K, figure 41(c). For the virtual mechanism, as the temperature decreases, the second stage moves towards the ignition up to the point of merging and disappearing at 650 K. The observed second stage is explained by the presence of the two intermediaries with significant concentrations during the NTC regime. The second stage disappears as soon as the NTC reaction paths dominate the chemistry. Therefore, this shows that virtual mechanisms can produce a second stage behavior if two distinct intermediates are present.

Even if the two stage ignition is observed when using the virtual chemistry, it was obtained by the optimization efforts to match the detailed IDT and not the temperature distribution as the latter has a much smaller weight to the fitness evaluation.

Figure 42 presents the temperature distribution for low temperature. The detailed mechanism continue presenting the two stage ignition, but the virtual chemistry does

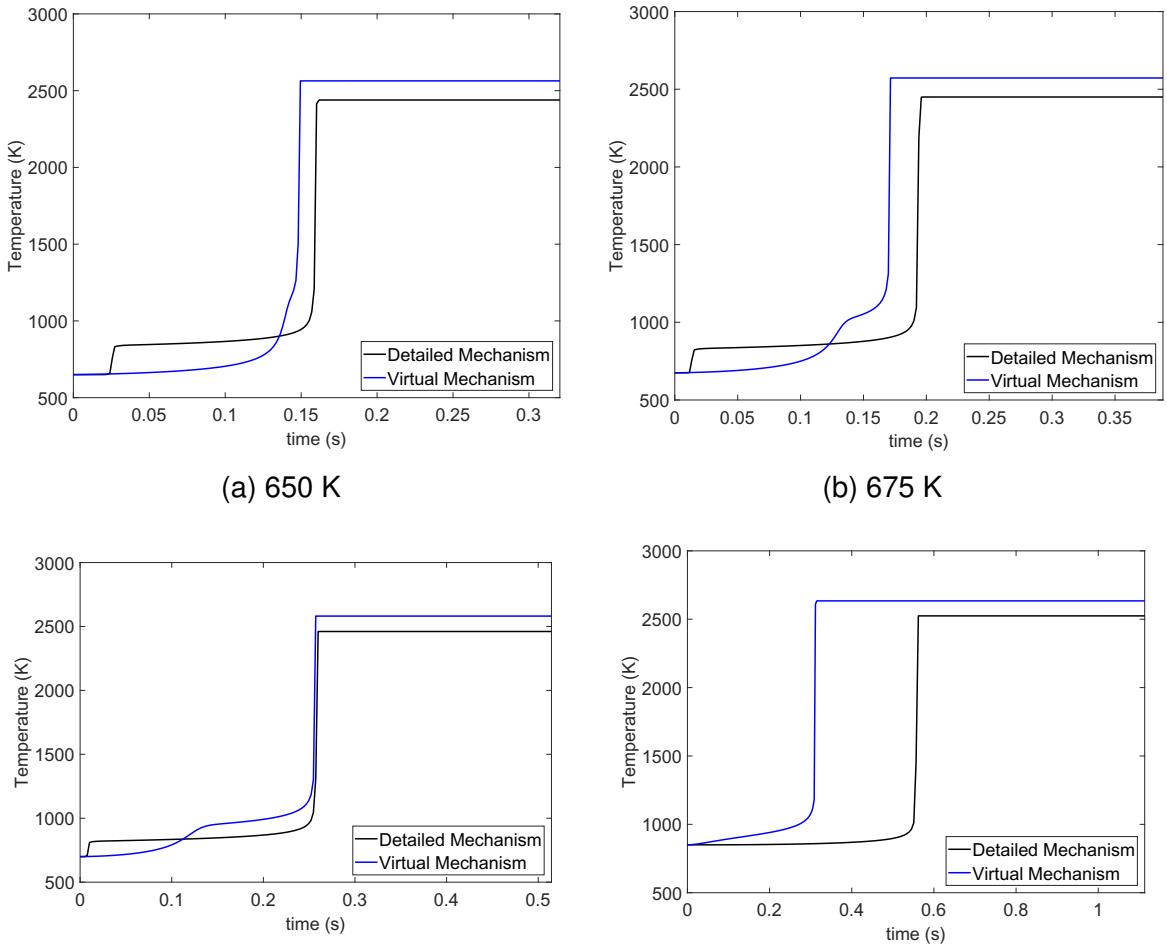

(a) 650 K (b) 675 K

(c) 700 K (d) 850 K

Figure 41 – Temperature distribution comparison between the detailed mechanism and the refined virtual mechanism at the NTC region (n-heptane + air, at stoichiometric ratio and 1 atm).

not. At those temperatures, the high temperature intermediary is not produced and, therefore, there is no difference on the enthalpy of the virtual species to simulate a second stage ignition. Even if the second stage is not present for the virtual mechanism, the overall prediction is very close to the detailed counterpart and the equilibrium temperature deviation is at its lower values.

4.2.2.3 Chemical species

The presence of two intermediaries in the model to represent two distinct regimes produces different mass fraction profiles. Additionally, as observed in the NTC temperature distribution, the virtual mechanism was able to reproduce a second stage mostly due to the presence of both intermediary during the ignition. Therefore, the mass fraction of the reactants and the intermediaries are analyzed next.

Figure 43 presents the maximum value of mass fraction for each intermediary for all the temperature cases. It is possible to note that at high temperature, the I_1, which was optimized in the high temperature paths, is the only one present. As the temperature decreases, I_2 appears and at very low temperatures, it is the main intermediary in

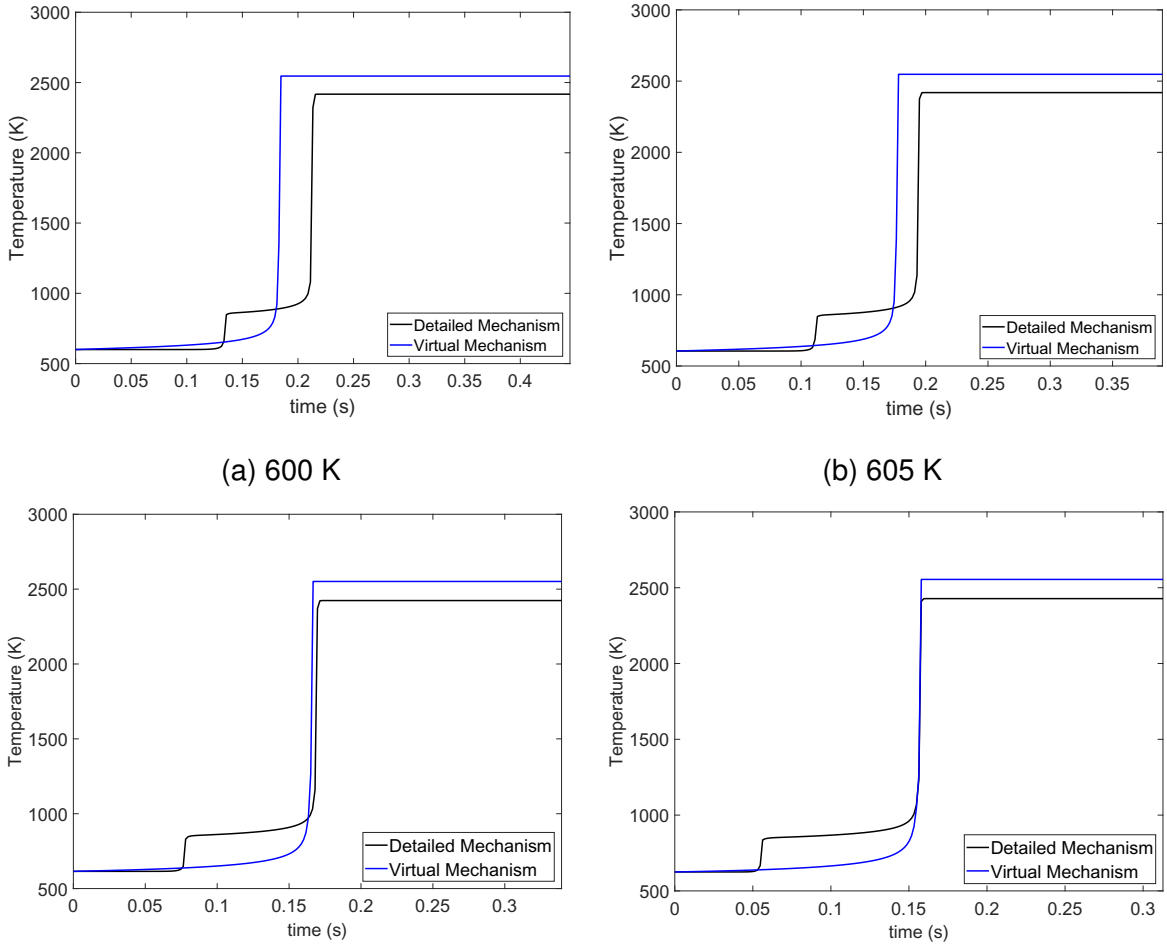

(a) 600 K

(b) 605 K

(c) 615 K

(d) 625 K

Figure 42 – Temperature distribution comparison between the detailed mechanism and the refined virtual mechanism at Low Temperature cases (n-heptane + air, at stoichiometric ratio and 1 atm).

the chemistry. The NTC region (temperature between 900 and 750 K) presents both intermediaries, which further explain the two stage ignition observed.

The next figures present the normalized mass fractions of O_2 for the detailed chemistry and O_2, I_1 and I_2 for the virtual chemistry. The results are divided into high temperature, NTC and low temperature cases.

Figure 44 presents the distribution of the species normalized mass fractions for the initial temperatures between 1500 and 900 K. Although I_2 is shown in the figures, its peak concentration is insignificant when compared to the I_1. In these figures we observe that both O_2 profiles are very similar, being off by the IDT error. At higher temperature conditions, the ignition coincides with the peak of I_1, presenting a similar role as an *OH* radical in the thermal ignition.

Additionally, the detailed mechanism does not consume all the available O_2 at the end of ignition, which could lead to the deviation in he equilibrium temperature. This availability persist throughout all the temperature range, decreasing as the temperature decreases, following the same behavior of the temperature deviation. The lack of reverse reactions and penalties for the intermediaries forces the existence of only virtual products at the end of ignition.

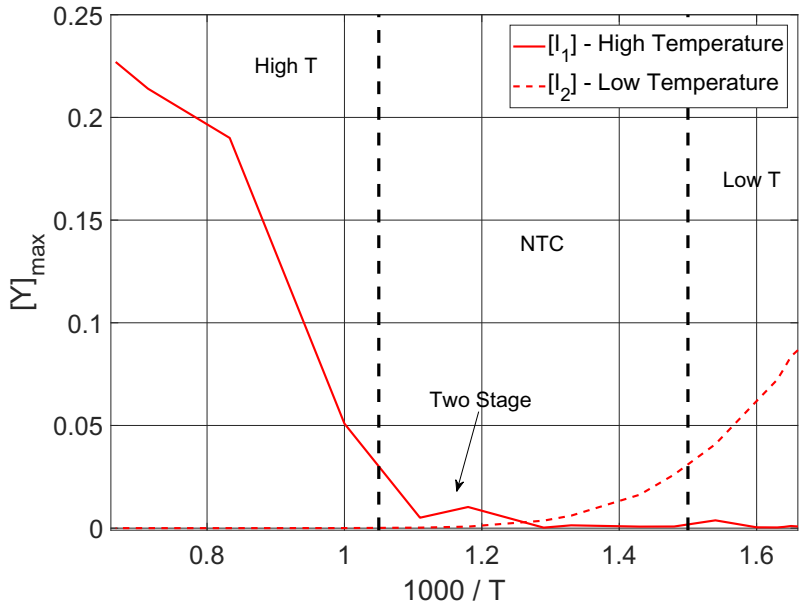

Figure 43 – Maximum recorded mass fraction for Intermediaries.

The distribution of the species in the NTC region is presented in figure 45. The two stage ignition for the detailed mechanism can be observed in the shape of the O_2 profile. There is a well defined step in the mass fraction in the initial ignition phase. The virtual mechanism predicts the overall shape of the curve at 650 K, with a smoother curve. The initial ignition of the virtual mechanism for the lower temperature cases presents a faster O_2 consumption. The penalties for reactants could be increased to force a slower initial rate.

The figure (d) is again the representation of the worst optimized condition. In those figures, the mass fraction of both intermediaries are of the same order of magnitude. The I_1 continues to appear near the IDT, with its peak almost at the ignition time. The I_2 intermediary is the first one to be produced and appears at the very early stages. As the temperature decreases and the IDT becomes faster during the NTC, the I_2 peaks move closer to the ignition, which leads to a reduced in the I_1 peak, assuming the radical role in the ignition.

For the low temperature cases, we refer to figure 46. The second stage ignition of the detailed mechanism is even strong during this conditions, as observed in the aggressive steps on the O_2 profiles. The virtual mechanism tries to reproduce the overall consumption, but it did not present any step on the prediction. The initial O_2 consumption rate for the virtual mechanism is even higher than the previous cases.

At these conditions, the maximum concentration of I_1 is basically zero compared to the I_2. The low temperature intermediary start to peak near the ignition and without the presence of the high temperature intermediary there is no second stage ignition. The overall ignition process is similar to the high temperature cases albeit using the I_2 as main radical.

At low temperature, the role of the reactants consumption penalization factor can be appreciated. To obtain an initial rate of consumption to be closer to the detailed mechanism (a close to zero rate), a more strict penalty should be used at initial ignition steps (two to five percent of the ignition time) to penalize any virtual mechanism that

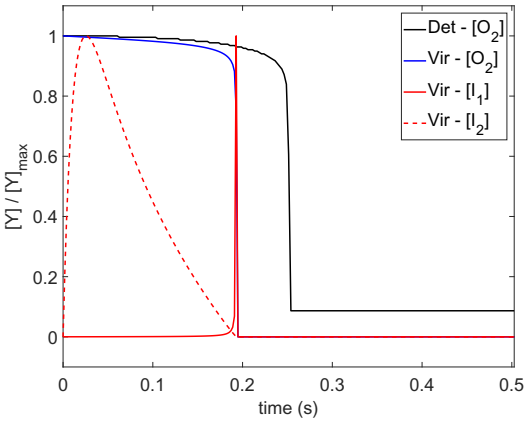

(a) 900 K

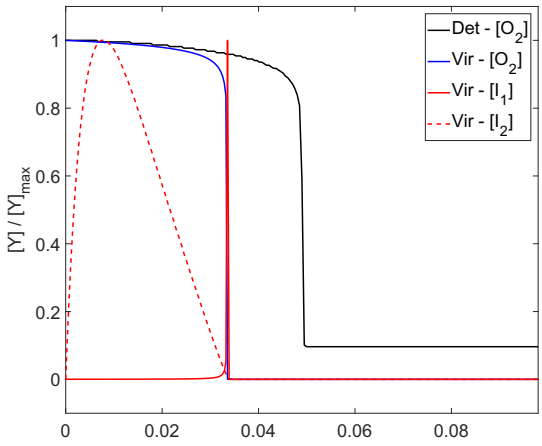

(b) 1000 K

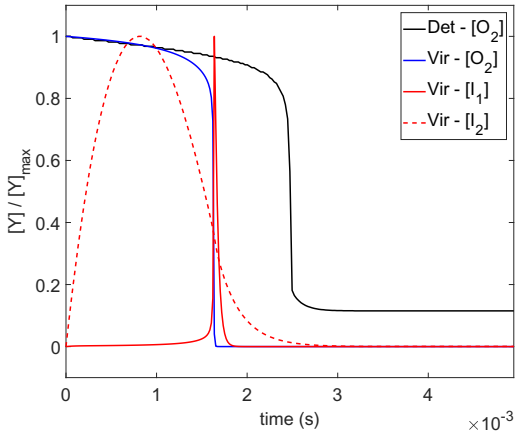

(c) 1200 K

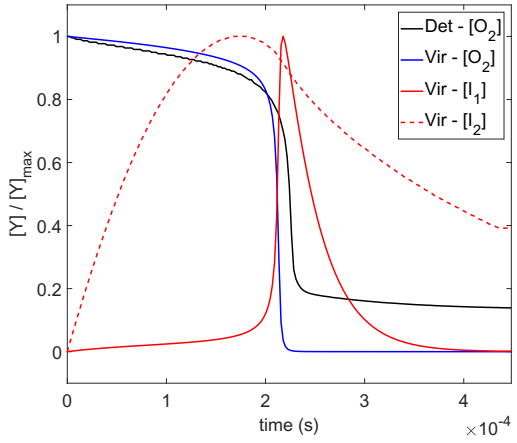

(d) 1400 K

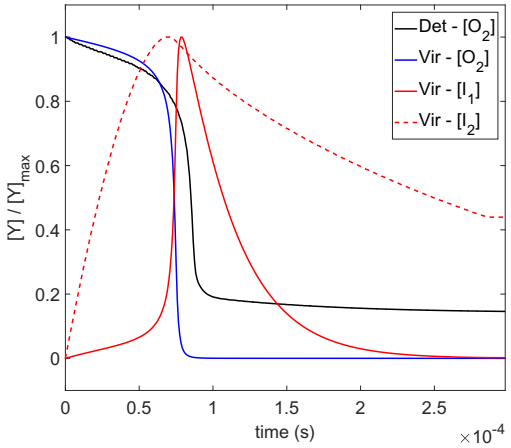

(e) 1500 K

Figure 44 – Normalized mass fraction profiles comparison between the detailed mechanism and the refined virtual mechanism at High Temperature cases (n-heptane + air, at stoichiometric ratio and 1 atm).

consumes more than one or two percent of the reactant mass during this region. The process of obtaining a valid NTC was already a challenge without such strict limits.

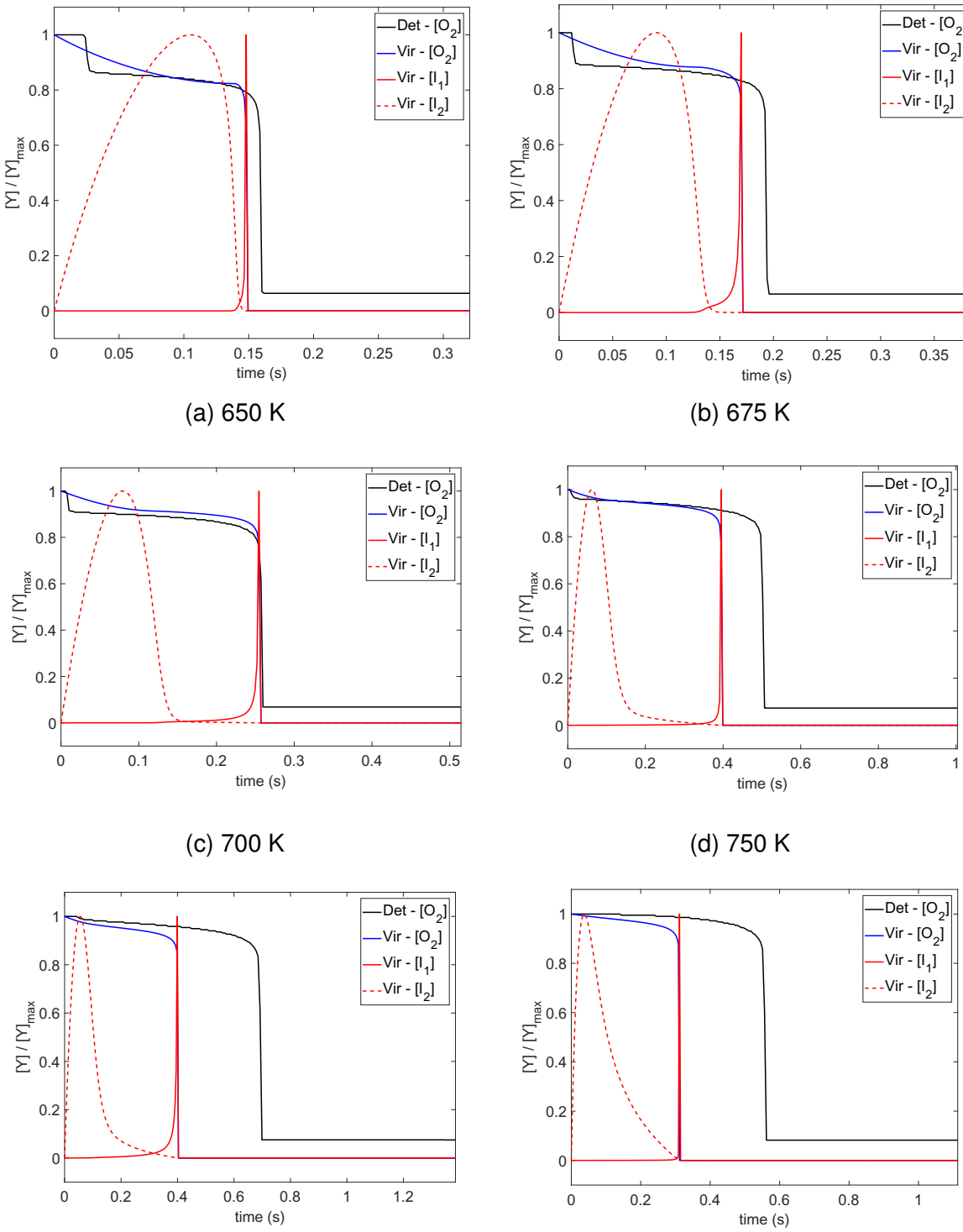

(a) 650 K (b) 675 K

(c) 700 K (d) 750 K

(e) 775 K (f) 850 K

Figure 45 – Normalized mass fraction profiles comparison between the detailed mechanism and the refined virtual mechanism at the NTC region (n-heptane + air, at stoichiometric ratio and 1 atm).

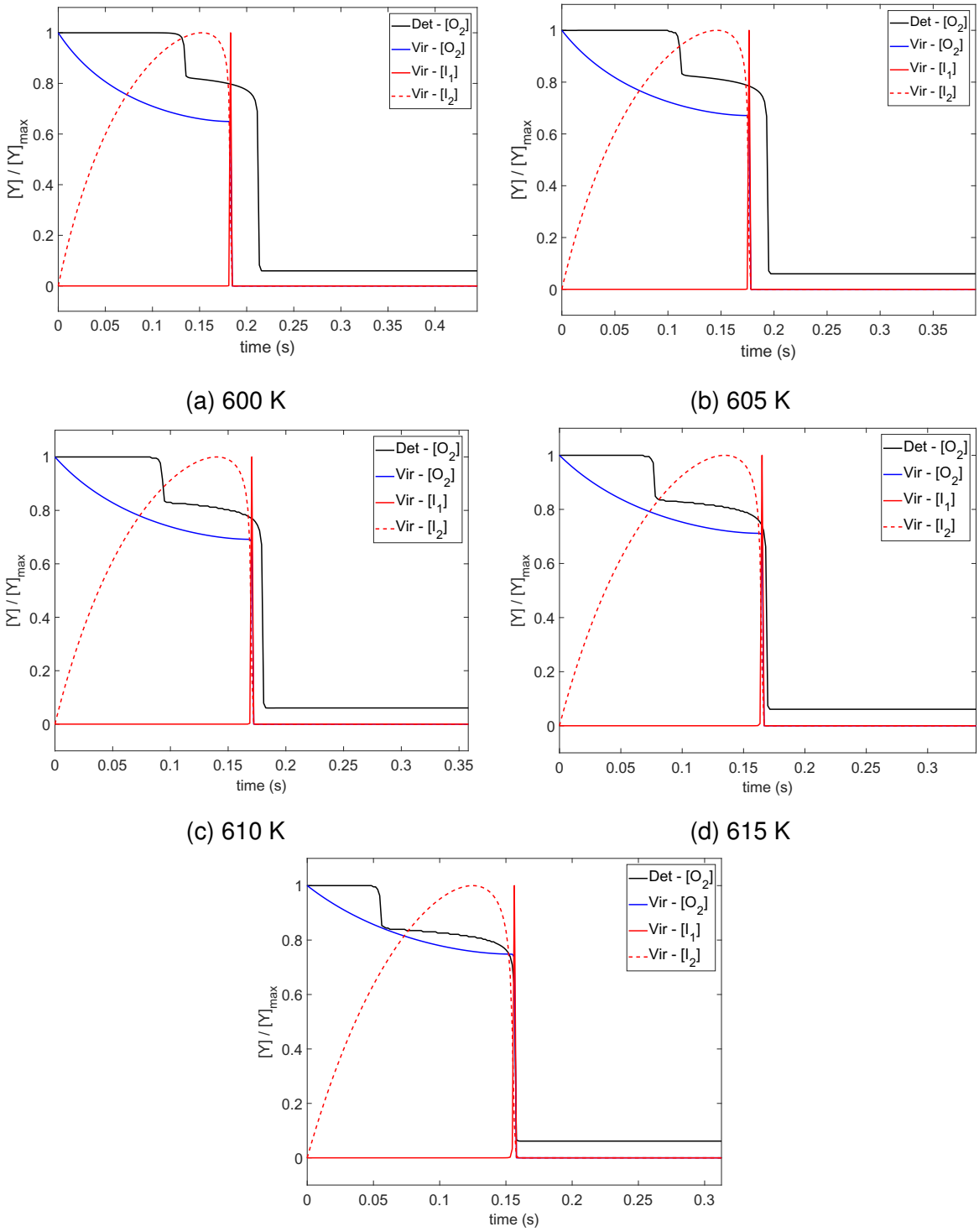

(a) 600 K

(b) 605 K

(c) 610 K

(d) 615 K

(e) 625 K

Figure 46 – Normalized mass fraction profiles comparison between the detailed mechanism and the refined virtual mechanism at Low Temperature cases (n-heptane + air, at stoichiometric ratio and 1 atm).

4.2.3 Computational Time

The computational time spent on simulations using the n-heptane virtual mechanism was assessed in the same way as used for the methane. The virtual and the detailed mechanisms run using the same code in the same machine. We recall that the detailed mechanism computational code relies heavily in the CANTERA library while the virtual uses an in-house code, with low effort to optimize it computationally for this task. The detailed mechanism has 1389 species interacting in 9603 reactions, while the current virtual chemistry used presents 10 virtual species and 6 virtual reactions, which represents a 0.07 % and 0.06 % of the number of the species and reactions of the detailed mechanism, respectively.

As before, the time required for the ignition has a major impact on the overall simulation time, as more time steps are required to achieve the ignition time. The computational time for the simulations for n-heptane differ from those for methane due to two main factors: the larger temperature range and the increased complexity of the detailed mechanism.

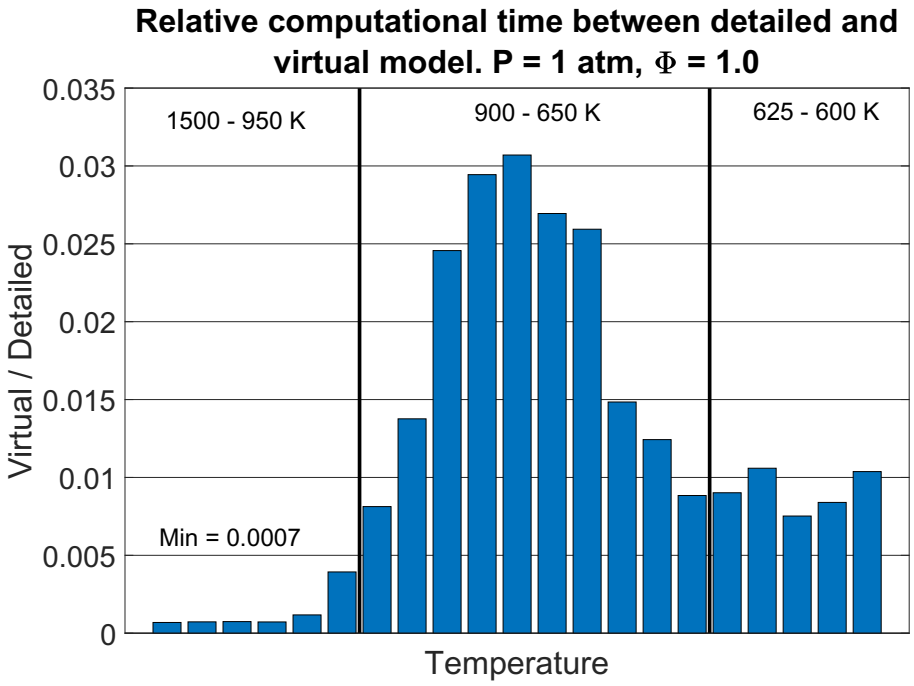

Figure 47 – Relative computational time between detailed and virtual model for n-heptane optimization

Figure 47 presents the relative computational time when using the virtual mechanism compared to the computational time when using the detailed mechanism. In the worst case, the CPU time for the virtual mechanism was approximately 4 % of the time spent using the detailed mechanism. Additionally, for the high temperature cases (1500 to 950 K region), the virtual mechanism results in a CPU time smaller than 1 % of the time spent when using the detailed mechanism, mostly due to the very simple reaction paths. The NTC region (900 to 650 K) results in the worse relative time, reaching up to 3 % of the detailed mechanism. In this region there is the superposition between the high and low temperature reaction paths, with the presence of the two intermediaries.

For the low temperature region (625 to 600 K) the low temperature intermediary is the only one present and, therefore, the results are similar to those of the high temperature region.

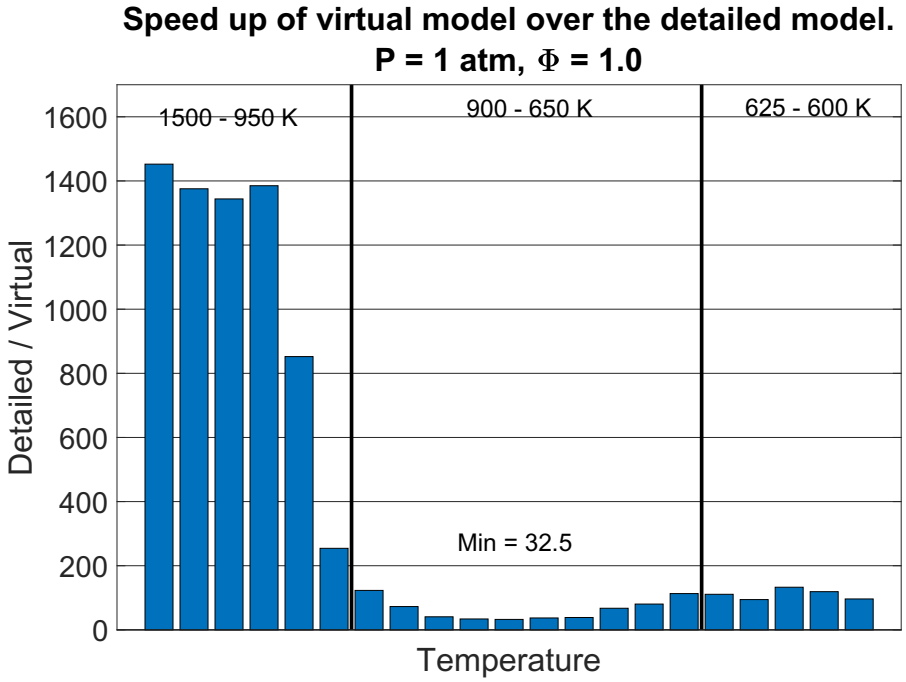

Figure 48 – Speed up factor for the n-heptane optimization.

Figure 48 presents the speed up factor for the virtual mechanism. For the High temperature cases, a speed up of 1400:1 was found for the cases above 1000 K. As the temperature decreases, the speed up also decreases, achieving a minimum value of 32.5:1 for the NTC region. The low temperature region presents the same type of behavior as the high temperature, albeit with an average of 80:1.

The results presented here also reflect the lack of optimization of the current code. More comparisons using different codes are recommended in the future.

5 CONCLUSION

This work develops virtual chemistry models to predicted the ignition delay time of methane-air and n-heptane-air mixtures. The focus is not only the prediction of the adiabatic flame temperature and the ignition delay time, but also the time distribution of the mixture temperature during a constant pressure, constant mass thermal ignition.

The virtual mechanism for methane-air mixtures was developed from intermediate to high temperatures and low pressures. The results indicate that the adiabatic flame temperature can be predicted with, at most, a 5 % over prediction of the thermodynamic equilibrium value. The IDT values in the range from 1000 K to 1500 K and 1 atm to 3 atm present a very good agreement with the results of the detailed mechanism, resulting in maximum deviations of, at most, 60 % at the higher temperature, with most predictions at $\pm$ 40 %. When these results are observed in a typical IDT diagram, the deviations are smaller than the common differences observed among predictions and shock-tube or rapid-compression machine measurements. Also, we notice that the optimization of the virtual mechanisms attempt to distribute the average deviation along the entire calculation domain and even the simplest global virtual mechanism (One RXN) presents a good compromise.

A harder test for the virtual mechanisms is the prediction of the temperature distribution along the thermal ignition. The simpler global mechanism (the One RXN model), although resulting in a good prediction of IDT, is not as well effective in predicting the temperature evolution. They lack the ability to emulate the formation and growth of a radical pool followed by a fast production of virtual species. Virtual mechanisms with intermediaries (such as the Three "One INTER" model) presents the closest agreement with the detailed temperature distribution, due to, mainly, the existence of an intermediary that allows for the emulation of the formation and growth of a radical pool during thermal ignition.

The comparison between the virtual models showed that, for a given structure (e.g. One RXN), increasing the number of parameters improve the fitness value. The same is not observed when comparing different structures, as the Two INTER (24 parameters) produced worse results when compared to models with a smaller set of parameters (One INTER with 13 parameters). The final combined models presented at most 10 species (18 % of the detailed chemistry) in the Two INTER model and 6 reactions (< 3 %) for the Three "One INTER" structure, values much smaller than common reduction techniques.

When comparing the CPU time spent to solve the same thermal ignition problem using a detailed or the virtual mechanisms using the same computer and numerical code, the smallest speed-up factor found was 1.6 times, which is already a very good result. However, for the slower ignition cases (e.g., at 1000 K), the speed-up was over 100 times the CPU time needed to compute the solution with the detailed mechanism. We also observe that the speed up grows exponentially as the IDT increases, becoming even more significant as the temperature decreases.

The virtual mechanism for the n-heptane-air constant pressure, constant mass thermal ignition focuses on predicting IDT and temperature distributions for conditions around the NTC region.

Similar to the methane case, the adiabatic flame temperature can be predicted with, at most, a 5 % over prediction of the thermodynamic equilibrium value. The IDT prediction for the n-heptane case presents a good accuracy when compared to the detailed mechanism for the high temperature cases. Along the NTC region, the

optimized virtual chemistry was able to reproduce the IDT with deviations smaller than 20% when compared to results of the detailed mechanism. The largest deviation, approximately 40 %, occurs at the transition from high temperature to NTC regions. Additionally, the optimized model was able to reproduce the change of the IDT curve from the NTC region to the low temperature with deviations smaller than 20 %.

The temperature distribution still requires improvement. The proposed virtual mechanism presented good overall results, however the two stage ignition presented by the mechanism of (MEHL et al., 2011) at low temperatures was not emulated. The virtual chemistry was only able to produce a similar effect during the transition from high temperature to the NTC region, where the two intermediaries were present during ignition. This indicates that a second stage ignition can be achieved by the addition of another active intermediary path during the conditions where such behavior is expected.

The final virtual mechanism present 10 virtual species and 6 virtual reactions corresponding to 0.07 % and 0.06 % of the detailed solution. The structure optimized contains 2 intermediaries and 4 virtual products, with a total of 20 optimization parameters.

The CPU time to calculate a thermal ignition problem was greatly reduced compared to methane, mostly due to the difference in size and complexity between the detailed and the virtual mechanism. Using the same procedure employed for the previous cases, the smallest speed up factor was 32.5 in the NTC region. Differently from the methane thermal ignition, the highest improvements were found in the high temperature region, which reached speed up factors of more than 1300 times. At the low temperature region, an average speed up factor of 80 times was observed. These results could be further improved by optimizing the numerical code.

5.1 FUTURE WORKS

There are many opportunities to improve the virtual chemistry for thermal ignition problems, and several opportunities to employ such strategies. Some of those opportunities are:

- To use an optimized code to further test the improvements of the virtual schemes;
- To test different fitness functions to produce mechanisms with better prediction of the temperature profile;
- To incorporate the current methodology in flame speed prediction models;
- To use local tabulated parameters to improve the solution;
- To optimize the mechanism from measurements instead of relying on detailed chemistry.

There are several opportunities to improve and to apply such methodologies, as the requirements for precision and computational time in the numerical simulation of applied combustion problems become stricter.

REFERÊNCIAS

ADHIKARI, Sudip; SAYRE, Alan; CHANDY, Abhilash J. In situ adaptive tabulation (ISAT) for combustion chemistry in a network of perfectly stirred reactors (PSRs). **Computers & chemical engineering**, Elsevier Ltd, v. 97, p. 124–134, 2017. ISSN 0098-1354.

AN, Jian; HE, Guoqiang; QIN, Fei; WEI, Xianggeng; LIU, Bing. Dynamic adaptive chemistry with mechanisms tabulation and in situ adaptive tabulation (ISAT) for computationally efficient modeling of turbulent combustion. **Combustion and flame**, Elsevier Inc, v. 206, p. 467–475, 2019. ISSN 0010-2180.

ANDROULAKIS, Ioannis P.; GRENDA, Jeffrey M.; BOZZELLI, Joseph W. Time-Integrated Pointers for Enabling the Analysis of Detailed Reaction Mechanisms. **American Institute of Chemical Engineers**, v. 50, n. 11, 2004. DOI: DOI10.1002/aic.10263.

BAHLOULI, Keyvan; SARAY, R. Khoshbakhi; ATIKOL, Ugur. Development of a reduced mechanism for *n*-heptane fuel in HCCI combustion engines by applying combined reduction methods. **Energy Fuels**, v. 26, p. 3244–3256, 2012. DOI: 10.1021/ef300073n.

BATTIN-LECLERC, Frédérique; SIMMIE, John M.; BLUROCK, Edward. **Cleaner Combustion: Developing Detailed Chemical Kinetic Models**, Springer, 2014. DOI: ISBN978-14-471-5308-5.

CAILLER, Mélody; DARABIHA, Nasser; FIORINA, Benoît. Development of a virtual optimized chemistry method. Application to hydrocarbon/air combustion. **Combustion and Flame**, v. 211, p. 281–302, 2020. DOI: https://doi.org/10.1016/j.combustflame.2019.09.013.

CAILLER, Mélody; DARABIHA, Nasser; VEYNANTE, Denis; FIORINA, Benoiît. Building-up virtual optimized mechanism for flame modeling. **Proceedings of the Combustion Institute**, v. 36, p. 1251–1258, 2017. DOI: http://dx.doi.org/10.1016/j.proci.2016.05.028.

CANCINO, Leonel R. **Desenvolvimento e Aplicação de Modelos Cinéticos Detalhados para Etanol e Combustíveis Hidrocarbonetos Contendo Etanol**. 2009. PhD thesis – Curso de Engenharia Mecânica, Programa de Pós-graduação em Engenharia Mecânica, Universidade Federal de Santa Catarina, Florianópolis.

CHENG, Xinwei; NG, Hoon Kiat; GAN, Suyin; HO, Jee Hou; PANG, Kar Mun. Development and validation of a generic reduced chemical kinetic mechanism for CFD spray combustion modelling of biodiesel fuels. **Combustion and flame**, Elsevier Inc, v. 162, n. 6, p. 2354–2370, 2015. ISSN 0010-2180.

CIOTTOLI, Pietro P; GALASSI, Riccardo Malpica; LAPENNA, Pasquale E; LECCESE, G; BIANCHI, D; NASUTI, F; CRETA, F; VALORANI, M. CSP-based chemical kinetics mechanisms simplification strategy for non-premixed combustion: An application to hybrid rocket propulsion. **Combustion and flame**, Elsevier Inc, v. 186, p. 83–93, 2017. ISSN 0010-2180.

CONTINO, Francesco; JEANMART, Hervé; LUCCHINI, Tommaso; D'ERRICO, Gianluca. Coupling of *in situ* tabulation and dynamic adaptive chemistry: An effective method for solving combustion in engine simulations. **Proceedings of the Combustion Institute**, v. 33, p. 3057–3064, 2011. DOI:10.1016/j.proci.2010.08.002.

CUI, Kai; LIU, Bing; ZHANG, Hai; WU, Yuxin; MATSUMOTO, Keigo; TAKENO, Keiji. Modeling of Pulverized Coal Combustion in Turbulent Flow with the Consideration of Intermediate Reactions of Volatile Matter. **Energy Fuels**, v. 27, p. 2246–2254, 2013. DOI: 10.1021/ef3017514.

CURTIS, Nicholas J.; NIEMEYER, Kyle E.; SUNG, Chih-Jen. An automated target species selection method for dynamic adaptive chemistry simulations. **Combustion and Flame**, v. 162, p. 1358–1374, 2015. DOI: 10.1016/j.combustflame.2014.11.004.

ECHEKKI, Tarek; MASTORAKOS, Epaminondas. **Turbulent Combustion Modeling: Advances, New Trends and Perspectives**, Springer, 2010. DOI: ISBN978-94-007-0411-4.

EMANI, S.; MAZAHERI, K.; SHAMOONI, A.; MAHMOUDI, Y. LES of flame acceleration and DDT in hydrogeneair mixture using artificially thickened flame approach and detailed chemical kinetics. **International Journal of Hydrogen Energy**, v. 40, p. 7395–7408, 2015. DOI: 10.1016/j.ijhydene.2015.03.165.

GALASSI, Riccardo Malpica; CIOTTOLI, Pietro P; SARATHY, S. Mani; IM, Hong G; PAOLUCCI, Samuel; VALORANI, Mauro. Automated chemical kinetic mechanism simplification with minimal user expertise. **Combustion and flame**, Elsevier Inc, v. 197, p. 439–448, 2018. ISSN 0010-2180.

GAO, Xiang; YANG, Suo; SUN, Wenting. A global pathway selection algorithm for the reduction of detailed chemical kinetic mechanisms. **Combustion and Flame**, v. 167, p. 238–247, 2016. DOI: Doi:10.1016/j.combustflame.2016.02.007.

GOODWIN, David G.; MOFFAT, Harry K.; SPETH, Raymond L. **Cantera: An Object-oriented Software Toolkit for Chemical Kinetics, Thermodynamics, and Transport Processes**. [S.l.: s.n.], 2017. http://www.cantera.org. Version 2.3.0. DOI: 10.5281/zenodo.170284.

GORDON, Robert L.; MASRI, Assad R.; POPE, Stephen B.; GOLDIN, Graham M. Transport budgets in turbulent lifted flames of methane autoigniting in a vitiated co-flow.

Combustion and Flame, v. 151, p. 495–511, 2007. DOI: 10.1016/j.combustflame.2007.07.001.

GOU, Xialong; CHEN, Zheng; SUN, Wenting; JU, Yiguang. A dynamic adaptive chemistry scheme with error control for combustion modeling with a large detailed mechanism. **Combustion and Flame**, v. 160, p. 225–231, 2013. DOI: 10.1016/j.combustflame.2012.10.015.

HE, Kaiyuan; ANDROULAKIS, Ioannis P.; IERAPETRITOU, Marianthi G. Numerical Investigation of Homogeneous Charge Compression Ignition (HCCI) Combustion with Detailed Chemical Kinetics Using On-the-Fly Reduction. **Energy Fuels**, v. 25, p. 3369–3376, 2011. DOI: 10.1021/ef200290z.

HE, Kaiyuan; ANDROULAKIS, Ioannis P.; IERAPETRITOU, Marianthi G. On-the-fly reduction of kinetic mechanisms using element flux analysis. **Chemical Engineering Science**, v. 65, p. 1173–1184, 2010a. DOI: DOI:10.1016/j.ces.2009.09.073.

HE, Kaiyuan; IERAPETRITOU, Marianthi G.; ANDROULAKIS, Ioannis P. Integration of On-The-Fly Kinetic Reduction with Multidimensional CFD. **American Institute of Chemical Engineers Journal**, v. 56, n. 5, p. 1305–1314, 2010b. DOI: 10.1002/aic.12072.

HIREMATH, Varun; LANTZ, Steven R.; WANG, Haifeng; POPE, Stephen B. Computationally-efficient and scalable parallel implementation of chemistry in simulations of turbulent combustion. **Combustion and Flame**, v. 159, p. 3096–3109, 2012. DOI: 10.1016/j.combustflame.2012.04.013.

HIREMATH, Varun; LANTZ, Steven R.; WANG, Haifeng; POPE, Stephen B. Large-scale parallel simulations of turbulent combustion using combined dimension reduction and tabulation of chemistry. **Proceedings of the Combustion Institute**, v. 34, p. 205–215, 2013. DOI: 10.1016/j.proci.2012.06.004.

HIREMATH, Varun; REN, Zhuyin; POPE, Stephen B. Combined dimension reduction and tabulation strategy using ISAT–RCCE–GALI for the efficient implementation of combustion chemistry. **Combustion and Flame**, v. 158, p. 2113–2127, 2011. DOI: 10.1016/j.combustflame.2011.04.010.

KAMMA, Panit; SUVANJUMRAT, CHAKRIT. Assessment of Partially Premixed Flame by In-Situ Adaptive Reduced Mechanisms in OpenFOAM. Universiti Malaysia Pahang, Kuantan, v. 18, n. 4, p. 9220, 2021. ISSN 2229-8649.

KONIAVITIS, Panos; RIGOPOULOS, Stelios; JONES, W.P. A methodology for derivation of RCCE-reduced mechanisms via CSP. **Combustion and flame**, Elsevier Inc, v. 183, p. 126–143, 2017. ISSN 0010-2180.

LAM, S. H. Singular Perturbation for Stiff Equations Using Numerical Methods. Ed. by Springer US. **Recent Advances In The Aerospace Sciences**, p. 3–19, 1985. DOI: doi:10.1007/978-1-4684-4298-4_1.

LAM, S. H.; GOUSSIS, D. A. Understanding complex chemical kinetics with computational singular perturbation. **The Combustion Institute**, p. 931–941, 1988.

LAM, Sau H. Model reductions with special CSP data. **Combustion and Flame**, v. 160, p. 2707–2711, 2013. DOI: doi:10.1016/j.combustflame.2013.06.013.

LAW, Chung K. **Combustion Physics**, Cambridge University Press, 2006. DOI: 10.1017/CBO9780511754517.

LI, Zhiyi; LEWANDOWSKI, Michał T; CONTINO, Francesco; PARENTE, Alessandro. Assessment of On-the-Fly Chemistry Reduction and Tabulation Approaches for the Simulation of Moderate or Intense Low-Oxygen Dilution Combustion. **Energy & fuels**, American Chemical Society, United States, v. 32, n. 10, p. 10121–10131, 2018. ISSN 0887-0624.

LIANG, Long; STEVENS, John G.; FARRELL, John T. A dynamic adaptive chemistry scheme for reactive flow computations. **Proceedings of the Combustion Institute**, v. 32, p. 527–534, 2009. DOI: doi:10.1016/j.proci.2008.05.073.

LIU, Z.; YANG, L.; SONG, E.; WANG, J.; ZARE, A.; BODISCO, T. A.; BROWN, R. J. Development of a reduced multi-component combustion mechanism for a diesel/natural gas dual fuel engine by cross-reaction analysis. **Fuel**, 2021 Elsevier Ltd, v. 293, 2021. ISSN 0016-2361.

LU, Tianfeng; LAW, Chung K. A directed relation graph method for mechanism reduction. **Proceedings of the Combustion Institute**, v. 30, n. 1, p. 1333–1341, 2005. DOI: 10.1016/j.proci.2004.08.145.

LU, Tianfeng; LAW, Chung K. Toward accomodating realistic fuel chemistry in large-scale computations. **Progress in Energy and Combustion Science**, v. 35, p. 192–215, 2009. DOI: 10.1016/j.pecs.2008.10.002.

LUO, Zhaoyu; LU, Tianfeng; MACIASZEK, Matthias J.; SOM, Sibendu; LONGMAN, Douglas E. A reduced mechanism for high-temperature oxidation of biodiesel surrogates. **Energy and Fuels**, v. 24, p. 6283–6293, 2010.

MAIO, Giampaolo; CAILLER, Mélody; MERCIER, Renaud; FIORINA, Benoît. Virtual chemistry for temperature and CO prediction in LES of non-adiabatic turbulent flames. **Proceedings of the Combustion Institute**, v. 37, p. 2591–2599, 2019. DOI: https://doi.org/10.1016/j.proci.2018.06.131.

MASEL, Richard I. **Chemical kinetics and catalysis**, Wiley-Interscience; Illustrated edition, 2001. DOI: ISBN978-04-712-4197-3.

MAZUMDER, Sandip. Adaptation of the in situ adaptive tabulation (ISAT) procedure for efficient computation of surface reactions. **Computer and Chemical Engineering**, v. 30, p. 115–124, 2005. DOI: 10.1016/j.compchemeng.2005.08.008.

MEHL, Marco; PITZ, William J.; WESTBROOK, Charles K.; CURRAN, Henry J. Kinetic modeling of gasoline surrogate components and mixtures under engine conditions. **Proceedings of the Combustion Institute**, v. 33, n. 1, p. 193–200, 2011. ISSN 1540-7489. DOI: https://doi.org/10.1016/j.proci.2010.05.027. Available from: http://www.sciencedirect.com/science/article/pii/S1540748910000787.

MINUZZI, Felipe; PINHO, Jean Monteiro de. A new skeletal mechanism for ethanol using a modified implementation methodology based on directed relation graph (DRG) technique. **Journal of the Brazilian Society of Mechanical Sciences and Engineering**, Springer Berlin Heidelberg, Berlin/Heidelberg, v. 42, n. 2, 2020. ISSN 1678-5878.

NAIK, C. V.; WESTBROOK, C. K.; HERBINET, O.; PITZ, W. J.; MEHL, M. Detailed chemical kinetic reaction mechanism for biodiesel components methyl stearate and methyl oleate. **Proceedings of the Combustion Institute**, v. 33, p. 383–389, 2011. DOI: 10.1016/j.proci.2010.05.007.

NIEMEYER, Kyle E; SUNG, Chih-Jen. Reduced Chemistry for a Gasoline Surrogate Valid at Engine-Relevant Conditions. **Energy & fuels**, American Chemical Society, v. 29, n. 2, p. 1172–1185, 2015. ISSN 0887-0624.

NIEMEYER, Kyle E.; SUNG, Chih-Jen. On the importance of graph search algorithms for DRGEP-based mechanism reduction methods. **Combustion and Flame**, v. 158, p. 1439–1443, 2011. DOI:10.1016/j.combustflame.2010.12.010.

OPPENHEIM, A. K. **Dynamics of Combustion Systems**, Springer, 2008. DOI: ISBN978-35-4077-363-4.

ORAN, Elaine S.; BORIS, Jay P. **Numerical Simulation of Reactive Flow**, Cambridge University Press, 2000. DOI: 10.1017/CBO9780511574474.

PACHECO, A. F.; OLIVEIRA, A. A. M.; FIORINA, B. Use of Virtual Kinetics Chemistry for Ignition Delay Times Predictions. In: EDITOR (Ed.). **18th Brazilian Congress of Thermal Sciences and Engineering**. [S.l.: s.n.], 2020.

PACHECO, Augusto F. **Analysis and reduction of detailed chemical kinetics mechanisms for combustion of ethanol and air**. 2016. MA thesis – Universidade Federal de Santa Catarina.

PACHLER, Robert F; RAMALINGAM, Ajoy K.; HEUFER, K. Alexander; WINTER, Franz. Reduction and validation of a chemical kinetic mechanism including necessity analysis and investigation of CH4/C3H8 oxidation at pressures up to 120 bar using a rapid compression machine. **Fuel**, v. 172, p. 139–145, 2016. DOI: Doi:10.1016/j.fuel.2015.12.044.

PANG, Kar Mun; NG, Hoon Kiat; GAN, Suyin. In-cylinder diesel spray combustion simulations using parallel computation: A performance benchmarking study. **Applied Energy**, v. 93, p. 466–478, 2012. DOI: 10.1016/j.apenergy.2011.12.023.

PEI, Y.; MEHL, M.; LIU, W.; LU, T.; PITZ, W. J.; SOM, S. A Multi-Component Blend as a Diesel Fuel Surrogate for Compression Ignition Engine Applications. **Journal of Engineering for Gas Turbines and Power**, v. 137, n. 11, 2015. DOI: 10.1115/1.4030416.

PEPIOT-DESJARDINS, P.; PITSCH, H. An efficient error-propagation-based reduction method for large chemical kinetic mechanisms. **Combustion and Flame**, v. 154, p. 67–81, 2008. DOI: 10.1016/j.combustflame.2007.10.020.

PEPIOT-DESJARDINS, p.; PITSCH, H. An efficient error-propagation-based reduction method for large chemical kinetic mechanisms. **Combustion and Flame**, v. 154, p. 67–81, 2008. DOI:10.1016/j.combustflame.2007.10.020.

PERINI, Federico; BRAKORA, Jessica L.; REITZ, Rolf D.; CANTORE, Giuseppe. Development of reduced and optimized reaction mechanisms based on genetic algorithms and element flux analysis. **Combustion and Flame**, v. 159, p. 103–119, 2012. DOI: doi:10.1016/j.combustflame.2011.06.012.

PETERS, Norbert. **Turbulent Combustion**, Cambridge University Press, 2000. DOI: 10.1017/CBO9780511612701.

In: PETERS, Norbert; ROGG, Bernd (Eds.). **Reduced Kinetic Mechanisms for Applications in Combustion Systems**. [S.l.]: Springer, Berlin, Heidelberg, 1993. (Lecture Notes in Physics Monographs). DOI: https://doi.org/10.1007/978-3-540-47543-9.

In: PILLING, M.J. (Ed.). **Low-Temperature Combustion and Autoignition**. [S.l.]: Elsevier, 1997. v. 35. (Comprehensive Chemical Kinetics). DOI: https://doi.org/10.1016/S0069-8040(97)80013-1.

POINSOT, Thierry. **Theoretical and Numerical Combustion**, R T Edwards Inc, 2001. DOI: ISBN978-19-302-1705-8.

POPE, S. B. Computationally efficient implementation of combustion chemistry using *in situ* adaptive tabulation. **Combustion Theory Modelling**, v. 1, p. 41–63, 1997.

QIU, Yue; YU, Liang; XU, Leilei; MAO, Yebing; LU, Xingcai. Workbench for the Reduction of Detailed Chemical Kinetic Mechanisms Based on Directed Relation Graph and Its Deduced Methods: Methodology and n-Cetane as an Example. **Energy & fuels**, American Chemical Society, v. 32, n. 6, p. 7169–7178, 2018. ISSN 0887-0624.

REN, Zhuyin; GOLDIN, Graham; HIREMATH, Varun; POPE, Stephen B. Simulations of a turbulent non-premixed flame using combined dimension reduction and tabulation for combustion chemistry. **Fuel**, v. 105, p. 636–644, 2013. DOI: 10.1016/j.fuel.2012.08.018.

REN, Zhuyin; LIU, Yufeng; LU, Tianfeng; LU, Liuyan; OLUWOLE, Oluwayemisi O.; GOLDIN, Graham M. The use of dynamic adaptive chemistry and tabulation in reactive flow simulations. **Combustion and Flame**, v. 161, p. 127–137, 2014. DOI: DOI:10.1016/j.combustflame.2013.08.018.

RUI, Zhao; LEPING, Xu; SHIQUAN, Feng. Construction of a reduced mechanism for diesel-natural gas -hydrogen using HCCI model with Direct Relation Graph and Sensitivity Analysis. **Polish journal of chemical technology**, Sciendo, v. 22, n. 4, p. 55–60, 2020. ISSN 1899-4741.

SAXENA, Vivek; POPE, Stephen B. PDF Simulations of Turbulent Combustion Incorporating Detailed Chemistry. **Combustion and Flame**, v. 117, p. 340–350, 1999. DOI: PIIS0010-2180(98)00081-9.

SI, Jicang; WANG, Guochang; LI, Pengfei; MI, Jianchun. A new skeletal mechanism for simulating MILD combustion optimized using Artificial Neural Network. **Energy (Oxford)**, Elsevier Ltd, v. 237, p. 121603, 2021. ISSN 0360-5442.

SMITH, Gregory P. et al. **GRI-mech 3.0**. [S.l.: s.n.], 2018. http://www.me.berkeley.edu/gri_mech/.

SUI, Ran; LIANG, Wenkai; MANTZARAS, John; LAW, Chung K. Coupled reaction mechanism reduction for the hetero-/homogeneous combustion of syngas over platinum. **Combustion and flame**, Elsevier Inc, v. 214, p. 37–46, 2020. ISSN 0010-2180.

SUN, Weiqi; GOU, Xiaolong; EL-ASRAG, Hossam A.; CHEN, Zheng; JU, Yiguang. Multi-timescale and correlated dynamic adaptive chemistry modeling of ignition and flame propagation using a real jet fuel surrogate model. **Combustion and Flame**, v. 162, p. 1530–1539, 2015. DOI: 10.1016/j.combustflame.2014.11.017.

SUN, Weiqi; JU, Yiguang. A multi-timescale and correlated dynamic adaptive chemistry and transport (CO-DACT) method for computationally efficient modeling of jet fuel combustion with detailed chemistry and transport. **Combustion and Flame**, v. 184, p. 297–311, 2017. DOI: 10.1016/j.combustflame.2017.05.032.

SUN, Wenting; CHEN, Zheng; GOU, Xiaolong; JU, Yiguang. A path flux analysis method for the reduction of detailed chemical kinetic mechanisms. **Combustion and Flame**, v. 157, p. 1298–1307, 2010.

TANG, Zhigang; ZHANG, Li; CHEN, Xi; TANG, Gangzhi. Improved Kinetic Mechanism for Diethyl Ether Oxidation with a Reduced Model. **Energy & fuels**, American Chemical Society, v. 31, n. 3, p. 2803–2813, 2017. ISSN 0887-0624.

TIAN, Zemin; YAN, Yingwen; LI, Jinghua. A simplified 1-butene mechanism with combined reduction method. **Fuel (Guildford)**, Elsevier Ltd, v. 241, p. 826–835, 2019. ISSN 0016-2361.

TOSATTO, L.; BENNETT, B. A. V.; SMOOKE, M. D. A transport-flux-based directed relation graph method for the spatially inhomogeneous instantaneous reduction of chemical kinetic mechanisms. **Combustion and Flame**, v. 158, p. 820–835, 2011. DOI:10.1016/j.combustflame.2011.01.018.

TOSATTO, Luca; BENNETT, Beth Anne V; SMOOKE, Mitchell D. Comparison of different DRG-based methods for the skeletal reduction of JP-8 surrogate mechanisms. **Combustion and flame**, Elsevier Inc, Amsterdam, v. 160, n. 9, p. 1572–1582, 2013. ISSN 0010-2180.

TURÁNYI, Tamás. Reduction of Large Reaction Mechanisms. **New Journal of Chemistry**, v. 14, p. 795–803, 1990. DOI: 0398-9836/90/117959.

TURÁNYI, Tamás; TOMLIN, Alison S. **Analysis of Kinetic Reaction Mechanisms**, Springer, Berlin, Heidelberg, 2014. DOI: 10.1007/978-3-662-44562-4.

VEERAPPAN, Devi Raghavee; RAMANATHAN, Karthik; KAISARE, Niket S. Automated Simulation Error based Reduction (ASER) of large chemical reaction mechanisms. **Computers & chemical engineering**, Elsevier Ltd, v. 130, p. 106560, 2019. ISSN 0098-1354.

VIGGIANO, Annarita; MAGI, Vinicio. Dynamic Adaptive Chemistry applied to homogeneous and partially stratified charge CI ethanol engines. **Applied Energy**, v. 113, p. 848–863, 2014. DOI: 10.1016/j.apenergy.2013.08.002.

VIRTANEN, Pauli et al. SciPy 1.0: Fundamental Algorithms for Scientific Computing in Python. **Nature Methods**, v. 17, p. 261–272, 2020. DOI: https://doi.org/10.1038/s41592-019-0686-2.

WANG, Quan-De; FANG, Ya-Mei; WANG, Fan; LI, Xiang-Yuan. Systematic analysis and reduction of combustion mechanisms for ignition of multi-component kerosene surrogate. **Proceedings of the Combustion Institute**, Elsevier Inc, v. 34, n. 1, p. 187–195, 2013. ISSN 1540-7489.

WARNATZ, J.; MAAS, U.; DIBBLE, R W. **Combustion: Physical and Chemical Fundamentals, Modeling and Simulation, Experiments, Pollutant Formation**, Springer, Sept. 2006. DOI: ISBN978-35-4025-992-3.

WU, Zuozhu; QIAO, Xinqi; HUANG, Zhen. A criterion based on computational singular perturbation for the construction of reduced mechanism for dimethyl ether oxidation. **Journal of the Serbian Chemical Society**, Journal of the Serbian Chemical Society, Belgrade, v. 78, n. 8, p. 1177–1188, 2013. ISSN 0352-5139.

WU, Zuozhu; QIAO, Xinqi; HUANG, Zhen. Development and validation of a reduced mechanism for methane using a new integral algorithm in a premixed flame. **Hemijska industrija**, Hemijska Industrija, Belgrade, v. 68, n. 5, p. 529–539, 2014. ISSN 0367-598X.

ZHANG, Shuliang; ANDROULAKIS, Ioannis P.; IERAPETRITOU, Marianthi G. A hybrid kinetic mechanism reduction scheme based on the on-the-fly reduction and quasi-steady-state approximation. **Chemical Engineering Science**, v. 93, p. 150–162, 2013. DOI: 10.1016/j.ces.2013.01.066.

ZHANG, Shuliang; BROADBELT, Linda J.; ANDROULAKIS, Ioannis P.; IERAPETRITOU, Marianthi G. Comparison of Biodiesel Performance Based on HCCI Engine Simulation Using Detailed Mechanism with On-the-fly Reduction. **Energy Fuels**, v. 26, p. 976–983, 2012. DOI: 10.1021/ef2019512.

ZHANG, Shuliang; BROADBELT, Linda J.; ANDROULAKIS, Ioannis P.; IERAPETRITOU, Marianthi G. Reactive Flow Simulation Based on the Integration of Automated Mechanism Generation and On-the-Fly Reduction. **Energy Fuels**, v. 28, p. 4801–4811, 2014. DOI: 10.1021/ef5010539.

ZHAO, Peng; LAM, S.H. Toward computational singular perturbation (CSP) without eigen-decomposition. **Combustion and flame**, Elsevier Inc, v. 209, p. 63–73, 2019. ISSN 0010-2180.

ZHOU, Lei; WEI, Haiqiao. Chemistry acceleration with tabulated dynamic adaptive chemistry in a realistic engine with a primary reference fuel. **Fuel**, v. 171, p. 186–194, 2016. DOI: 10.1016/j.fuel.2015.12.055.